



GEOLOGICAL SURVEY OF CANADA  
COMMISSION GÉOLOGIQUE DU CANADA

This document was produced  
by scanning the original publication.

Ce document est le produit d'une  
numérisation par balayage  
de la publication originale.

BULLETIN 330

**URANIUM GEOLOGY OF THE EASTERN BAKER  
LAKE BASIN, DISTRICT OF KEEWATIN,  
NORTHWEST TERRITORIES**

A.R. Miller



Energy, Mines and  
Resources Canada

Énergie, Mines et  
Ressources Canada

1980



**GEOLOGICAL SURVEY  
BULLETIN 330**

**URANIUM GEOLOGY OF THE EASTERN BAKER  
LAKE BASIN, DISTRICT OF KEEWATIN,  
NORTHWEST TERRITORIES**

A.R. Miller

© Minister of Supply and Services Canada 1980

Available in Canada through

authorized bookstore agents  
and other bookstores

or by mail from

Canadian Government Publishing Centre  
Supply and Services Canada  
Hull, Québec, Canada K1A 0S9

and from

Geological Survey of Canada  
601 Booth Street  
Ottawa, Canada K1A 0E8

A deposit copy of this publication is also available  
for reference in public libraries across Canada

Cat. No. M42-330E                      Canada: \$5.00  
ISBN 0-660-10707-4                  Other countries: \$6.00

Price subject to change without notice

**Critical readers**

*A.N. LeCheminant*  
*I.R. Jonasson*

*Original manuscript submitted: 1978 - 12 - 06*  
*Approved for publication: 1979 - 06 - 29*

## Preface

Reconnaissance geological mapping by the Geological Survey in the southeastern barren grounds of the Northwest Territories during the mid-1950s and 1960s, outlined the distribution of supracrustal rocks and revealed many geological similarities to the actively explored uraniferous Beaverlodge-Athabasca districts. This in turn stimulated the initial phases of uranium exploration in the districts of Keewatin and Mackenzie. Commencing in the early 1970s and continuing to the present, mapping at a scale of 1:250 000 has allowed the acquisition and interpretation of geological data for a region which possesses a very long and complex history of basin development. This information is necessary to the interpretation and evaluation of the uranium metallogeny in a region where uranium is clearly not time bound.

This report represents the initial phase in a continuing research project to document and interpret the uranium metallogeny of the Archean-Paleohelikian basins in the districts of Keewatin and Mackenzie, Northwest Territories. By bringing together information on regional geology and metallogeny, the Geological Survey of Canada is providing a service desired by the mining industry as well as fulfilling one of its principal objectives – determining the mineral and energy resources available to Canada.

OTTAWA, June 1980

D.J. McLaren  
Director General  
Geological Survey of Canada



## CONTENTS

vii	Abstract/Résumé
1	Introduction
1	Acknowledgments
1	Scope and purpose of the project
1	Regional geology
4	Age of the Dubawnt Group
4	Uranium occurrences in the Dubawnt Group and underlying gneisses
4	Analytical techniques
4	Geology of the Christopher Island region
5	Chemistry of the Christopher Island intrusive rocks
5	Fracture-controlled mineralization in the Christopher Island region
8	Age of mineralization
8	Chemistry of the uranium minerals, selenides, and noble metals
10	Origin of the U-Cu-Ag-Au-Se mineralization
10	Geology of the diatreme breccia mineralization
13	Geology and fracture-controlled mineralization in the Bissett-Thirty Mile Lake region
13	General geology
13	Fracture-controlled mineralization within the basement
18	Age of basement mineralization
18	Geology and fracture-controlled mineralization within the Dubawnt Group
22	Geology of the redbed mineralization
22	Paleoenvironment of the South Channel and Kazan formations
24	Geological setting of the Kazan type mineralization
25	Petrography of the Kazan arkose
26	Lithological relationships associated with Kazan type mineralization
27	Petrography of the altered Kazan arkose associated with mineralization
27	White altered Kazan arkose
29	Pink altered Kazan arkose
31	Red altered Kazan arkose
32	Ore mineralogy of Kazan type mineralization
38	Geochemistry of the Kazan type mineralization
38	Sodium and potassium
39	Iron
39	Magnesium
39	Carbonate
40	Copper
40	Silver
40	Uranium
40	Vanadium
40	Molybdenum
41	Zinc
41	Barium
41	Fluorine
41	Geochemistry of the altered Kazan arkose adjacent to the Martell intrusions
41	Genetic model for the Kazan type mineralization
45	Comparison of the geology and mineralization of the eastern Baker Lake basin and Beaverlodge District, Saskatchewan
49	References

## Tables

11	1. Electron microprobe analyses of uranium phases associated with fracture-controlled mineralization
12	2. Electron microprobe analyses of selenide minerals, occurrence 4
13	3. Electron microprobe analyses of electrum associated with selenide-pitchblende mineralization, occurrence 3
30	4. Electron microprobe analyses of chlorite associated with the Kazan type mineralization
36	5. Electron microprobe analyses of illitic clay associated with the Kazan type mineralization, occurrence 10
37	6. Electron microprobe analyses of pitchblende and uraniferous titanates associated with the Kazan type mineralization
46	7. Comparison of the geology and uranium occurrences in the eastern Baker Lake basin, N.W.T. and Beaverlodge District, Saskatchewan

## Figures

- 2 1. Geology of the Dubawnt Group, eastern Baker Lake basin with locations of the various types of uranium occurrences
- 5 2. Total alkali vs. silica for lamprophyre dykes and subvolcanic stocks related to the Christopher Island Formation
- 6 3. Geology of Christopher Island with the locations of the various types of uranium occurrences
- 13 4. Generalized geology of the diatreme breccia occurrence
- 15 5. Geology of the fracture-controlled mineralization, Kazan Falls area
- 20 6. Geology of uranium occurrence 18, Thirty Mile Lake area
- 24 7. Geology of uranium occurrences 9, 10 and 11 in the Bissett Lake-Martell Lake-Kazan River area
- 25 8. Geology of uranium occurrence 20, Thirty Mile Lake area
- 31 9. Compositional variation of interstitial chlorites associated with the Kazan type mineralization
- 40 10.  $\text{Na}_2\text{O}$  vs.  $\text{CO}_2$  for altered and unaltered arkose, Kazan type mineralization
- 40 11.  $\log \text{Cu}$  vs.  $\log \text{CO}_2$  for altered and unaltered arkose, Kazan type mineralization
- 41 12.  $\log \text{U}$ ,  $\log \text{Cu}$  vs.  $\log \text{Ag}$  for altered and unaltered arkose, Kazan type mineralization
- 42 13.  $\log \text{Cu}$ ,  $\log \text{Mo}$ ,  $\log \text{V}$ ,  $\log \text{Pb}$  vs.  $\log \text{U}$  for altered and unaltered arkose, Kazan type mineralization
- 43 14. Schematic cross-sectional model for the Kazan type U-Cu-Ag mineralization

Plates 1-37 -- in text

## Appendixes

- 53 1. Location of uranium occurrences
- 54 2. Whole rock and trace element analyses of Dubawnt Group rocks
- 61 3. Summary of the uranium occurrences in the eastern Baker Lake basin, Northwest Territories

## URANIUM GEOLOGY OF THE EASTERN BAKER LAKE BASIN, DISTRICT OF KEEWATIN, NORTHWEST TERRITORIES

### Abstract

Proterozoic sequences associated with major unconformities are potential uranium metallogenic provinces. Late Aphebian to Paleohelikian Dubawnt Group continental clastic sedimentary and subaerial alkaline volcanic rocks and underlying Archean gneisses, District of Keewatin, Northwest Territories, represent one such uraniumiferous metallogenic province.

Three types of uranium mineralization are present in the eastern Baker Lake basin, which extends from Christopher Island at the eastern end of Baker Lake southwestwards to the western limit of Thirty Mile Lake. The three uranium associations are: 1) fracture controlled mineralization in the Dubawnt Group and basement gneisses (U-Cu-Ag-Au-Se or U-Cu-Pb-Mo-Zn), 2) diatreme breccia mineralization in basement gneisses (U-Cu-Zn), and 3) impregnation and microfracture mineralization in altered arkose peripheral to lamprophyre dykes (U-Cu-Ag).

Hydrothermal fracture related mineralization is controlled by northwest- and east-northeast-trending fault-fracture zones. Diatreme breccia mineralization results from the channelling of groundwaters through highly permeable brecciated gneiss. Mineralization within the altered Kazan arkose peripheral to alkaline dyke complexes formed by a two stage process. Iron and copper sulphides and silver were deposited within the outer portions of the thermal aureole in response to a temperature and Eh gradient across a convective cell created by the thermal anomaly of the dyke complex. The epigenetic sulphide mineralization subsequently provided the reducing environment for precipitation of uranium from groundwater. All three uranium associations show a close spatial distribution to the basal Dubawnt unconformity.

The lithological and structural relationships of the Dubawnt Group rocks, types of mineralization and associated alteration assemblages are strikingly similar to the Beaverlodge District, Saskatchewan.

### Résumé

Les successions protérozoïques associées à d'importantes discordances pourraient représenter des provinces métallogéniques uranifères. Dans le district de Keewatin (Territoires du Nord-Ouest), les roches sédimentaires clastiques continentales et les roches volcaniques alcalines subaériennes du groupe de Dubawnt, qui datent de l'Aphébien supérieur au Paléohélikien, et les gneiss archéens sous-jacents constituent une province métallogénique uranifère de ce genre.

On rencontre trois types de minéralisation uranifère dans l'est du bassin du lac Baker, qui s'étend dans une direction sud-ouest entre l'île Christopher (extrémité est du lac Baker) et la limite ouest du lac Thirty Mile. Les trois groupes de minéralisation uranifère sont: 1) une minéralisation liée à des fractures, dans le groupe de Dubawnt et les gneiss du soubassement (U-Cu-Ag-Au-Se ou U-Cu-Pb-Mo-Zn), 2) la minéralisation de brèches d'explosion volcanique dans les gneiss du soubassement (U-Cu-Zn) et 3) des imprégnations et minéralisations des microfractures qui traversent les arkoses altérées situées à la périphérie de dykes de lamprophyre (U-Cu-Ag).

Les minéralisations hydrothermales des fractures sont limitées par des zones de failles et fractures orientées nord-ouest et est-nord-est. La minéralisation des brèches d'explosion volcanique est due au passage des eaux souterraines à travers le gneiss bréchoïde et fortement perméable. À l'intérieur de l'arkose altérée de Kazan, qui entoure le complexe de dykes alcalins, la minéralisation s'est effectuée en deux phases. Les sulfures de fer et de cuivre et les minerais d'argent se sont déposés dans les portions extérieures de l'aureole thermique, sous l'effet du gradient de température et de Eh caractérisant la cellule de convection créée par l'anomalie thermique qu'a engendrée le complexe de dykes. La minéralisation épigénétique en sulfures a ensuite produit le milieu réducteur favorable à la précipitation des minerais uranifères à partir des eaux souterraines. Ces trois types de minéralisation en uranium manifestent dans leur distribution spatiale un lien étroit avec la discordance basale de Dubawnt.

Les relations lithologiques et structurales qui caractérisent les roches du groupe de Dubawnt, les types de minéralisation et les assemblages associés de minéraux altérés, rappellent de façon étonnante le district de Beaverlodge en Saskatchewan.





## URANIUM GEOLOGY OF THE EASTERN BAKER LAKE BASIN, DISTRICT OF KEEWATIN, NORTHWEST TERRITORIES

### INTRODUCTION

Various Proterozoic sequences associated with major unconformities are potential uranium metallogenic provinces. The Proterozoic Dubawnt Group sedimentary and volcanic rocks and underlying gneisses, Districts of Keewatin and Mackenzie, Northwest Territories represent one such uranium-bearing metallogenic province. The Baker Lake basin refers to a continuous belt of Dubawnt Group rocks which extends from the east end of Baker Lake to Tulemalu Lake (LeCheminant and Miller, 1978). This report is concerned with the eastern portion of the Baker Lake basin located between Baker Lake and Thirty Mile Lake (Fig. 1). The discussion of the uranium geology is restricted to the South Channel, Kazan and Christopher Island formations and underlying basement complex. The term 'occurrence' is used throughout this report to designate the presence of a uranium-bearing phase and has no connotation of grade or tonnage. Pitchblende, as used in this report, refers to a non-thorium bearing uraninite occurring as sooty, colloform and botryoidal forms and rarely as euhedra.

The Dubawnt basin in the Baker Lake region is an east-northeast elongate structure approximately 55 km wide. The Dubawnt Group rests unconformably on the basement complex along the southern and eastern margins of the basin (LeCheminant et al., 1977) and lies in fault contact with the basement complex along the northern margin (Donaldson, 1965). The Dubawnt Group has been regionally faulted about east and east-northeast directions that parallel the distribution of these rocks, and about a northwest direction. The distribution of faults suggests that the Dubawnt rocks in the Baker Lake region were deposited in a graben.

### Acknowledgments

The writer acknowledges the following officers of the Geological Survey of Canada: A.N. LeCheminant for the many discussions on the regional geology of the Baker Lake Basin; L.P. Tremblay for the discussions on the regional geology of the Beaverlodge district; A.N. LeCheminant and I.R. Jonasson for critically reading the manuscript; J.A. Kerswill for the statistical processing of the geochemical data; A.G. Plant and G.J. Pringle for the energy dispersive investigations and quantitative electron microprobe analyses, D.M. Watson, A.C. Roberts and A.L. Littlejohn for X-ray identifications and the staff of the Analytical Chemistry Section for the rock geochemistry.

### SCOPE AND PURPOSE OF THE PROJECT

This study began in 1976 and is the first part of an ongoing research project on the uranium mineralization in the Dubawnt Group rocks and underlying gneiss complex, District of Keewatin, Northwest Territories. The petrological study has been conducted by the Economic Geology Division in association with geological studies undertaken by Precambrian Division, Geological Survey of Canada.

The investigation was initiated to study: 1) the mineralogy of the uranium occurrences within the Dubawnt Group rocks and underlying gneisses, 2) the relationship of mineralization to their host rocks, and 3) to interpret the results with regards to genetic modelling for the uranium mineralization.

During the 1976 field season, detailed mapping, examination, and sampling of 20 uranium occurrences was completed. These occurrences are numbered 1 to 20 going from east to west (Fig. 1). From fall 1976 to spring 1978, research involved characterizing the petrography, ore microscopy, and geochemistry of the various mineralization types.

### REGIONAL GEOLOGY

The Dubawnt Group is a relatively flat lying sequence of Late Archean to Paleohelikian sedimentary rocks, volcanic rocks, and related intrusive equivalents. Donaldson (1965) subdivided the Dubawnt Group into six formations: South Channel conglomerate, Kazan arkose, Christopher Island volcaniclastic and volcanic rocks and related Martell intrusions, Pitz volcanic rocks, and the Thelon sandstone.

The Dubawnt Group rests unconformably upon and in fault contact with Archean felsic gneisses and mafic to ultramafic intrusions. The basement rocks in the vicinity of Christopher Island consist of granitoid and granulitic gneisses and an intrusive gabbroic-noritic anorthosite complex (Schau and Hulbert, 1977; Wright, 1967). Southwestwards from the Christopher Island region, the basement complex adjacent to the unconformity includes gneissic quartz monzonite and granodiorite, cataclastic migmatitic gneisses, and major metavolcanic and metasedimentary units (LeCheminant et al., 1976, 1977).

The basal redbeds of the Dubawnt Group include the South Channel and Kazan formations. The South Channel Formation, ranging from 0-1800 m in thickness (LeCheminant et al., 1977), is principally a pebble supported conglomerate with minor sandstone interbeds. The predominant framework lithologies are granitic and granodioritic gneiss ranging from angular blocks to rounded granules (>256 mm-2 mm). The maroon matrix consists of sand- to silt-sized quartz and feldspar cemented by finely dispersed hematite and calcite. Clast size variations, channel scours, and pebble imbrication outline bedding planes. Locally the basement complex adjacent to the unconformity is hematitized and contains banded hematite veinlets. The locally derived nature of the framework lithologies and the immaturity of the conglomerate suggest that the South Channel conglomerate is an alluvial fan deposit or possibly local scree deposits along the margin of the Dubawnt Basin.

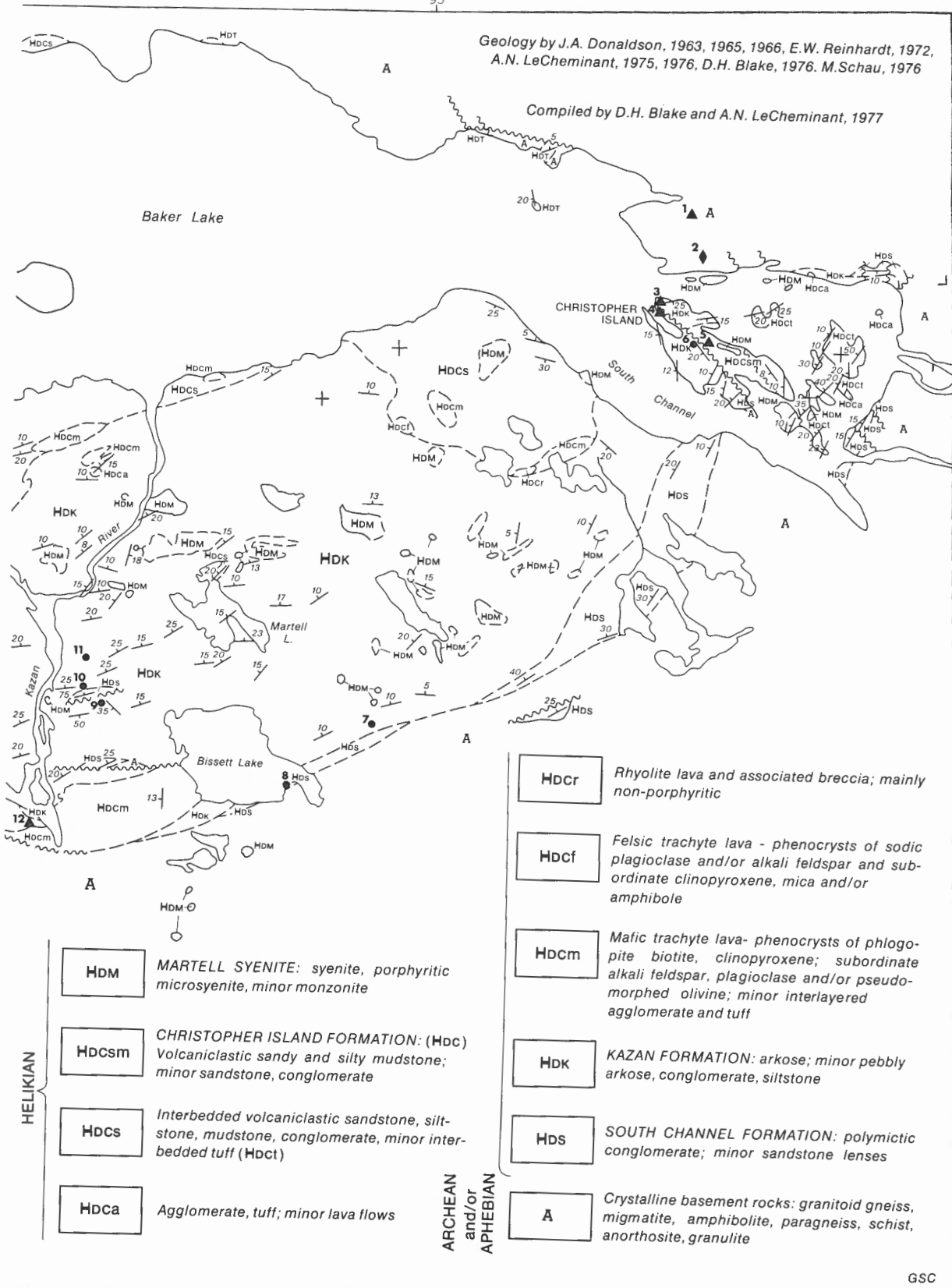
The Kazan Formation is conformable with the South Channel Formation and is estimated to be approximately 1000 m thick in the Baker Lake area. The Kazan Formation is a crossbedded plagioclase-rich arkose interbedded with mudstone and siltstone. The arkose is typically pink, red to maroon, fine- to medium-grained, well sorted, and indurated with hematite, calcite, and albite. Variation in lithologies represented by fining upward cycles and structures represented by desiccation cracks and mudchip arkoses suggest repeated subaerial exposure of a braided fluvial river system (Donaldson, 1965; Macey, 1973). The lower redbed formations, South Channel and Kazan, are interpreted as a sequence of northwestward overlapping alluvial fans derived from basement uplifts to the south and east.



95°

Geology by J.A. Donaldson, 1963, 1965, 1966, E.W. Reinhardt, 1972, A.N. LeCheminant, 1975, 1976, D.H. Blake, 1976, M.Schau, 1976

Compiled by D.H. Blake and A.N. LeCheminant, 1977



64°

HELIKIAN

- HDM** MARTELL SYENITE: syenite, porphyritic microsyenite, minor monzonite
- HDCsm** CHRISTOPHER ISLAND FORMATION: (Hdc) Volcaniclastic sandy and silty mudstone; minor sandstone, conglomerate
- HDCs** Interbedded volcaniclastic sandstone, siltstone, mudstone, conglomerate, minor interbedded tuff (Hdct)
- Hdca** Agglomerate, tuff; minor lava flows

- Hdcr** Rhyolite lava and associated breccia; mainly non-porphyritic
- Hdcf** Felsic trachyte lava - phenocrysts of sodic plagioclase and/or alkali feldspar and subordinate clinopyroxene, mica and/or amphibole
- HDCm** Mafic trachyte lava- phenocrysts of plagioclase, biotite, clinopyroxene; subordinate alkali feldspar, plagioclase and/or pseudomorphed olivine; minor interlayered agglomerate and tuff
- HDK** KAZAN FORMATION: arkose; minor pebbly arkose, conglomerate, siltstone
- HDS** SOUTH CHANNEL FORMATION: polymictic conglomerate; minor sandstone lenses
- A** Crystalline basement rocks: granitoid gneiss, migmatite, amphibolite, paragneiss, schist, anorthosite, granulite

ARCHEAN and/or APHEBIAN

63°30'

GSC

95°

The Christopher Island Formation is conformable on the Kazan Formation in the eastern portion of the basin and unconformable in the region north of Thirty Mile Lake (LeCheminant et al., 1977). The Christopher Island Formation consists of subaerial potassic alkaline lavas and pyroclastic rocks and derived volcanoclastic sediments estimated to be up to 300 m thick locally (LeCheminant et al., 1977; Blake, 1980). Subvolcanic intrusions, termed the Martell Syenite by Donaldson (1965), range in composition from syenite to monzonite (Wine, 1976). The intrusions which are equivalent compositionally to the volcanic rocks, intrude the basement complex, South Channel, Kazan, and Christopher Island formations (Fig. 1) and occur principally as large sills and sill complexes near Martell Lake and as single or complex dyke swarms and stocks within the lower redbed and basement complex (Donaldson, 1965; LeCheminant et al., 1977).

The upper formations of the Dubawnt Group comprise the calc-alkaline Pitz volcanic rocks and Thelon sandstone. The Pitz Formation has a maximum thickness of 100 m and consists of porphyritic acid lava flows. The Thelon Formation, at least 100 m thick in the eastern Baker Lake basin, abuts and overlies lavas of the Pitz and Christopher Island formations (LeCheminant et al., 1977). These sediments are locally derived and consist of flat-lying, cross-bedded, red to cream orthoquartzites and conglomerates. Northwest-trending Mackenzie diabase dykes transect all of the above formations.

#### AGE OF THE DUBAWNT GROUP

The Dubawnt Group has not been affected by regional metamorphism or major folding but has been faulted extensively. A whole rock Rb/Sr isochron on trachytic and felsic volcanic rocks of the Christopher Island Formation indicates an age of  $1786 \pm 26$  Ma (Wanless and Loveridge, 1972; decay constant  $\gamma_{\text{Rb}^{87}} = 1.42 \times 10^{-11}$  yr). This represents a minimum age for the South Channel and Kazan formations and suggests that the lower redbeds were deposited during the latest stages of the Hudsonian Orogeny or immediately thereafter. Thus the basal redbeds may range from late Apebian to earliest Paleohelikian.

#### URANIUM OCCURRENCES IN THE DUBAWNT GROUP AND UNDERLYING GNEISSES

Epigenetic uranium mineralization is localized near the present trace of the basement-Dubawnt Group contact in the eastern Baker Lake basin. The epigenetic mineralization has been subdivided into three types:

- 1) Fracture controlled mineralization in
  - a) Christopher Island volcanic and volcanoclastic rocks and subvolcanic pipes,
  - b) basement gneisses
- 2) Mineralization in altered Kazan arkose (Kazan type)
- 3) Mineralization in the breccia envelope peripheral to a diatreme structure.

Fracture-controlled and diatreme-breccia mineralization within the basement gneisses and supercrustal rocks is concentrated within approximately 5 km of the basal Dubawnt unconformity. The zones of Kazan-type mineralization occur up to 16 km from the unconformity; however these mineralized areas are restricted to specific stratigraphic portions of the Kazan arkose.

#### Analytical Techniques

Major elements were analyzed by X-ray fluorescence on a Philips sequential X-ray spectrometer, Model 1450 and the trace elements Ba, Sr, V, and Cu by emission spectroscopy in the Analytical Chemistry Section, Geological Survey of Canada. Other trace elements Pb, Zn, Mo, and Ag were determined by atomic absorption, Bondar-Clegg Co., Ottawa. The lower limit of detection for the Pb, Zn, Mo and Ag analyses is 2, 1, 1, and 0.1 ppm respectively with a precision of 10 to 15 per cent. Uranium analyses on whole rock powders were determined by delayed neutron activation, Atomic Energy of Canada Ltd., Commercial Products Division, Ottawa. The level of detection for uranium by delayed neutron activation is  $0.4 \mu\text{g}$  uranium with a precision of  $\pm 20$  per cent at 1 ppm and  $\pm 5$  per cent at  $>100$  ppm.

Very fine grained silicates, sulphides and radioactive minerals and phases were studied using a Mineral Analysis Company electron microprobe equipped with a Kevex energy dispersive spectrometer for spectra identification followed by quantitative analyses. Minerals were analyzed using an accelerating voltage of 15 and 20 kV and a specimen current of about  $0.3 \mu\text{amps}$ .

#### Geology of the Christopher Island Region

The Dubawnt Group rests with angular unconformity and in fault contact with anorthosite, granulitic and granodioritic gneisses. Basement rocks to the north and east of Christopher Island include granulitic and granitoid gneisses and a gabbroic-noritic anorthosite complex. The granulitic gneisses are strongly banded and consist of a slightly retrograded equigranular assemblage of hypersthene + diopside + garnet + hornblende + biotite + chlorite + quartz + plagioclase + potash feldspar + apatite + iron oxide and sulphides. The gabbroic-noritic anorthosite complex is intrusive into the granulitic and granitoid gneisses and has been deformed about an east-west trend (Schau and Hulbert, 1977). Uranium contents of the granulitic gneisses and intrusive complex range from  $<0.1$  to 2.4 ppm. To the south and southeast of Christopher Island, the basement complex consists of retrograded amphibolite grade granodioritic and granitic gneisses, paragneiss, and amphibolite.

The distribution of basal clastic sedimentary rocks of the Dubawnt Group outlines the eastern terminus of the Baker Lake basin east of Christopher Island (Fig. 1). The South Channel Formation consists of conglomerate-breccia and conglomerates locally derived from granulite, anorthosite, and granodioritic gneisses (Schau and Hulbert, 1977; Donaldson, 1965) and averages approximately 100-120 m thick in this segment of the Dubawnt basin (Schau, personal communication, 1977). The Kazan Formation, a sequence of interbedded carbonate and hematite cemented arkose and siltstone, is conformable with the South Channel conglomerate and is estimated to be approximately 150-175 m thick.

The Christopher Island Formation is conformable with and gradational from the Kazan arkose through a zone of tuffaceous arkose. This formation comprises maroon tuffaceous arkose, sandy and silty maroon mudstone, trachytic flow rocks, and equivalent stocks, sills and dykes.

The tuffaceous sediments of the Christopher Island Formation contain ash to block size fragments (0.25 to  $>64$  mm) of porphyritic trachyte set in an arkosic matrix (Plate 1). Tuffaceous and lapilli size fragments commonly exhibit fiamme structures. The tuffaceous arkose indurated with hematite and calcite consists of medium to fine sand size, angular to subrounded grains of quartz, plagioclase, potash feldspar, and lithic clasts of granoblastic gneiss and

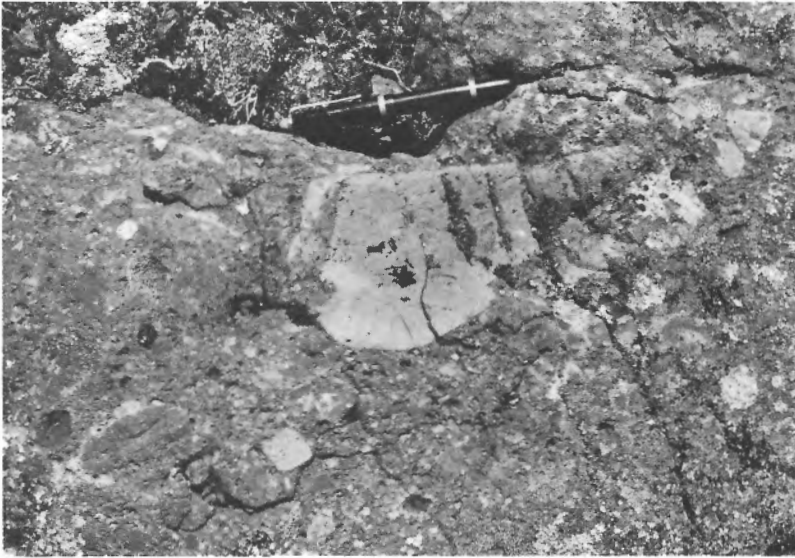


Plate 1

Tuffaceous arkose, Christopher Island Formation, Christopher Island. (GSC 203591)

trachyte. The upper sedimentary unit on Christopher Island is a massive to poorly bedded, silty to sandy maroon mudstone which consists of angular grains of quartz and feldspar, and minor trachyte clasts cemented by hematite and calcite.

The igneous rocks in the Christopher Island area intrude the basement complex and Dubawnt supercrustal rocks. These occur as intrusive breccias occupying volcanic vents and as dykes, sills, laccoliths, stocks and flow units. Dykes and stocks commonly contain subangular to subrounded fragments of Kazan arkose as well as xenoliths of granitic gneiss and white quartz whereas sills and laccoliths commonly contain rafts of Kazan or Christopher Island sediments (Blake et al., 1977). Bleached contact aureoles ranging from cream to mauve in colour and up to 1 m in width occur within rocks of the adjacent Kazan or Christopher Island formations.

The intrusive rocks are porphyritic biotite or olivine(?) biotite syenites. These have been extensively propylitized with chlorite or carbonate or both replacing olivine(?) and chlorite partially to completely replacing biotite. Biotite commonly occurs as euhedral phenocrysts, to 2 mm in length and as fine subhedral grains to 0.15 mm intergrown with the feldspar groundmass. The groundmass consists of varying proportions of biotite, feldspar, microphenocrysts of apatite and altered magnetite and very fine grained calcite and chlorite, with calcite and chlorite varying with the degree of propylitization. The presence of irregular hematite concentrations through the groundmass, along cleavage planes in biotite and pseudomorphs after magnetite microphenocrysts indicates extensive oxidation accompanying propylitization.

On Christopher Island, aphanitic pyrite-bearing diabase dykes, which trend northwest, transect all of the Dubawnt Group rocks. The Dubawnt Group and basement complex in the Christopher Island region have been intensely faulted along northwest and subparallel directions.

## Chemistry of the Christopher Island Intrusive Rocks

Mafic syenite stocks that intrude the Dubawnt sedimentary rocks (Appendix 2, analyses 1, 2) and the granulitic gneisses (Appendix 2A, analysis 3) are highly propylitized as shown by the varied  $\text{CO}_2$  contents. The alkaline character is shown by high total alkali and high  $\text{K}_2\text{O}/\text{Na}_2\text{O}$  (>1) ratios similar to Christopher Island volcanic rocks (Fig. 2). The incompatible trace elements Ba, Sr, Zr, and P are enriched in these stocks, typical for rocks of alkaline affinities (Carmichael et al., 1974). Uranium contents of these subvolcanic stocks (3.5-8.3 ppm) are similar to uranium abundances of Christopher Island volcanic and intrusive rocks in the Thirty Mile Lake area (Blake, 1980).

## Fracture-controlled Mineralization in the Christopher Island Region

Epigenetic uranium mineralization exhibits a close spatial relationship between trachytic dykes, stocks and sills and fracture systems. Mineralization comprising uranium, various selenides and noble metals is present in narrow zones of compound fracturing and brecciation in Kazan arkose and in tuffaceous arkose and biotite trachyte of the Christopher Island Formation. Fracture zones vary from a network of random hairline veinlets with sparse mineralization to branching vertical to subvertical veins containing massive black metal-bearing concentrations to 1 cm in width.

The mineralization at occurrence 1 is contained entirely within a fractured subvertical alkaline trachyte dyke, trending  $310^\circ$ , which crosscuts well layered granulitic gneiss. The dyke, 9-12 m in width and approximately 275 m long, terminates against northeast-trending linears at its southeastern and northwestern extremities. The barren segments of the dyke have a red to greyish red, aphanitic to

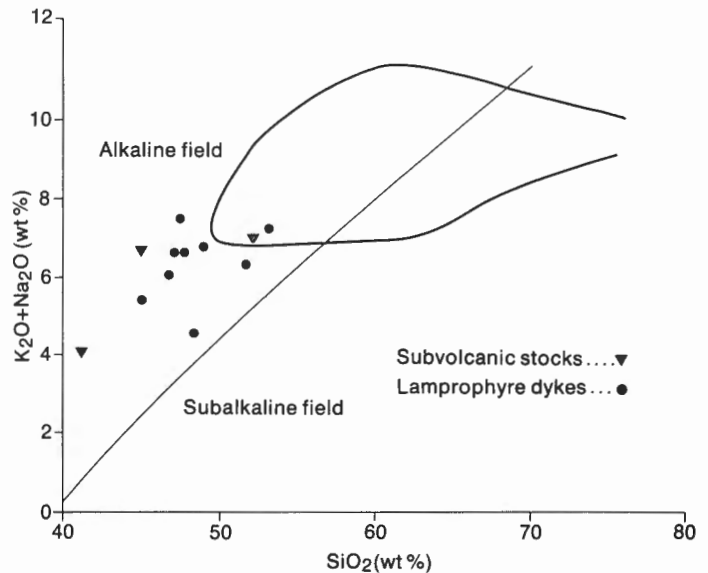
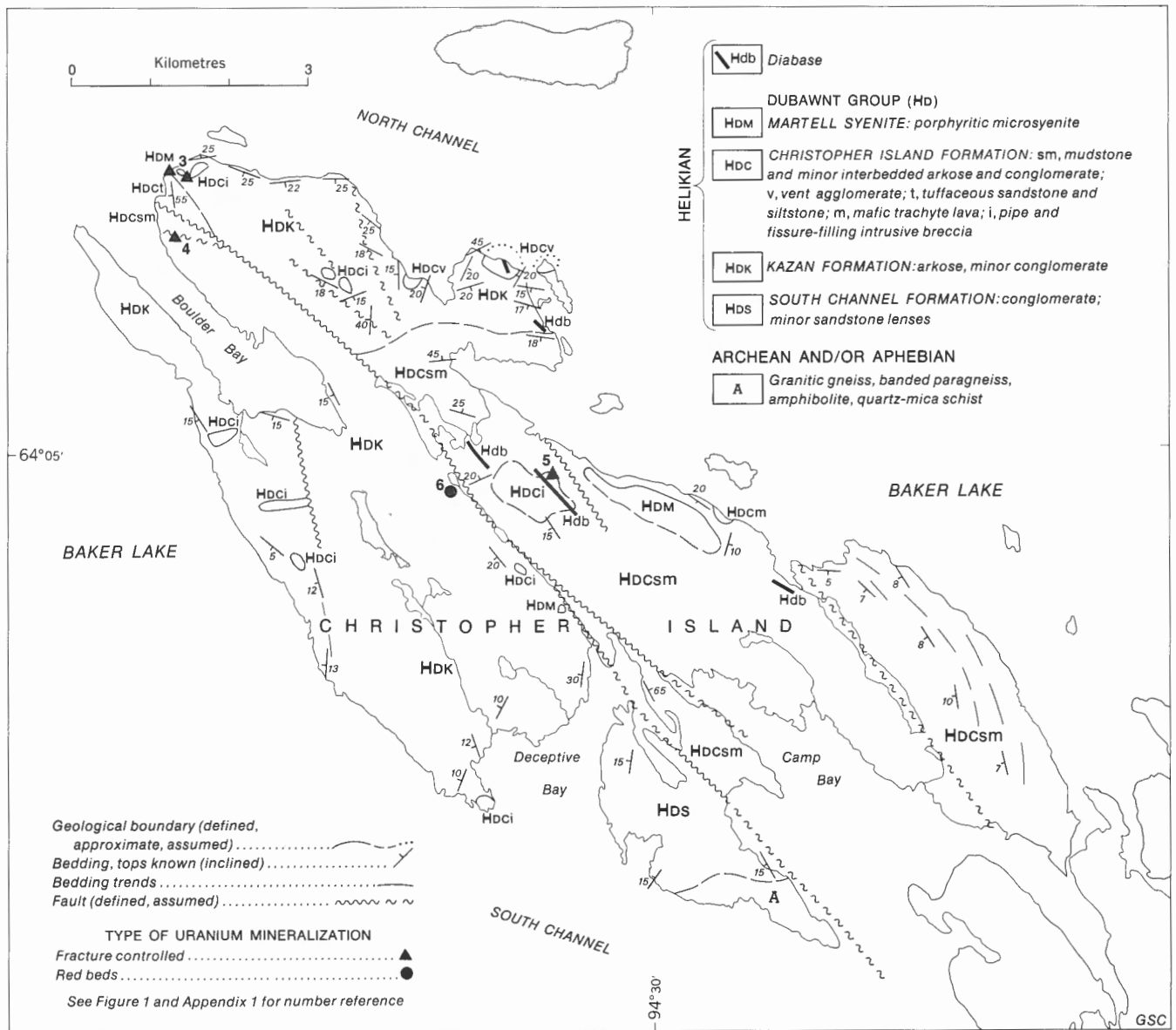


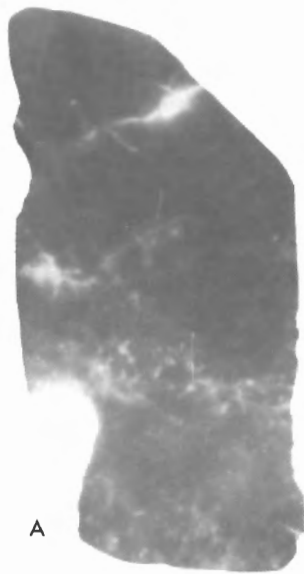
Figure 2.  $\text{Na}_2\text{O} + \text{K}_2\text{O}$  vs.  $\text{SiO}_2$  for lamprophyre dykes and subvolcanic stocks related to the Christopher Island Formation. Dashed polygon represents the range of Christopher Island volcanic rocks and Martell syenite (from Blake, 1980, Fig. 31). All analyses (Appendix 2A, B) recalculated to 100 per cent without  $\text{H}_2\text{O}$  and  $\text{CO}_2$ .



**Figure 3.** Geology of Christopher Island with the locations of the various types of uranium occurrences (from Blake, 1980, Fig. 18).

aphanitic porphyritic texture with 1-5 mm phenocrysts of biotite and potassic feldspar. Aphanitic finely banded chilled margins, 10-15 cm wide, are present along the entire length of the dyke. Xenoliths of subangular granulitic gneiss and subrounded granitic gneiss and white quartz are sparsely distributed through the entire length of the dyke. However in and adjacent to the zone of mineralization the dyke is choked with 5-15 cm rounded to subrounded granitic gneiss and white quartz xenoliths. Propylitic alteration is pervasive throughout the dyke. However in the intensely fractured and mineralized segment, it is completely altered to a fine grained mixture of calcite, chlorite and pyrite, with pyrite accounting for the prominent gossan. Pinkish white calcite and chlorite replace feldspar and biotite phenocrysts and fill fractures; the prominent fracture set trend is parallel to the dyke direction. Laporte (1974a) reported that the mineralized zone, 9 m wide and 45 m long, is pipe shaped and plunges at 25° to the north. Uranium and molybdenum concentrations have been reported in the fracture controlled pipe shaped mineralized zone.

On the northwestern peninsula of Christopher Island occurrences 3 and 4 were examined, each occurrence consisting of several areas of fracture-controlled uranium and base metal mineralization (Fig. 3). Three mineralized zones were examined in the area of occurrence 3, all of which are controlled by fractures that trend 045°, 065° and 320°, the last direction parallels the regional fracture zones that transect Christopher Island. Sparse mineralization is carried by hairline fractures within the peripheral zones of the propylitized porphyritic olivine(?)-biotite syenite stocks and the adjacent thermally metamorphosed mottled white to purple Kazan arkose. The fractured and mineralized trachyte is characterized by narrow irregular orange to pink reduced fracture walls and very fine grained green to limy green mixtures of secondary uranium minerals (Plate 2). The fracture assemblage includes pitchblende, hematite, calcite and chlorite.



A

Autoradiograph of fractured and mineralized olivine(?) biotite trachyte stock, occurrence 3. (GSC 203591-A)



B

Polished slab with mineralized fractures outlined by black lines. (GSC 203345-C)



C

Weathered surface of polished slab exhibiting altered and bleached fracture walls outlined by black lines. (GSC 203345-C)

### Plate 2

A major trachytic intrusion, on the northwestern peninsula, is in fault contact with crossbedded Kazan arkose and Christopher Island tuffaceous arkose. The intrusion is a fine grained biotite trachyte similar to the above described small plugs but contains sparsely distributed rounded 20-25 cm granitic gneiss xenoliths. The trachyte is intensely fractured and sheared about subvertical northwesterly trending fractures that parallel the faulted contacts. Pitchblende and copper selenides are associated with chlorite and chlorite-pink calcite filled fractures.

The third mineralized zone of occurrence 3, located 20-30 m east of the small circular trachytic plugs is present within a narrow 0.5-1.0 m wide north-trending subvertical fracture zone in tuffaceous Christopher Island arkose. Aphanitic and aphanitic porphyritic trachyte fragments range from 5 mm to 7 cm in size with lapilli sized fragments the most common. The fracture zone is a branching network of calcite, chlorite, minor quartz and black metaliferous concentrations. The metaliferous assemblage includes: pitchblende, copper, lead and copper-silver selenides and electrum.

Two mineralized zones were examined in the area of occurrence 4. The major zone of mineralization is contained in an intensively fractured trachytic unit which is faulted against Kazan arkose and Christopher Island tuffaceous sediments. Mineralization is controlled by subvertical north-east fractures that parallel the faults bounding the igneous unit. The trachytic unit is intensely propylitized and fractured and consists of pseudomorphs of mica and olivine(?) set in a very fine grained mat of relict feldspar, calcite, dolomite, hematite and chlorite. Mineralized veinlets contain pitchblende, copper and lead selenides, hematite with carbonates, chlorite and minor quartz. The structural control of the mineralization is strikingly similar to mineralization at occurrence 3.

The second zone of erratically distributed mineralization was traced for approximately 500 m in fractured maroon Kazan arkose and is associated with a quartz-calcite stockwork zone that parallels the prominent northwest linear that transects Christopher Island. The stockwork consists of a branching network of white and pink calcite, the latter Mn-rich, anhedral and euhedral white quartz, hematite, and chlorite, with disseminated chalcopyrite, minor chalcocite, pitchblende, uranophane, and marcasite.

The fracture controlled mineralization at occurrence 5 is hosted within a xenolithic porphyritic maroon trachyte stock. The stock is roughly circular in plan measuring approximately 60 m along a north-west-southeast direction and approximately 45 m along a northeast-southwest direction and intrudes sandy mudstone of the Christopher Island Formation. The stock exhibits a xenolithic marginal rim with subrounded arkosic fragments and non-xenolithic core. The entire stock displays an aphanitic porphyritic texture with 1-3 mm chloritized biotite phenocrysts across its entire width. The southwestern segment of the stock is intruded by a northwesterly trending fine grained sulphide-bearing diabase dyke.

Uranium mineralization is confined to 1-3 mm wide discontinuous fractures within the central core of the intrusion. The west-northwest-trending fractures contain pitchblende, copper selenides, hematite, calcite, and chlorite.

The branching vertical to subvertical fracture systems of occurrence 3, 4, and 5 represent the common mode of mineralization on Christopher Island. These fracture systems exhibit microscopic open space filling textures. These occurrences contain the following metallic minerals in varying proportions but always with similar textural and paragenetic relations: colloform and crystalline pitchblende,



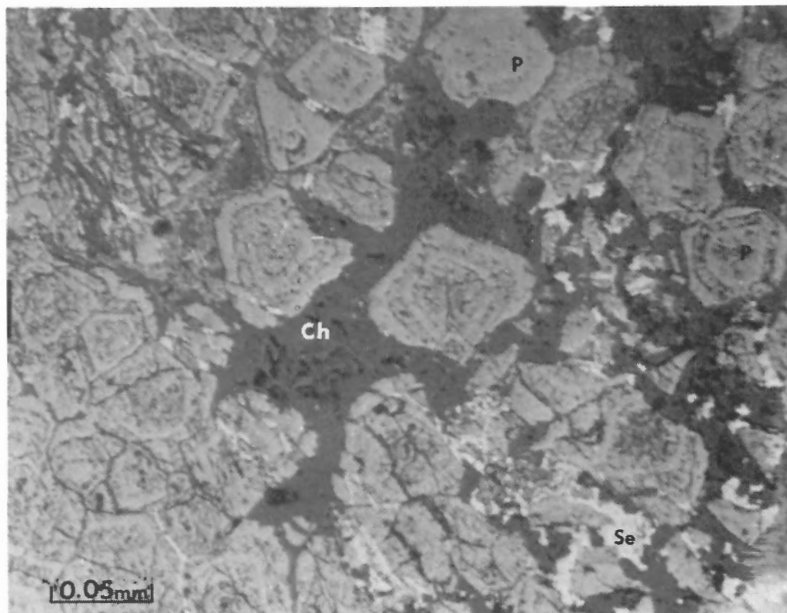


**Plate 3**

Photomicrograph of zoned urania (P) set in chlorite (Ch), urania is fractured and infilled by chlorite and copper selenides (Se). Zones with a high polish are high in lead compared to the zones with a pitted appearance which are low in lead, occurrence 5, reflected light. (GSC 203179-A)

the selenides umangite ( $\text{Cu}_3\text{Se}_2$ ), athabascaite ( $\text{Cu}_5\text{Se}_4$ ), berzelianite ( $\text{Cu}_2\text{Se}$ ), clausthalite ( $\text{PbSe}$ ), eucairite ( $\text{CuAgSe}$ ) and electrum of variable composition, Au-Ag and Ag-Au.

The fracture-controlled selenium-uranium mineralization is represented mineralogically and texturally by a composite series of fracturing and metal and gangue deposition. The initial phase of mineralization is represented by open space filling textures of colloform pitchblende. Colloform pitchblende commonly contains chlorite pseudomorphs after euhedral carbonate. These pseudomorphs suggest carbonate deposition along with pitchblende. The central portions of colloform pitchblende veinlets may contain euhedral occasionally zoned, crystals of pitchblende, termed urania (Plate 3). The principle zoning element of the urania is lead. Chlorite and hematite are intergrown with colloform pitchblende and acts as matrix to urania grains.

The second phase of deposition following fracturing and brecciation of the uraniferous assemblage consists of various selenide minerals intergrown with subhedral to euhedral hematite, very fine grained chlorite, calcite, and cerussite. The most abundant selenides, athabascaite and berzelianite, occur as very fine grained intergrowths associated with subhedral to euhedral bladed hematite (Plate 4A). Umangite occurs as fine anhedral intergrowths with athabascaite-berzelianite or is mantled by the latter (Plate 4B). Grey fluid inclusions (0.001-0.005 mm) are randomly distributed through umangite. Clausthalite occurs as very fine (<0.05 mm) anhedral grains in or adjacent to umangite. Eucairite with or without intergrowths of athabascaite-berzelianite is present as veinlets within pitchblende (Plate 5) or infills brecciated subhedral pitchblende and syneresis cracks in colloform pitchblende (Plate 6). Wispy fine grained selenides and hematite were impregnated into the wall rocks during the second phase of mineralization.

The third stage involves refracturing of the previous assemblages followed by deposition of ragged stringers of gold and silver-rich electrum associated with hematite,

fine grained (0.2-0.4 mm) quartz, and Mn-rich calcite (Plate 7). Secondary minerals coating fracture walls and fracture filling assemblages include boltwoodite, kasolite, wölsendorfite, and malachite.

### Age of Mineralization

The noble metal-selenium-uranium mineralization occurs within fractured Kazan arkose, Christopher Island arkose and trachytic intrusions which intrude the upper mudstone unit on Christopher Island. The mineralization is related to northwest-southeast fracture zones which displace all the Dubawnt lithologies in the Christopher Island region. Thus this mineralization is considered to be post Christopher Island Formation.

A U-Pb isotopic analysis on pitchblende from the fracture controlled selenium-uranium mineralization at occurrence 4 resulted in the ratios:  $\text{Pb}^{206}/\text{U}^{238} = 0.1699$ ,  $\text{Pb}^{207}/\text{U}^{235} = 2.211$  and  $\text{Pb}^{207}/\text{Pb}^{206} = 0.0945$  (Little, unpublished G.S.C. data). Calculated ages are highly discordant and the analysis lies below the concordia plot suggesting a loss of lead relative to uranium. The age is 1516 Ma ( $\text{U}^{238} = 1.55125 \times 10^{-10}/\text{y}$  and  $\text{U}^{235} = 9.8485 \times 10^{-11}/\text{y}$ ). A Rb/Sr isochron on mudstones from Christopher Island suggests a depositional age of  $1750 \pm 50$  Ma and a resetting of the Rb/Sr isochron at  $1510 \pm 60$  Ma (Bell, personal communication, 1978). The resetting of the

Rb/Sr isochron in the Christopher Island mudstones may be associated with the remobilized age displayed by the pitchblende analysis.

### Chemistry of the Uranium Minerals, Selenides, and Noble Metals

Two electron microprobe analyses of the central portions of colloform pitchblende associated with selenides and noble metals from occurrence 3 indicate that the pitchblende is non-thorium-bearing and contains high lead values (17.0 and 17.1 wt %, Table 1). The ratio of uranium to lead is 3.78. The consistent calcium content of 1.4 wt % in optically homogenous pitchblende suggests that calcium is substituting for uranium in the pitchblende structure. Minor iron and silicon were detected in the botryoidal pitchblende. The low oxide totals of the analyses, uranium taken as  $\text{UO}_2$ , suggest the pitchblende may be hydrous or carbonate-bearing. The presence of euhedral pseudomorphs of chlorite after carbonate within colloform pitchblende suggests coprecipitation of carbonate and pitchblende and may indicate that uranium was in solution as uranium carbonate complexes.

Electron microprobe analyses of the selenides athabascaite, berzelianite, and umangite show that these phases are essentially Cu-Se minerals with minor substitution of Fe and S, respectively (Table 2). Broad beam electron microprobe analyses of fluid inclusions and host umangite indicate that the inclusions contribute minor concentrations of Pb (3.2-7.0 wt %), Cl (0.3-0.5 wt %), and possibly Fe (0.4-2.1 wt %) to the totals (Table 2). Low totals for umangite analyses are unexplained but it is possible that the inclusions may contain  $\text{H}_2\text{O}$  or  $\text{CO}_2$ . Gold-silver electrum (Table 3) and silver-gold electrum are associated with selenide-pitchblende mineralization. The low sulphur contents of the selenides, lack of sulphide minerals associated with the selenide period of mineralization, and the lack of silver sulphides indicate a very low partial pressure of sulphur during selenide-noble metal deposition.

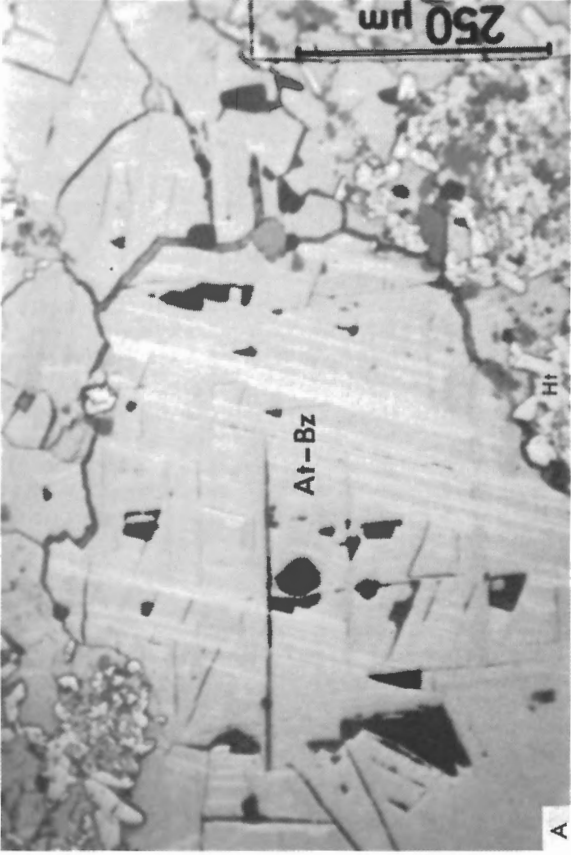
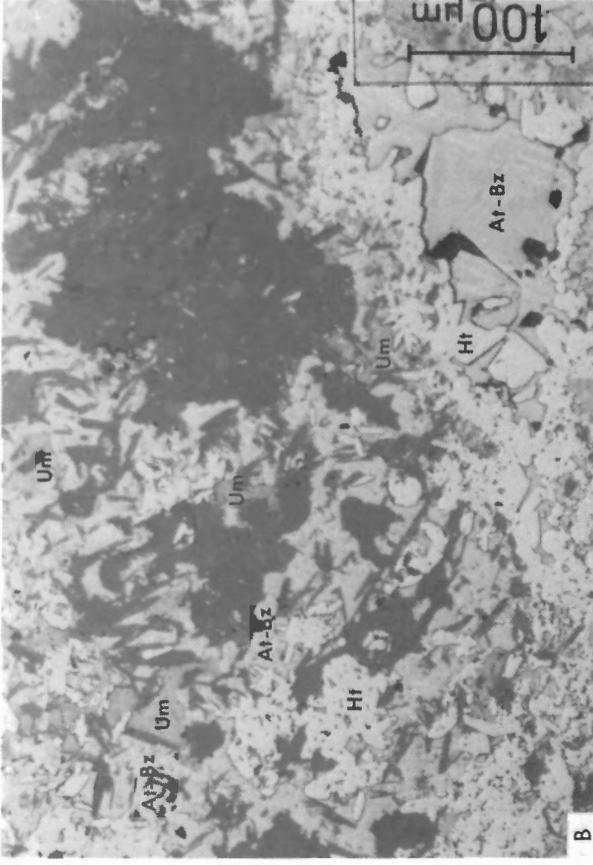


**Plate 4**

**4A.** Photomicrograph of intergrowths of athabascaite and berzelianite, collectively marked At-Bz with hematite (Ht), occurrence 4, reflected light. (GSC 203591-B)



**4B.** Photomicrograph of umangite (Um) intergrown with twinned intergrowths of athabascaite-berzelianite (At-Bz) and blades of hematite (Ht). This assemblage is impregnated into the propylitized trachyte host, black areas, adjacent to pitchblende-selenide veinlets, occurrence 4, reflected light. (GSC 203591-C)

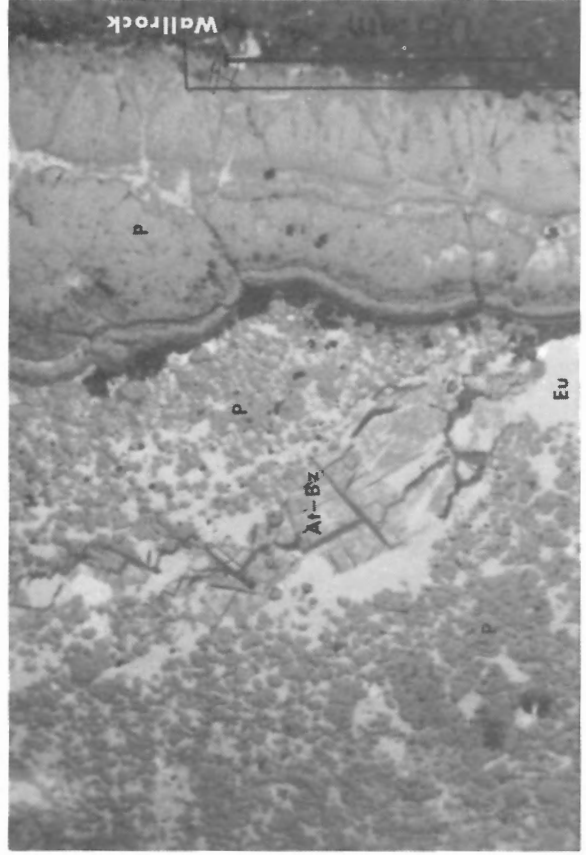


**Plate 5**

Photomicrograph of pitchblende (P) infilled by athabascaite-berzelianite (At-Bz) and eucairite (Eu), occurrence 4, reflected light. (GSC 203591-D)

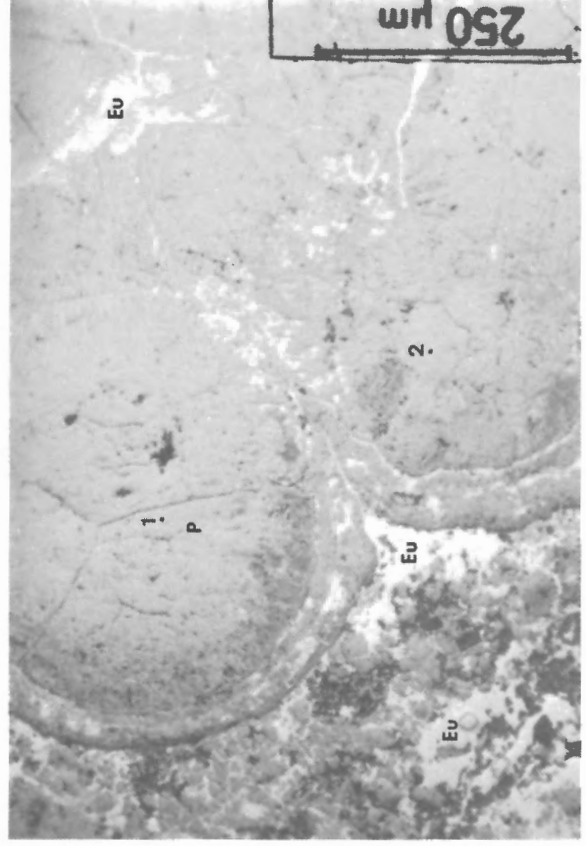


**Plate 6**

Photomicrograph of eucairite (Eu) infilling syneresis cracks in pitchblende (P), occurrence 3, reflected light. Pitchblende analyses 1,2 (Table 1). (GSC 203591-E)

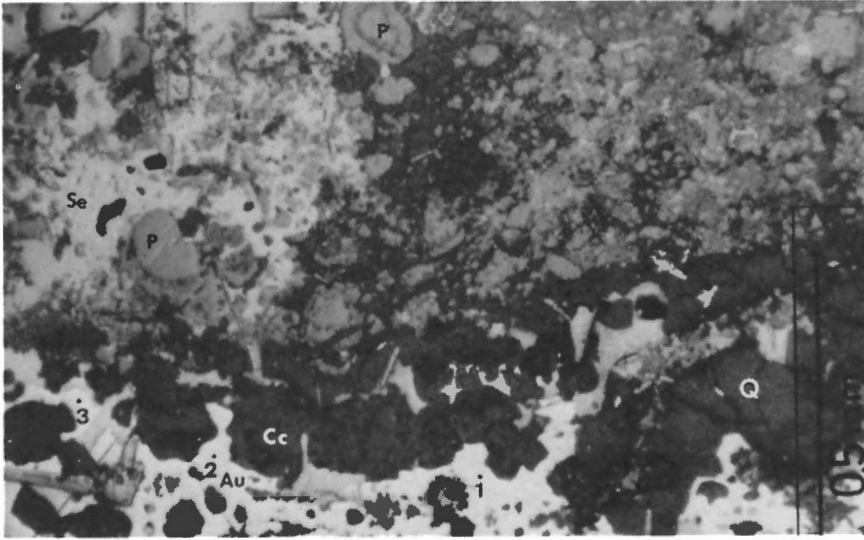


Plate 7

Photomicrograph of native gold (Au) with quartz (Q) and Mn-calcite (Cc) associated with selenide (Se)-pitchblende (P) mineralization, occurrence 3, reflected light. Electron analyses 1,2,3 (Table 3). (GSC 203591-F)

### Origin of the U-Cu-Ag-Au-Se Mineralization, Christopher Island

Vein-type pitchblende mineralization can be accompanied by a varied and complex mineral assemblage of sulphides, selenides, arsenides, antimonides, and native minerals. Various uranium districts such as Beaverlodge area, Canada (Robinson, 1955) and numerous areas in Czechoslovakia (Ruzicka, 1971; Kvacsek, 1973) exhibit mineral textures that indicate the selenide period of mineralization is paragenetically later than initial pitchblende deposition but closely related in time. The U-Cu-Ag-Au-Se mineralization is the product of a composite sequence of fracturing and metal deposition. The three distinct stages of vein mineralization on Christopher Island are similar to stages recognized in the uraniumiferous districts mentioned above.

Bernardini and Catani (1968) showed that umangite ( $\text{Cu}_3\text{Se}_2$ ) breaks down to berzelianite ( $\text{Cu}_{2-x}\text{Se}$ ) and klockmannite ( $\text{CuSe}$ ) at  $150^\circ\text{C}$ . Harris et al. (1970a, b) unsuccessfully attempted to synthesize athabascaite ( $\text{Cu}_5\text{Se}_4$ ) at  $100^\circ\text{C}$  in the "dry" system with 3 per cent S. Umangite was synthesized at  $120^\circ\text{C}$ . The low temperature synthesis and breakdown of various selenide phases and the intergrowths of umangite and athabascaite suggest a low temperature for the selenide depositional period. The low sulphur content of the selenide-noble metal mineralization and inferred low temperature of deposition implies a  $f_{\text{S}_2} < 10^{-7}$  assuming a temperature of  $150^\circ\text{C}$  (Barton and Toulmin, 1964).

Studies in active geothermal areas, such as the Red Sea geothermal system (Shanks and Bischoff, 1977), Broadlands geothermal fields (Ewers and Keays, 1977), and the Salton Sea geothermal system (Skinner et al., 1967), indicated a relative enrichment of Na, Ca, K and Cl and various heavy metals in the hydrothermal fluids compared to seawater. Experimental data on the complexing of various base and noble metals (Seward, 1973, 1976; Henley, 1973) with chlorine and sulphur indicated that these complexes play an important role in the transport and deposition of hydrothermal ore solutions. The chlorine-rich fluid inclusions within umangite along with the presumed presence of  $\text{H}_2\text{O}$  or  $\text{CO}_2$  suggests a chlorine-rich brine as the transporting media for the base metal and noble metal mineralization.

### Geology of the Diatreme Breccia Mineralization

The lithologies and structures associated with this type of mineralization occur within the basement granulitic gneisses to the north of Christopher Island (NTS area 56D/2). The granulitic gneisses are host to xenolithic dykes and stocks belonging to the Christopher Island igneous suite.

The generalized geology of the diatreme breccia in NTS area 56D/2 is shown in Figure 4. The igneous complex consisting of a central vertical sided ovoid stock, approximately 55 m north-south and 45 m east-west with peripheral radial and tangential dykes is interpreted as a subvolcanic neck and related dyke swarm. The central stock and dykes are xenolithic, porphyritic biotite syenite.

The stock and dykes are porphyritic to glomeroporphyritic with phenocrysts of biotite and minor sericitized and chloritized plagioclase. The groundmass is a very fine grained (0.20 mm) mat of biotite and feldspar, predominantly potassic feldspar, and minor apatite microphenocrysts. The groundmass is oxidized, chloritized and intensely carbonatized as shown by the high carbonate content (8.0 wt %  $\text{CO}_2$ , Appendix 2B, analysis 3). In spite of the pervasive alteration of the groundmass, the stock still maintains the alkaline characteristics of the Christopher Island igneous suite. Xenoliths within the central stock and peripheral dykes consist of 1 to 25 cm rounded white vein quartz, granitic to granodioritic gneiss as well as minor angular granulitic gneiss.

Brecciated granulitic gneiss surrounds the central stock and peripheral dykes. The degree of packing of the brecciated country rock varies away from the central stock. The brecciated granulitic gneiss has been subdivided on the basis of texture into a closely packed breccia adjacent to intrusive stock and a loosely packed breccia peripheral to the intrusive stock (Fig. 4; Plates 8A, B).

The closely packed breccia zone rimming the central vertical stock consists of angular fragments of granulite (5 mm to 40 cm in size) with minor rounded exotic clasts of vein quartz and granitic gneiss. The breccia is cemented by carbonate, rock flour, and minor aphanitic trachyte. The loosely packed breccia consists of an open framework of granulitic gneiss fragments cemented by a series of minerals displaying successive open space filling textures.

An irregular mineralized pod, approximately 10 m in diameter, occurs within the loosely packed breccia unit. The metallic assemblage includes colloform pitchblende,

Table 1

Electron microprobe analyses of uranium phases associated with fracture-controlled mineralization

Analysis Occurrence	1	2	3	4	5	6	7	8
Texture Wt%	Colloform Pitchblende	Colloform pitchblende	Botryoidal pitchblende	Colloform pitchblende	Disseminated Ti-U phase	Colloform pitchblende		
U	64.3	64.7	60.6	60.2	68.6	37.6	36.4	70.8
Pb	17.0	17.1	17.9	18.4	7.0	1.0	2.5	7.0
Th	0.00	N.A.	0.00	0.00	Tr	0.00	N.A.	0.00
Ca	1.4	1.4	1.6	1.3	3.3	0.4	0.4	2.4
Ti	N.D.	N.D.	0.5	0.5	0.5	21.0	16.9	0.02
Fe	0.02	0.04	0.2	0.2	1.1	0.7	0.6	0.5
Si	0.1	0.1	0.2	0.3	0.6	3.0	3.4	0.3
Al	N.D.	N.D.	0.1	0.1	N.D.	0.3	0.4	0.03
Zr	N.D.	N.D.	0.6	1.0	1.0	0.6	0.7	0.6
Mn	N.D.	N.D.	N.D.	N.D.	N.D.	N.D.	N.D.	0.4
S	0.00	N.A.	0.00	0.00	Tr	0.00	0.1	0.00
Total	82.82	83.34	81.70	82.00	82.10	64.60	61.40	82.05

N.D. = Not detected during energy dispersive spectra investigation  
N.A. = Not analyzed  
Tr = Trace on crystal spectrometer  
Analyst: A.G. Plant

Table 2  
Electron microprobe analyses of selenide minerals, occurrence 4

	Elements Wt. %						Total	Formula (Se, S) = 4.00
	Cu	Se	S	Fe	Pb	Cl		
Athabascaite	51.8	43.4	3.6	1.5	-	-	100.3	Cu <sub>4.92</sub> Fe <sub>0.16</sub> Se <sub>3.32</sub> S <sub>.68</sub>
Athabascaite	52.3	43.5	3.3	0.2	-	-	99.3	Cu <sub>5.03</sub> Fe <sub>0.02</sub> Se <sub>3.37</sub> S <sub>.63</sub>
Athabascaite	52.1	43.1	3.3	0.4	-	-	98.9	Cu <sub>5.05</sub> Fe <sub>0.04</sub> Se <sub>3.37</sub> S <sub>.63</sub>
Athabascaite	52.9	43.1	3.6	0.1	-	-	99.7	Cu <sub>5.06</sub> Fe <sub>0.01</sub> Se <sub>3.32</sub> S <sub>.68</sub>
Athabascaite + Berzelianite	55.0	42.5	3.1	0.4	-	-	101.0	Cu <sub>5.46</sub> Fe <sub>0.04</sub> Se <sub>3.39</sub> S <sub>.61</sub>
Athabascaite + Berzelianite	56.1	41.7	3.0	0.2	-	-	101.0	Cu <sub>5.68</sub> Fe <sub>0.02</sub> Se <sub>3.40</sub> S <sub>.60</sub>
Athabascaite + Berzelianite	57.2	40.0	3.4	0.1	-	-	100.7	Cu <sub>5.87</sub> Fe <sub>0.01</sub> Se <sub>3.31</sub> S <sub>.69</sub>
Berzelianite + Athabascaite	56.9	39.7	3.0	0.2	-	-	99.8	Cu <sub>6.00</sub> Fe <sub>0.03</sub> Se <sub>3.37</sub> S <sub>.63</sub>
Berzelianite + Athabascaite	58.2	38.3	3.0	0.2	-	-	99.7	Cu <sub>6.33</sub> Fe <sub>0.03</sub> Se <sub>3.35</sub> S <sub>.65</sub>
Berzelianite	60.0	37.2	2.9	0.3	-	-	100.4	Cu <sub>6.73</sub> Fe <sub>0.04</sub> Se <sub>3.36</sub> S <sub>.64</sub>
Umagite	49.1	43.8	0.0	0.4	3.2	0.3	96.8	Cu <sub>5.57</sub> Fe <sub>0.05</sub> Se <sub>4.00</sub> S <sub>.00</sub>
Umagite	46.7	40.7	0.0	2.1	7.0	0.5	97.0	Cu <sub>5.71</sub> Fe <sub>0.30</sub> Se <sub>4.00</sub> S <sub>.00</sub>
Umagite	47.7	40.0	0.0	1.6	4.3	0.3	93.9	Cu <sub>5.93</sub> Fe <sub>0.23</sub> Se <sub>4.00</sub> S <sub>.00</sub>

Data from Pringle and Miller, 1977.

chalcopyrite, rare resinous sphalerite and traces of pyrite. The granulitic breccia fragments within the zone of mineralization are retrograded with the partial to complete development of chlorite after all mafic minerals. Pyrite and chalcopyrite within the fragments have been remobilized into fine bands paralleling and crosscutting the relict gneissosity. Paragenetically the initial open space filling assemblage involved the deposition of pitchblende on hematitized breccia fragments or intergrown with drusy white and smoky quartz, minor hematite, pyrite and chlorite. An analysis of colloform pitchblende contains greater uranium and calcium and less lead (Table 1, analysis 8) than the colloform pitchblendes from occurrence 3 (Table 1, analyses 1, 2). Drusy quartz crusts and pitchblende are succeeded by fine- to medium-grained pink calcite, white dolomite, fine chlorite rosettes and white barite. Subhedral chalcopyrite tetrahedrons and minor sphalerite dodecahedrons are associated with the carbonate-sulphate cement. Pitchblende moulds in calcite-dolomite aggregates and calcite, dolomite, and hematite encrusting drusy quartz indicate that the uranium mineralization was associated with an early oxidizing quartz-hematite assemblage. Secondary uranium minerals coating colloform pitchblende include yellow and orange crusts of uranophane, kasolite, and wölsendorfite.

The brecciation of the granulitic gneiss surrounding the circular alkaline trachyte stock and dyke complex prepared the ground for the passage of mineralizing fluids. Restriction of uranium-copper-zinc mineralization to the outer margins of the brecciated gneiss envelope illustrates the importance of a permeable horizon or conduit for access and transmission of the ore-bearing solutions. This occurrence can be interpreted as an epigenetic uranium-base metal concentration resulting from the channelling of an aqueous system through a zone of high permeability or alternatively the mineralization may have accompanied or closely followed volatile degassing during formation of the alkalic subvolcanic pipe (Tilsley, 1978). Preliminary energy dispersive studies on interstitial calcite, dolomite and barite cements indicate no Sr and traces of Mn and Fe within carbonates and traces of Sr within barite. Sr-rich calcite in the matrix of coarse agglomerates and lapilli tuffs from an eruptive centre (NTS 65 P/11) was interpreted to be of a primary magmatic origin associated with an explosive carbonate-bearing alkaline magma (LeCheminant et al., 1979). The lack of Sr-rich carbonates associated within the interpreted volcanic structure at occurrence 2 suggests that mineralization resulted from groundwater migration along the basal Dubawnt unconformity with subsequent channelling through a zone of high permeability.

A similar quartz-carbonate breccia structure in granulitic gneiss (Plate 8C) with associated trachytic dykes was investigated in NTS area 56D/1, approximately 4.5 km northeast of the mineralized diatreme breccia. The breccia displays various degrees of packing and interstitial cements but no mineralization was

Table 3

Electron microprobe analyses of electrum associated with selenide-pitchblende mineralization, occurrence 3

	Grain 1	Grain 2	Grain 3
Au	91.5	91.5	91.9
Ag	9.1	9.0	9.0
Total	100.6	100.5	100.9

recognized. Reinhardt and Chandler (1973) described a similar breccia pipe in NTS area 55M/16 near the Dubawnt unconformity. No mineralization was reported nor was this structure examined by the author.

### Geology and Fracture-Controlled Mineralization in the Bissett-Thirty Mile Lake Region

#### General Geology

The basement complex immediately south of the Dubawnt Group rocks in the Bissett-Thirty Mile Lake region consists of gneissic quartz monzonite and granodiorite, cataclastic migmatites and augen gneisses. Uranothorite-bearing pegmatites and allanite-bearing gneisses are present within the basement complex.

The southern margin of the eastern Baker Lake basin extending from the Christopher Island area southwest to the Thirty Mile Lake area is locally controlled by northwest, east-northeast, to east-trending faults and the trace of the basal unconformity (Fig. 1). The structures containing the uranium mineralization in the Bissett-Thirty Mile Lake area are parallel to the northwest fault systems that control the uranium-selenium-noble metal mineralization on Christopher Island.

Numerous fracture-controlled uranium occurrences are present near the trace of the basal unconformity from Kazan Falls to the western end of the Thirty Mile Lake. All of these occurrences are present within approximately 13 km of the unconformity (Fig. 1).

In the Kazan Falls area intense fracturing, faulting and accompanying alteration have been superimposed upon the basement gneisses and Christopher Island volcanic flows and volcanoclastic sediments. The basement rocks consist of a sequence of interlayered potassic feldspar augen gneisses, granoblastic granitic and granodioritic gneisses and migmatites. Garnet-hornblende and hornblende amphibolites are interlayered with the gneisses. Regional gneissosity is east-west with vertical to subvertical attitudes. Mineral lineations and small parasitic folds within the gneisses and folded amphibolitic bands suggest an isoclinal structure plunging west.

The amphibolite grade gneissic rocks have been retrograded to the greenschist facies with the development of chlorite after biotite and hornblende, sericite within sodic plagioclase, and the development of epidote as veinlets and as intergrowths with chlorite, biotite, and hornblende. The felsic character and locally well developed layering of leucocratic and mesocratic bands may indicate a sedimentary parentage for some of the basement complex. Several molybdenite-pyrite gossans are present within amphibolites interlayered with the leucocratic gneisses.

In the Kazan Falls area, Dubawnt rocks north of the unconformity dip south and are presumed faulted against the gneiss complex. The succession exposed in the immediate

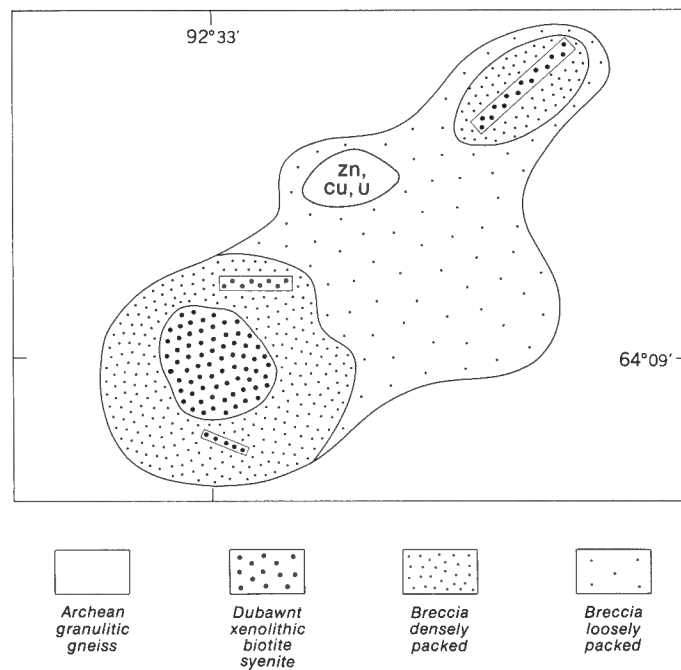


Figure 4. Generalized geology of the diatreme breccia occurrence (55 D/2).

area north of the fault is maroon Kazan sandstone overlain by several fining upward sequences of volcanoclastic sediments capped by porphyritic feldspar-biotite trachytic flows.

#### Fracture-Controlled Mineralization Within the Basement

The leucocratic basement gneisses in the Kazan Falls area are cut by a series of en echelon fracture and fault zones. The dimensions of this dislocation zone are estimated to be at least 2.5 km long and at least 2 km wide. Mineralization is controlled by fractures and faults that trend 335 to 360° and exhibit either right or left lateral displacements. Individual mineralized zones, up to 0.5 m in width, vary from mylonitic zones to zones of fractured and brecciated gneiss. All zones display varying degrees of hematitization, chloritization, silicification, and carbonatization.

Uranium occurrences 13 and 14, immediately southeast of Kazan Falls, exhibit similar alteration assemblages, metallic minerals, textures, paragenetic sequences and structural relationships to the hosting gneisses. The mineralization at occurrence 13 is contained in a series of three subparallel fault and fracture zones approximately 90 m apart that trend 335 to 360° (Fig. 5). Although each zone displays the same alteration assemblage, each exhibits varying degrees and amounts of fracturing, brecciation and cataclasis. The western zone consists of a fractured and brecciated gneiss in which relict equigranular quartz-feldspar fragments occur in a crushed matrix of quartz and feldspar. The gneiss has been pervasively impregnated with hematite along grain boundaries and through quartz and feldspar grains. Plagioclase and potassic feldspar are overgrown by fine sericite and chlorite mats. Fracture filling assemblages include white calcite, pink Mn-rich calcite, chlorite (clinoclone) and hematite coating fracture walls and disseminated through chlorite and calcite. Pitchblende is confined to the crushed matrix between brecciated gneiss fragments (Plate 9).

Plate 8

- A. Densely packed angular granulitic gneiss breccia adjacent to xenolithic biotite trachyte core, occurrence 2. (GSC 203261-A)

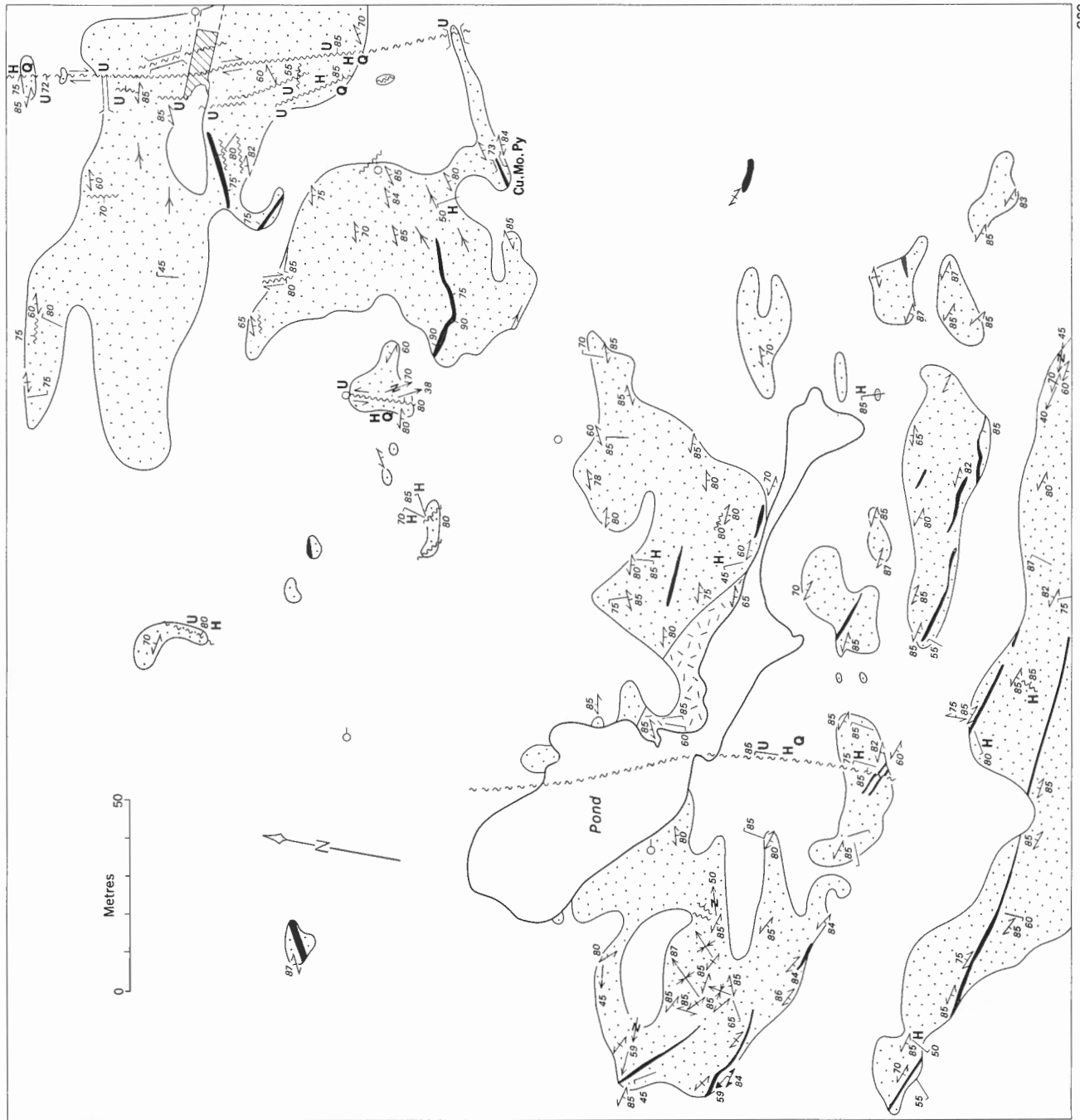





- B. Loosely packed angular granulitic gneiss breccia with hematite-quartz-carbonate-chlorite-sulphate filling assemblage, occurrence 2. (GSC 203261-C)



- C. Breccia structure (56 D/1; 7117400 N, 427950 E) similar to breccia at occurrence 2. (GSC 203591-G)





-  Hornblende feldspar augen granodiorite gneiss
-  Amphibolite and hornblende rich granodiorite gneiss
-  Amphibolite or garnet amphibolite

- Limit of outcrop .....
- Foliation layering in gneiss (inclined, vertical) .....
- Foliation in amphibolite .....
- Lineation in amphibolite .....
- Trend, plunge of minor fold sense of motion (with, without) .....
- Trend of quartz rods or augens .....
- Fault (defined, assumed, arrows indicate relative movement) .....
- Joint with alteration (hematite H, quartz Q) .....
- Synform with plunge .....
- Mineralization; uranium, copper molybdenum, pyrite .....
- Trench .....
- Drill hole (inclined, vertical) .....

**Figure 5**  
 Geology of the fracture-controlled mineralization, Kazan Falls area (55 M/12).



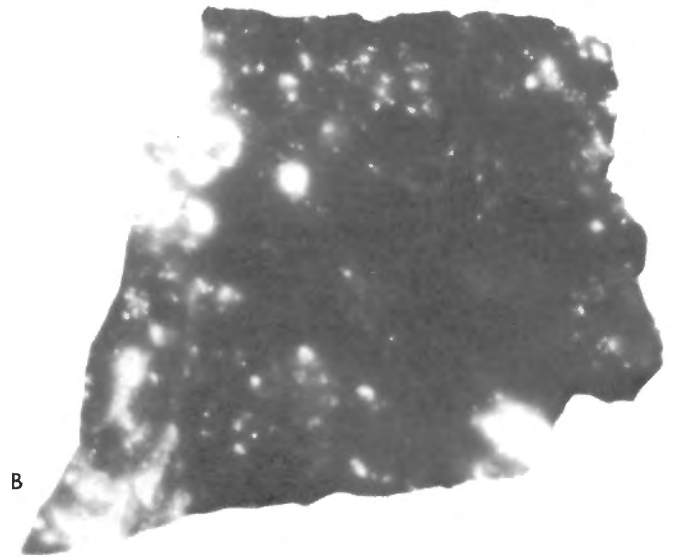
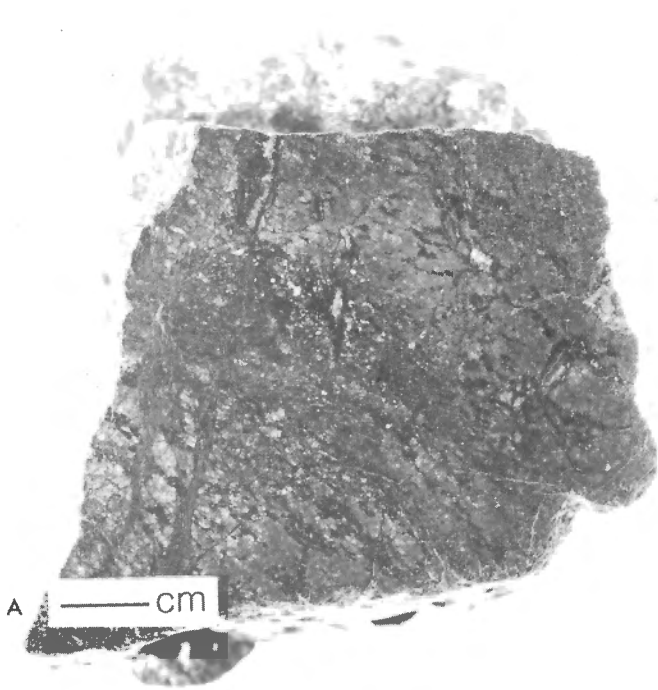


**Plate 9**

**A.** Intensely altered and brecciated granitoid gneiss, western zone, occurrence 13. (GSC 203345-K)

**B.** Autoradiograph of Figure 9A showing distribution of uranium mineralization. (GSC 203591-H)

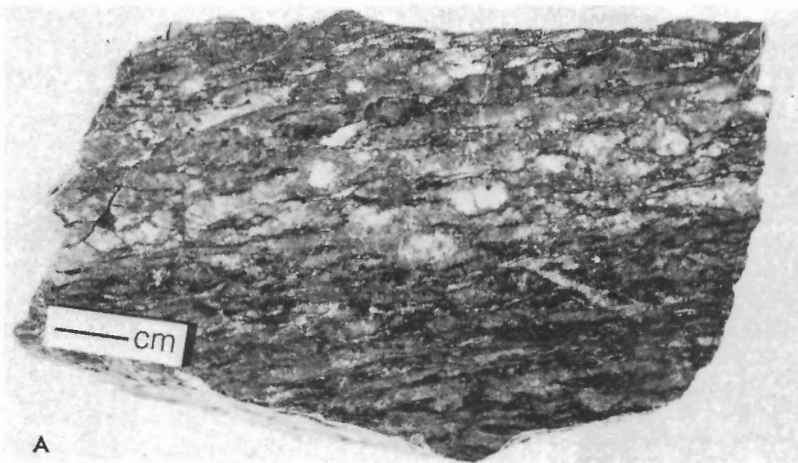


**Plate 10**

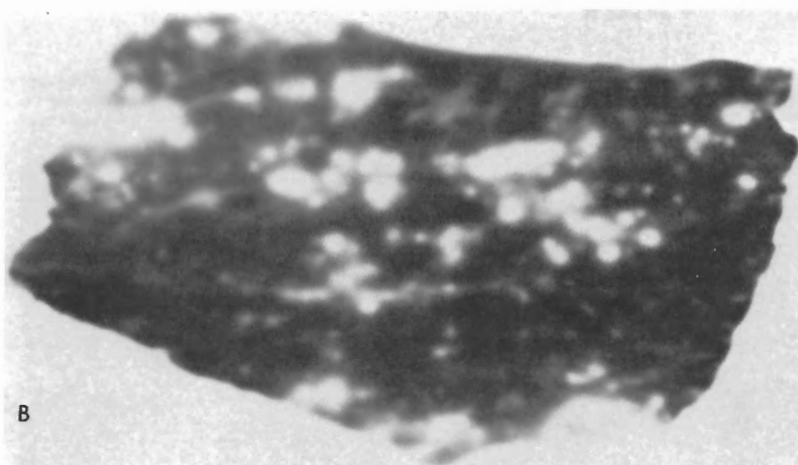
North-trending hematitized and mineralized fault, central zone occurrence 13. Note the drag of the interlayered leucocratic gneiss and amphibolite into the fault plane. (GSC 203261-B)

The central mineralized area is a narrow mylonite zone characterized by intense hematite alteration. The mylonite zone transects interlayered leucocratic potassic feldspar augen gneiss, leucocratic granodioritic gneiss and amphibolite. The units immediately adjacent to the mylonite zone exhibit drag structures indicating left lateral motion (Plate 10). The zone of cataclasis, hematitization, silicification and carbonatization is 30-36 cm wide and consists of mylonitic gneiss, containing angular fragments of leucocratic gneiss, epidotized gneiss and amphibolite all of which are criss-crossed by veinlets and lensoid fractures filled with drusy quartz, calcite and chlorite. Finely banded portions of the mylonitic zone exhibit numerous small scale structures such as boudins of competent gneissic fragments and parasitic folds and faults. Relatively late lensoid fractures can contain sugary and euhedral white to clear drusy quartz, chlorite, disseminated and colloform hematite, and intergrowths of calcite, prehnite and pumpellyite. Uranium and sulphide mineralization is associated with composite fracture filling assemblages and is concentrated along a narrow-band, about 6 cm wide on the western side of the mylonite zone.

The mineralized eastern zone, approximately 15 to 20 m wide, consists of a hematitized northerly trending fault zone flanked by subparallel zones the latter characterized by very closely spaced fractures that transect biotite-potassic feldspar augen granitic gneiss and interlayered amphibolite (Plate 11). On an outcrop scale the intensely fractured and mineralized gneiss displays a fine ribbed structure with chlorite and hematite coating fracture planes. Microscopically this crosscutting structure comprises very fine granoblastic feldspar and quartz crush bands and finely hematitized hairline fractures. Hematite and chlorite alterations predominate in the fractured gneiss with minor quartz and calcite veining.



A. Finely fractured and mineralized potassic feldspar augen gneiss, eastern zone, occurrence 13. (GSC 203345-L)



B. Autoradiograph of Figure 11A showing distribution of uranium mineralization. (GSC 203591-I)

### Plate 11

Occurrence 14 (about 2 km south-southeast of occurrence 13) exhibits similar structural and mineralogical characteristics to occurrence 13. A principal vertical to subvertical fault zone up to 0.6 m wide with subparallel minor faults trending north-northwest to north and displaying right lateral movements transects isoclinally folded potassic feldspar augen granodiorite gneiss and interlayered amphibolites. The main fault zone has an outcrop expression of approximately 150 m and has sporadic mineralization confined to the southern 45 m of the fault zone. This zone is characterized by hematite altered wall rocks and a drusy fault filling assemblage of calcite, chlorite and quartz. The northern segment of the fault is unmineralized and consists of a branching network of predominantly quartz filled fractures with minor hematite alteration of the wall rocks.

The fracture-fault filling assemblages and associated metallic phases in both occurrences exhibit a similar paragenetic sequence. The initial stage of mineralization involved fracturing and mylonitization with the accompanying assemblage of pitchblende, hematite, quartz and chlorite (clinocllore). Several morphological and

textural varieties of pitchblende are present and the textural relationships with sulphide minerals suggest at least two generations of pitchblende.

Pitchblende associated with pink Mn-rich calcite-chlorite-quartz veinlets is present as individual or coalescing colloform grains or as rare crystals. The fine spherical grains are disseminated through quartz rich veinlets with calcite and spherical chlorite rosettes (Plate 12). Crystalline pitchblende, 0.10 to 1.50 mm in size, are subhedral in form and are brecciated and recemented by quartz (Plate 13).

Gneisses that have been microfractured but not pervasively invaded by calcite-chlorite-quartz veinlets contain extremely fine delicate colloform and botryoidal pitchblende associated with hematite (Plate 14A, B). Hematitized quartz and feldspar adjacent to these pitchblende concentrations commonly exhibit fine radial fracture patterns resulting from radioactive bombardment.

Pitchblende is present as irregular grains and wispy sooty mats associated with chlorite-rich veinlets. These mats commonly enclose very finely disseminated iron-copper and iron sulphides. This textural relationship may represent a remobilized pitchblende.

The initial sulphide, pyrite, is present as discrete subhedral to euhedral cubes and stringers which are in turn fractured and replaced by chalcopyrite and bornite (Plate 15). The latter sulphides are predominantly associated with chlorite-calcite filled veinlets but are also present as disseminated grains through the hematite-chlorite-quartz-carbonate filled fractures. Exsolution textures of bornite in chalcopyrite or *visa versa* indicate re-equilibration of sulphide solid solutions (Craig, 1974b). Chalcopyrite commonly envelops and fills syneresis cracks in fine colloform buckshot pitchblende (Plate 16).

Galena has two textural variations, the most common being anhedral discrete grains or aggregates with chalcopyrite-bornite. The second mode interpreted to be a radiogenic product is present as minute anhedral grains (<0.01 mm) peripheral to and in shrinkage cracks of colloform and sooty pitchblende (Plate 16). Minor molybdenite is present with the metallic assemblage.

Bloom minerals on mineralized fracture-fault planes include malachite, very fine grained crusts of uranophane, kasolite, boltwoodite and very fine 0.1-0.2 mm anhedral to subhedral crystals and crusts of wölsendorfite. Numerous highly oxidized and highly radioactive specimens contained digenite and covellite as disseminated grains and mantles on chalcopyrite, bornite and galena.

A northwest-trending fault zone located at 7058370N, 614850E (65P/10) is approximately 1 km south of the basal Dubawnt unconformity. This structure transects leucocratic potassic feldspar augen granodioritic gneiss. Amphibolites, locally pyrrhotite-chalcopyrite bearing, are interlayered with and crosscut the gneissic layering. The non-radioactive fault zone has an outcrop expression of approximately 60 m and is approximately 15-20 cm wide. The fault filling assemblage contains chalcopyrite, galena, bornite and pyrite disseminated in a sugary white quartz, chlorite, and white calcite matrix. The fault trace is marked by abundant

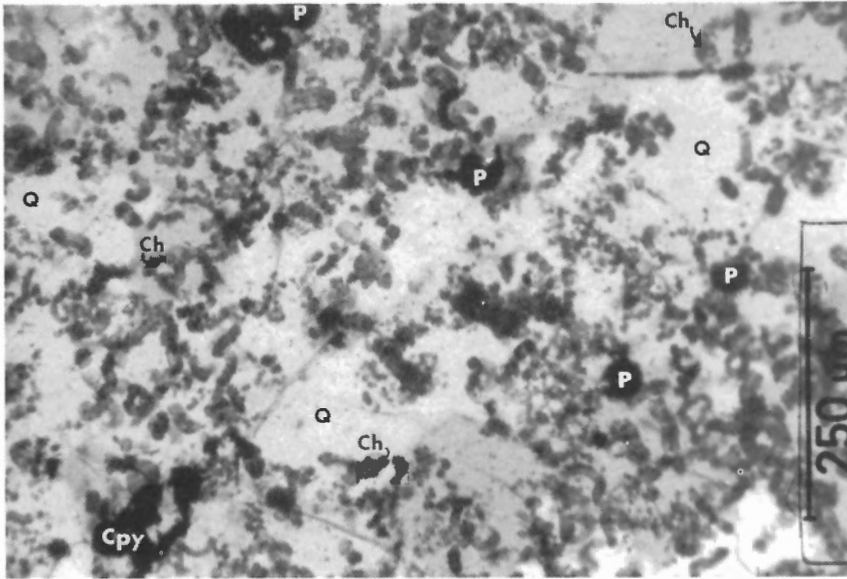
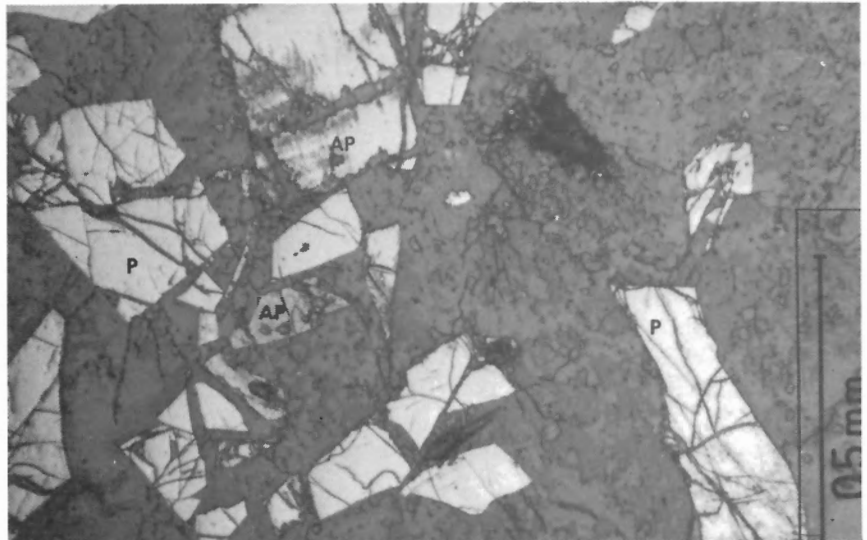


Plate 12

Photomicrograph of colloform pitchblende (P) associated with spherical chlorite (Ch), quartz (Q), occurrence 14, transmitted light. (GSC 203591-J)

Plate 13

Photomicrograph of fractured subhedral pitchblende (P) set in chlorite-quartz-calcite host. Mottled appearance of altered pitchblende grains (AP) represents first stage in the replacement of pitchblende by wölsendorfite and uranophane, occurrence 13, reflected light. (GSC 203591-K)



malachite, azurite and limonite straining. Even though this fault zone is non-radioactive it displays fracture filling assemblages and structural features similar to the radioactive fracture zones near Kazan Falls.

Sparsely disseminated uranium-molybdenum mineralization, occurrence 15, is present approximately 5 km southwest of occurrence 13. The basement complex consists of interlayered biotite-rich paragneiss, leucocratic biotite-potassic feldspar augen gneiss and garnet amphibolite all of which are cut by amphibolite and diabase dykes. The radioactive minerals include very fine grained monazite and pitchblende, both of which occur within biotite-rich bands which mantle potassic feldspar augens. Extremely fine grained molybdenite, 0.5 mm, is disseminated throughout the augen gneiss. The lack of fracture zones associated with this occurrence may suggest that the disseminated mineralization within the layered felsic gneisses is syngenetic.

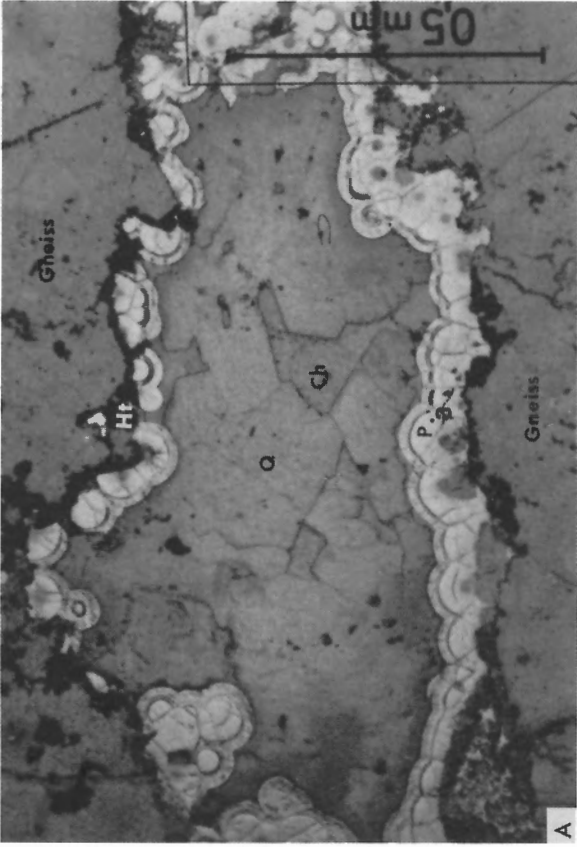
#### Age of Basement Mineralization

A U-Pb isotopic analysis on pitchblende from the fracture-controlled mineralization at occurrence 13

immediately south of the unconformity resulted in the ratios:  $Pb^{206}/U^{238} = 0.34947$ ,  $Pb^{207}/U^{235} = 5.34056$  and  $Pb^{207}/Pb^{206} = 0.1109$  (Little, unpublished GSC data). The calculated ages are discordant and the isotopic ratios for the analysis lie above the concordia plot suggesting a loss of uranium relative to lead. The similarity of this U-Pb age, 1813 Ma and the Rb-Sr age of 1786 Ma suggests a genetic relationship between mineralization and Christopher Island volcanism.

#### Geology and Fracture-controlled Mineralization Within the Dubawnt Group

Fracture controlled mineralization in the Thirty Mile Lake area is localized near the southern margin of the eastern Baker Lake basin similar to the U-Cu-Ag-Au-Se association on Christopher Island and the U-Cu-Pb-Mo association in the area of Kazan Falls. The basement complex, north of the eastern end of Thirty Mile Lake, is directly overlain by the Christopher Island Formation and to the west by the South Channel Formation. The presence of the Christopher Island Formation in contact with the



**A.** Photomicrograph of colloform pitchblende (P) with hematite (Ht) mantling fracture walls and infilled by quartz (Q) and chlorite (Ch), occurrence 13, reflected light. Pitchblende analysis 3, Table 1. (GSC 203591-L)

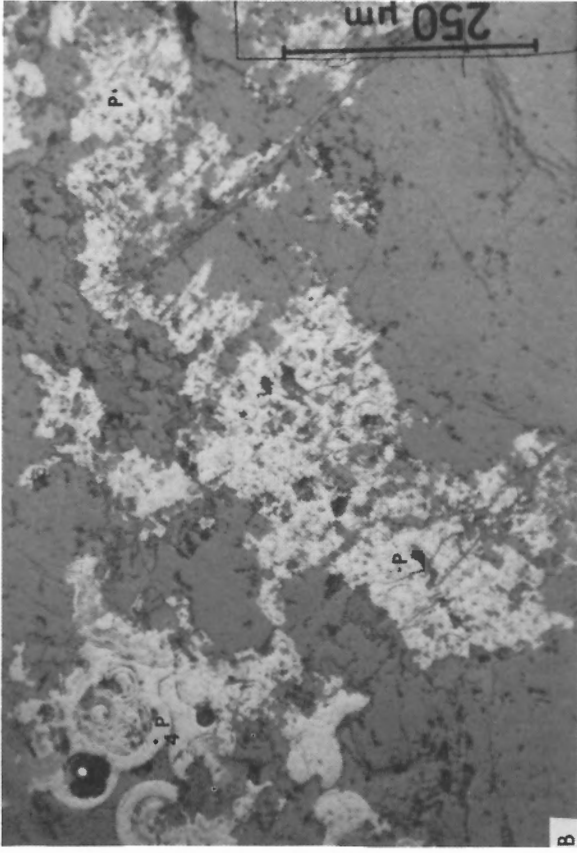


**Plate 14**

**B.** Photomicrograph of botryoidal pitchblende in hairline fractures, occurrence 13, reflected light. Pitchblende analysis 4, Table 1. (GSC 203591-M)

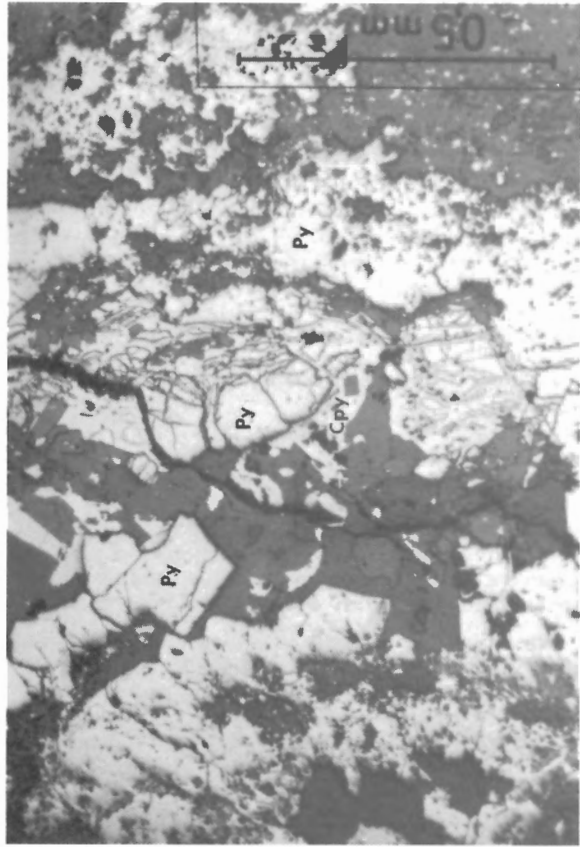


**Plate 15**

Photomicrograph of pyrite (Py) fractured and replaced by chalcopyrite (Cpy), occurrence 14, reflected light. (GSC 203591-N)

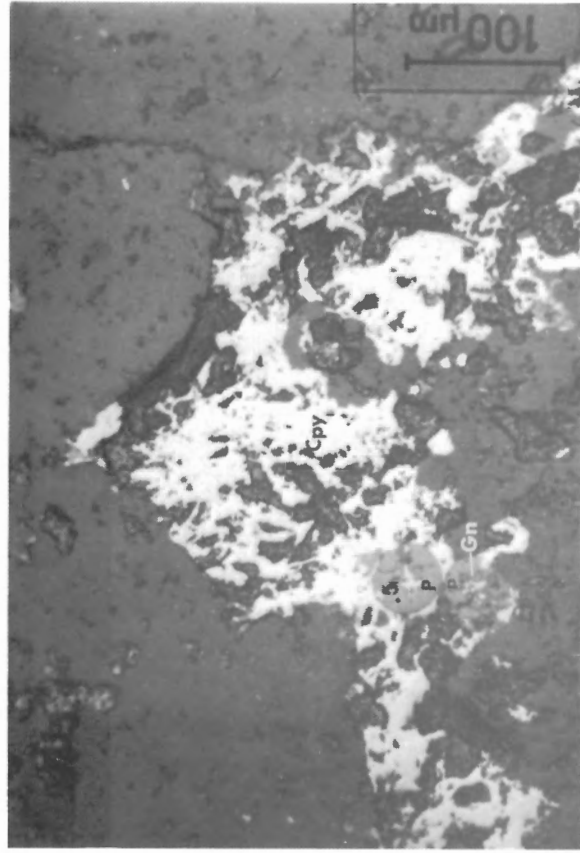


**Plate 16**

Photomicrograph of colloform pitchblende (P) mantled by chalcopyrite (Cpy). Note the very fine grained galena (Gn) within pitchblende syneresis cracks, occurrence 14, reflected light. Pitchblende analysis 5, Table 1. (GSC 203591-O)

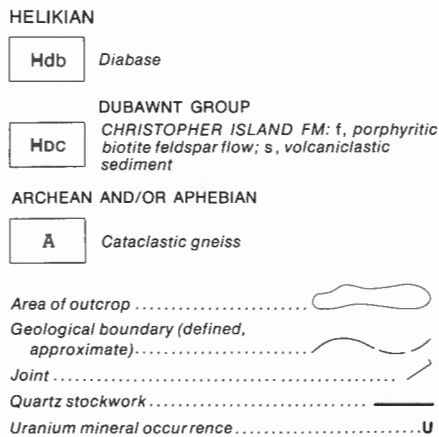
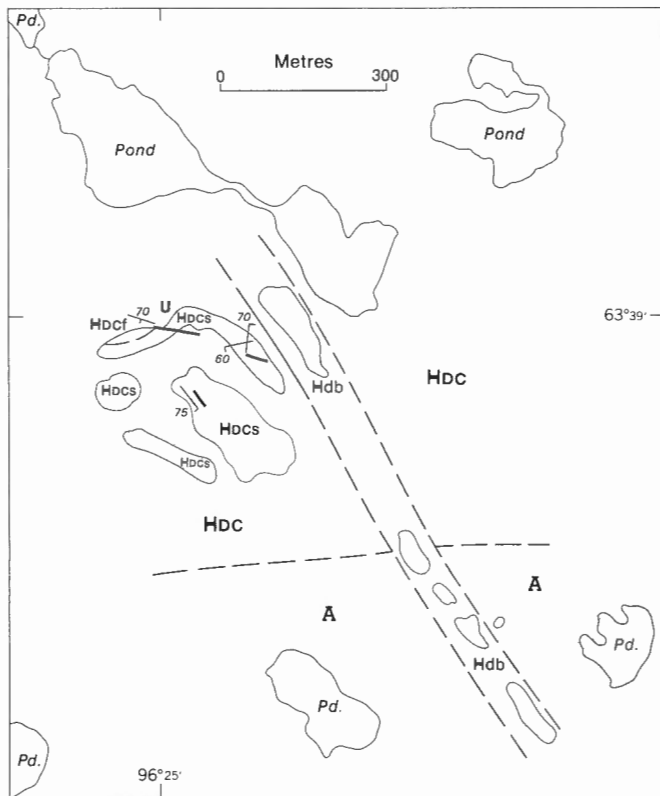


**Figure 6.** Geology of uranium occurrence 18, Thirty Mile Lake area (65 P/9).

basement gneisses and the apparent interfingering of the redbeds with the volcanic rocks north of Thirty Mile Lake suggest that the Christopher Island Formation may be faulted against the basement complex. Three fracture-controlled uranium occurrences are present in the Christopher Island Formation near the unconformity or its faulted equivalent.

The westerly of three uranium occurrences, occurrence 18, is located approximately 400 m north of the unconformity. Volcanoclastic sedimentary rocks of the Christopher Island Formation predominate in the occurrence area and are overlain by an aphanitic porphyritic trachytic flow unit. A northwest-trending medium grained ophitic diabase dyke, belonging to the Mackenzie dyke swarm, intrudes the cataclastic gneisses and Christopher Island Formation (Fig. 6).

The southerly outcrops in the occurrence area are massive coarse volcaniclastic sediments containing clasts of maroon porphyritic trachyte and minor granitic gneiss. Clasts range from pebbles to boulders in size, subangular to subrounded in form, and are set in a maroon medium to coarse sandy matrix of feldspar and quartz. The content of basement clasts decreases northwards until the sediment contains only volcanic clasts. The northern edge of the occurrence area is a massive reddish maroon aphanitic porphyritic trachyte flow. Phenocrysts of plagioclase and biotite to 2 mm in size and glomeroporphyritic plagioclase to 5 mm in size are set in an aphanitic feldspar-rich groundmass.

The volcanic and volcaniclastic rocks are brecciated by quartz stockworks trending west to northwest. The uranium-copper mineralization is confined to a bleached and brecciated zone within aphanitic porphyritic trachyte. The mineralized zone is approximately 4 m wide and 9 m along strike. The bleached trachyte is reddish orange to orange and highly hematitized compared to the unaltered maroon trachyte. In addition to the oxidized groundmass of the brecciated and bleached trachyte, the plagioclase and biotite phenocrysts are partially and completely replaced by chlorite and very fine grained hematite.

The stockwork exhibits open space filling textures with sugary milky crystalline quartz crystals encrusting the fracture walls. The associated assemblage includes calcite, orange barite, chlorite and minor hematite. Pitchblende is present as fine irregular sooty mats associated with calcite-chlorite rich veinlets. Copper sulphides, chalcopyrite, and bornite are disseminated through the breccia fragments and intergrown with the vein filling minerals. Chalcopyrite and bornite occur as separate grains and as extremely fine exsolution intergrowths (Plate 17). Bornite commonly exhibits irregular rims of chalcocite and covellite interpreted to be oxidation products. Secondary minerals in the mineralized stockwork are malachite, azurite and uranophane.

Approximately 3.5 km to the west, two uranium-base metal occurrences (numbers 16 and 17) are related to structural elements that have been superimposed upon the Dubawnt Group. The Christopher Island Formation in this region consists of a series of trachyte flows striking east-west and interpreted to dip north based on the presence of low angle joint planes. The flows are aphanitic porphyritic in texture, with phenocrysts of feldspar and biotite with or without hornblende. Locally narrow biotite trachyte dykes containing granitic gneiss xenoliths crosscut the porphyritic flows. Glomeroporphyritic plagioclase and potassic feldspar to 7 mm in size are set in a trachytic groundmass. The flows are highly propylitized with the development of fine grained calcite impregnated through the groundmass and calcite and/or chlorite after feldspar, hornblende and biotite phenocrysts. Olivine(?) pseudomorphs are associated with porphyritic feldspar-biotite flows. Altered biotite phenocrysts consist of iron-rich chlorite, very fine grained anatase and very fine grained hematite which is disseminated through and outlines the pseudomorphs.

The porphyritic trachyte flows in the vicinity of occurrence 17 are fractured about west to northwest and north- to north-northeast sets. Mineralization is contained within the latter set but is carried principally by the west to northwest fracture set. The mineralization is contained in a highly radioactive gossan about 8 m long by 3 m wide trending 030° with northwest-southeast-trending mineralized fractures extending up to 75 m from the high grade zone. Peripheral radioactive fracture zones are characterized by thin reddish orange to orange reduced walls containing malachite coated chlorite, calcite, and quartz filled veinlets. The area immediately adjacent to the gossan is chloritized

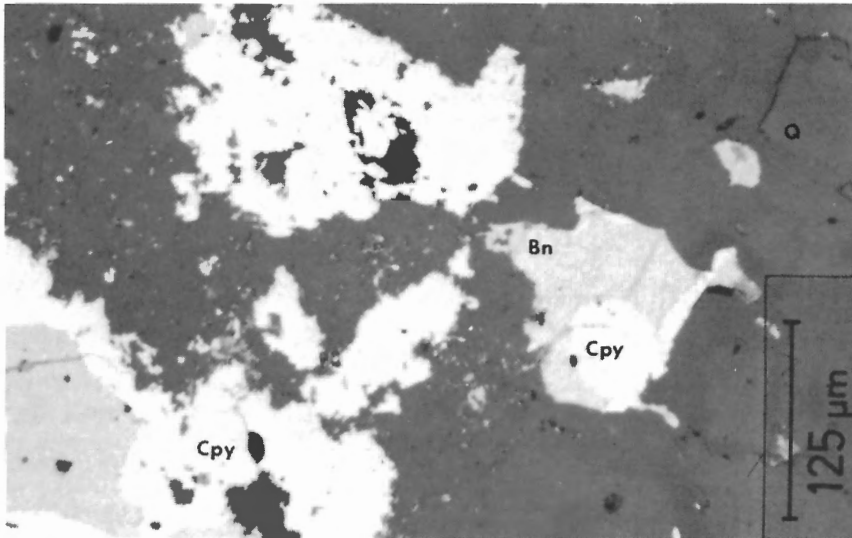


Plate 17

Photomicrograph of chalcopyrite (Cpy) and bornite (Bn) in quartz (Q)-chlorite veinlet. Note the extremely fine intergrowth of chalcopyrite in bornite, occurrence 18, reflected light. (GSC 203591-P)

and carries disseminated chalcopyrite. The gossan consists of angular brecciated fragments of intensely chloritized porphyritic trachyte in a fine grained, 0.2-0.04 mm mosaic of quartz, chlorite, calcite, hematite, yellow barite and anatase.

The fine grained sulphides (0.2-0.5 mm) galena, pyrite, sphalerite, bornite and principally chalcopyrite are disseminated through the altered and brecciated trachyte fragments and barite-carbonate-quartz-chlorite veinlets. Pitchblende is present as fine anhedral grains 0.1-0.2 mm and as sooty mats disseminated through the vein filling assemblage.

Occurrence 16, approximately 2 km east of occurrence 17, contains disseminated sulphide and uranium mineralization in northwesterly trending fractures. The Christopher Island volcanic rocks in the area consist of massive porphyritic trachyte flows and breccia zones the latter consisting of fine to medium (<1 cm to 5 cm) angular to subrounded fragments of porphyritic trachyte. These zones are interpreted as flow top or bottom breccias. The biotite phenocrysts within the zone of fracturing are replaced by chlorite and rarely epidote both of which are intergrown with a very fine grained assemblage of hematite, anatase and a uraniferous phase. The opaque minerals outline and are disseminated throughout the biotite pseudomorphs (Plate 18A, B).

Sporadic sulphide and uranium mineralization is confined to the fracture systems, the widest fracture zone being approximately 10-15 cm. Autoradiographs of the fractured porphyritic trachyte show that a uranium phase is associated with hematite in calcite-chlorite veinlets and in chlorite, anatase, and hematite bearing pseudomorphs after biotite. The pseudomorphs are set in a fine grained oxidized and chloritized matrix of feldspar microlites, apatite and possibly devitrified glass. Within the fracture zone, chalcopyrite, galena, covellite and digenite are disseminated through the trachytic groundmass and in the calcite-chlorite veinlets.

Energy dispersive investigations and quantitative electron microprobe crystal spectrometry of the uraniferous phase within a biotite pseudomorph indicate that the principal elements are uranium and titanium with minor silicon and lead (Table 1). Energy dispersive spectra on numerous grains and the quantitative analyses indicate variable abundances of uranium and titanium. The analyzed uraniferous phase is too fine grained (5-10 $\mu$ ) for X-ray identification. The uraniferous phase is intimately

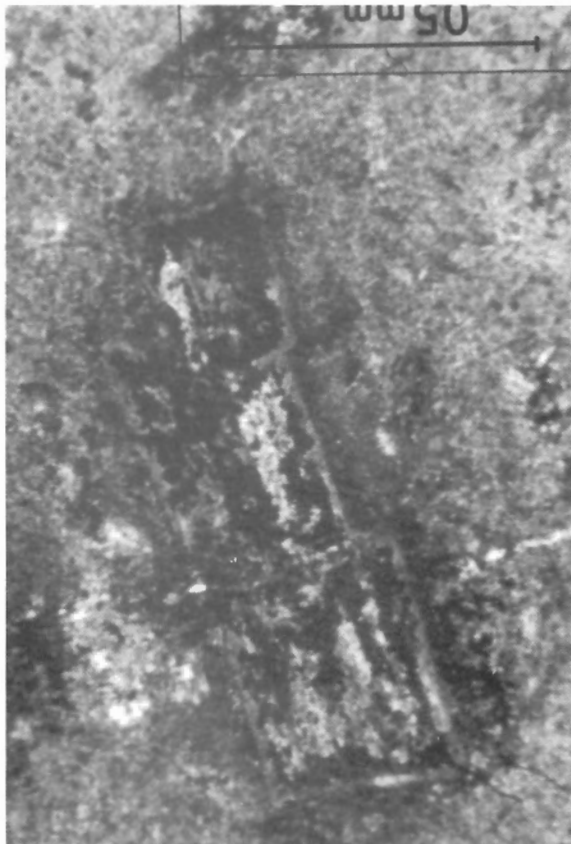
intergrown with anatase. Secondary minerals within the fracture zone are very thin crusts of malachite and pale yellow kasolite.

The restriction of sulphides and uranium-titanium phases to the northwest fractures suggests that fracture zones channelled metal-bearing fluids. The intimate intergrowth of anatase and uranium-titanium phases suggests complexing of uranium around anatase developed during or after chloritization of the mica phenocrysts.

Occurrence 19 is located in an area of limited exposure of interbedded Christopher Island volcanoclastic sediments and massive aphanitic porphyritic trachyte flows. The sediments consist of subrounded cobble to granule sized (15 cm-1 cm) aphanitic porphyritic trachyte set in a maroon sand to silt sized matrix. The volcanic units are typically reddish maroon to maroon, aphanitic porphyritic with euhedral to subhedral phenocrysts of feldspar and biotite. Propylitization of phenocrysts and groundmass is common.

The anomalous radioactivity is confined to a zone of massive reddish orange amygdaloidal biotite-feldspar trachyte (Appendix 2A, analysis 4), about 7 m wide (north-south) and 15 m long (east-west). The feldspathic groundmass contains subhedral microphenocrysts of plagioclase (0.1-0.3 mm) and chloritized and carbonatized biotite phenocrysts. The zoned amygdales are equant to elongate in shape and filled with chlorite followed by calcite. No radioactive minerals or sulphides have been identified, however, the bleached amygdaloidal trachyte contains 87.3 ppm U and 1910 ppm Pb compared to the range of 3.0-13.1 ppm U for Christopher Island volcanic rocks (Blake, 1980). This radioactive zone is interpreted as an epigenetic concentration within a propylitized vesicular flow top.

A sequence of southerly dipping sedimentary, volcanic and volcanoclastic rocks of the Kazan and Christopher Island formations is poorly exposed immediately north of the fracture-fault controlled mineralization of occurrences 13 and 14. These rocks are presumed to be in fault contact with the basement complex. A fracture zone with anomalous radioactivity, occurrence 12, is present within maroon porphyritic biotite trachyte flows. The fracture zone trending 350° is exposed for approximately 40 m along strike and up to 7 m in width. Trachyte within the fracture zone is bleached to a light orange to peach hue and contains quartz, calcite, and hematite filled fractures. No radioactive minerals or sulphide minerals have been recognized. However, this radioactive anomaly is related to northwest- to north-trending fracture zones similar to the mineralization in the adjacent gneisses.



A. Photomicrograph of chloritized biotite phenocryst within a propylitized trachytic groundmass, occurrence 16, transmitted light. (GSC 203591-Q)

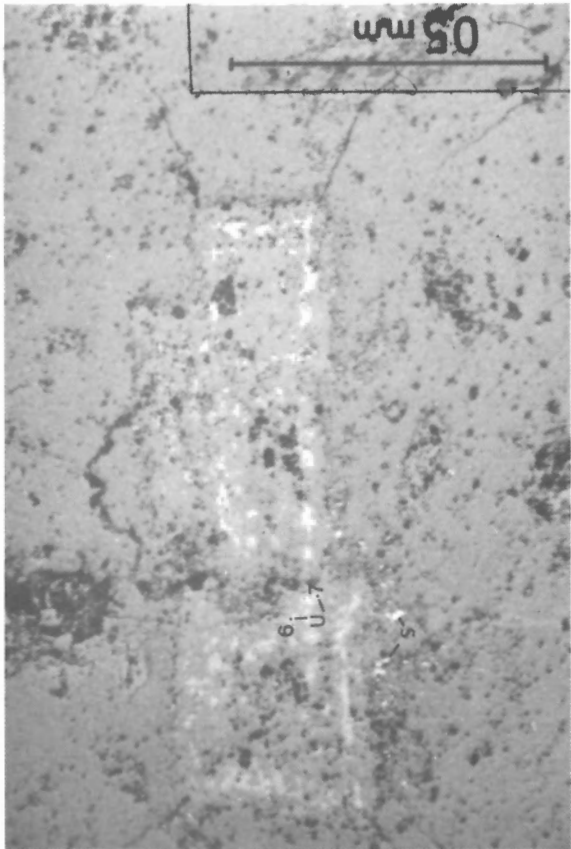


Plate 18

B. Photomicrograph of chloritized biotite phenocryst with very fine grained uraniferous titanates (U) disseminated through the anatase-hematite-chlorite pseudomorph. Very fine grained chalcopyrite (S) and galena (S) adjacent to the altered phenocrysts, occurrence 16, reflected light. Analyses 6 and 7, Table 1. (GSC 203591-R)

## Geology of the Redbed Mineralization

### Paleoenvironment of the South Channel and Kazan Formations

The lower redbeds of the Dubawnt Group, South Channel and Kazan formations, outcrop in the area south of Baker Lake and east of the Kazan River. Donaldson (1965, 1967) and Macey (1973) studied the sedimentology of these formations and stated that these formations represent fluvial sedimentary rocks accumulated in a structurally controlled basin marginal to a tectonically unstable provenance area to the southeast and south.

The polymictic South Channel conglomerate consists of locally derived rounded to angular basement clasts, predominantly felsic gneisses, but metavolcanic, metasedimentary and metaplutonic rocks are present. Matrix material varies from coarse sand to silt size muscovite, quartz and feldspar cemented by hematite and calcite. The great variability in clast shape and roundness indicates a high degree of immaturity. In addition, the massive character, poor sorting and bimodal distribution of clasts in the conglomerate suggest a high transport energy and rapid deposition due to loss in gradient.

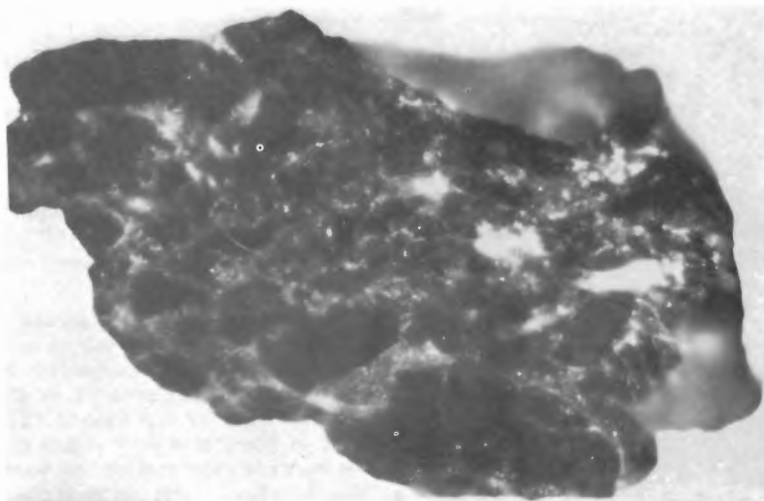
The Kazan Formation is conformable with and gradational from the South Channel Formation. With increasing sand interbeds and a decreasing coarse lithic component, the South Channel conglomerate is gradational into coarse to pebbly Kazan arkosic sandstone. The arkose is well bedded with thin maroon siltstone-mudstone laminae and typically consists of wedge shaped planar and trough cross stratification. Towards the northwest, the arkose contains a greater siltstone-mudstone component suggesting that it is a more basinward facies of the Kazan arkose.

The Kazan arkose is plagioclase-rich, typically well bedded and cemented with hematite, albite, calcite and minor quartz, with hematite accounting for the pink to maroon hues of the arkose-siltstone-mudstone units. Modal variations of the principal clasts are: albite 20-32%, potassium feldspar 7-12% and quartz 18-39% with the cements: albite 1-7%, carbonate 1-10% and hematite 2-6%. Sedimentary structures such as fining upward cycles, desiccation cracks, mudstone-siltstone rip-up structures and a variety of ripple marks in arkosic beds and siltstone-mudstone interbeds indicate a shallow water environment with varying water velocity and frequent subaerial exposure. Northwest-trending paleocurrents in the Kazan Formation (Donaldson, 1965) as well as the above sedimentological structures strongly indicate a braided fluvial river system.

The Kazan arkose characteristically displays planar and trough stratification on the scale of 20-60 cm, however, locally within the lower segments of the Kazan Formation there are large crossbedded arkosic units termed the giant crossbedded arkose that attain dimensions of tens of metres across and several metres thick. The giant crossbedded arkose is a discontinuous subfacies of the Kazan Formation occurring in a broad arc extending from west of Bissett and Martell lakes to Christopher Island. It is restricted to the basal portions of the Kazan Formation at the transition between coarse pebbly arkose and medium to fine grained arkose-siltstone units (Fig. 7). In detail, the giant crossbedded unit is a complexly interbedded sequence of large crescent shaped crossbedded arkose and small scale planar and trough crossbedded arkose-siltstone and minor pebbly arkose.



A. Photograph of mineralized uranium-copper bearing polymictic South Channel conglomerate, occurrence 8. (GSC 203345-H)



B. Autoradiograph of Figure 19A showing the distribution of uranium mineralization. (GSC 203591-S)

**Plate 19**



**Plate 20**

Angular clasts from the basal portion of the South Channel conglomerate at occurrence 8. (GSC 203591-T)

The giant crossbedded arkose is characterized by medium to coarse, subrounded to rounded sand size detritus and by arkosic beds up to 30-40 cm interbedded with thin (1-5 mm) maroon siltstone laminae. Bedding characteristics and the high degree of sorting of arkosic beds and siltstone laminations, subrounded to rounded shape of quartz and feldspar, absence of clay or micaceous detritus, scarcity of desiccation cracks, and a high angle of repose ( $28^{\circ}$  to  $33^{\circ}$ ) for the internal stratification of cross sets suggest the unit represents transverse eolian dunes. In outcrop plan, the large crescent shaped structures resemble truncated festoons of eolian dunes.

Giant crossbedded structures can be created within a fluvial system (Freeman and Visser, 1975; Coleman, 1969) or by eolian processes (Reineck and Singh, 1975; Bigarella, 1972). Eolian processes could have been active during periods of arid conditions or created simultaneously within the braided fluvial environment. The change in grain and clast size from the South Channel conglomerate to the Kazan arkose indicates varying flow conditions typical of a braided stream environment. Decrease in grain size from conglomerate to sandstone represents the change from a proximal to a distal braided stream facies (Schumm, 1977). The distribution of distal arkosic sandstones overstepping proximal conglomeratic facies as overlapping clastic wedges may be the result of a lowering of the stream gradient.

Paleomagnetic data from the Kazan and Christopher Island formations indicate that the Dubawnt basin was located at  $07^{\circ}\text{N}$ ,  $083^{\circ}\text{W}$  during Dubawnt sedimentation and volcanism (Park et al., 1973). Dubawnt sediments representing a series of clastic wedges may have been deposited in a wadi-like environment having its provenance area the gneissic and intrusive rocks to the southeast and south. The near source coarse clastic sediments represented by the South Channel conglomerate would be deposited as alluvial fans and possibly scree deposits at the margin of the basin. Ephemeral braided streams could create the sedimentary structures and lithological relationships existing between the South Channel conglomerate and Kazan arkose. Reworking of the fluvial deposited arkoses by winds could produce eolian dunes represented by giant crossbedded arkoses that are interbedded with braided stream deposits.



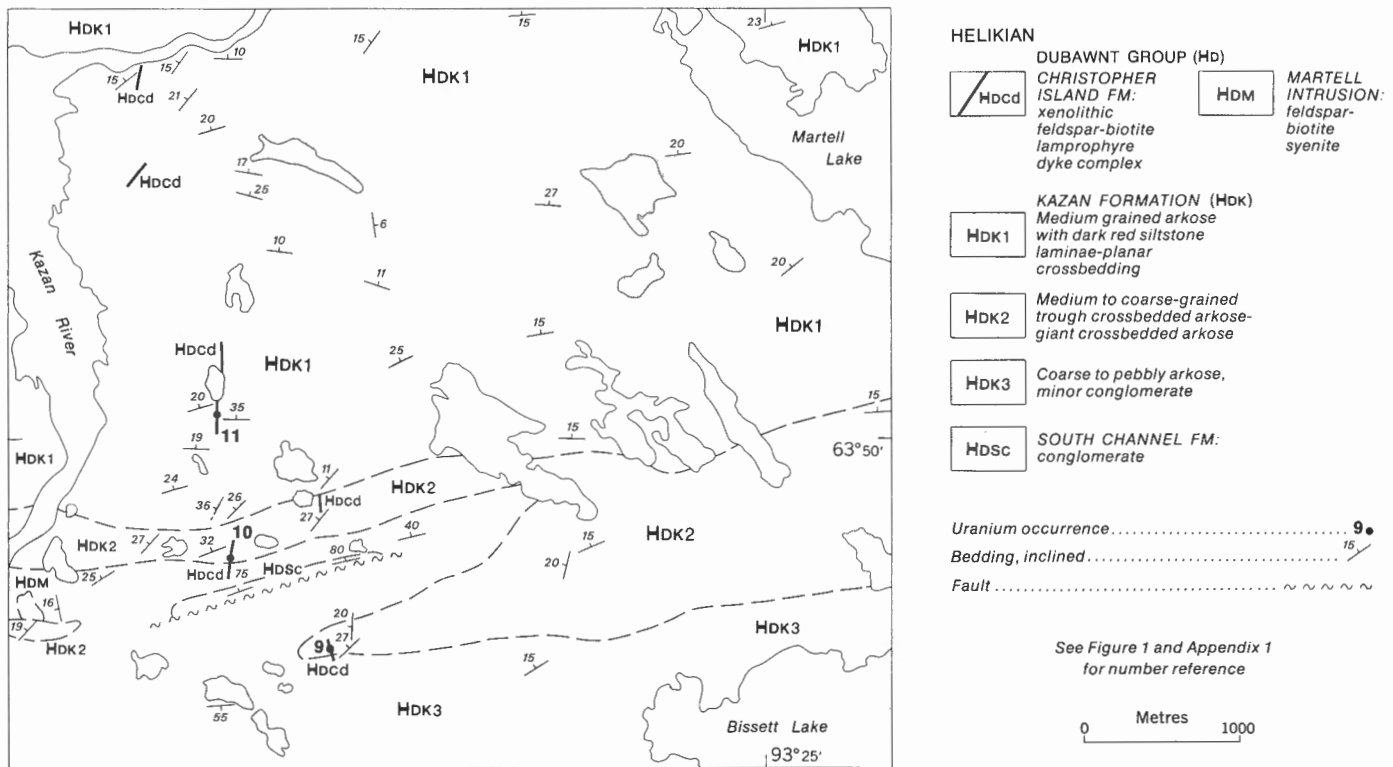


**Figure 7.** Geology of uranium occurrences 9, 10 and 11, Bissett Lake-Martell Lake-Kazan River area (55 M/13,14). Mapped by A. Miller and A.N. LeCheminant in 1975 and 1976.

GSC

### Geological Setting of the Kazan Type Mineralization

The term 'Kazan type mineralization' is used here to describe epigenetic concentration of silver, copper and uranium phases as impregnations and as fracture fillings within altered Kazan and South Channel conglomerate. The mineralization is irregularly distributed within thermally metamorphosed sedimentary rocks peripheral to altered lamprophyre dyke rocks equivalent to the Christopher Island potassic volcanic rocks.

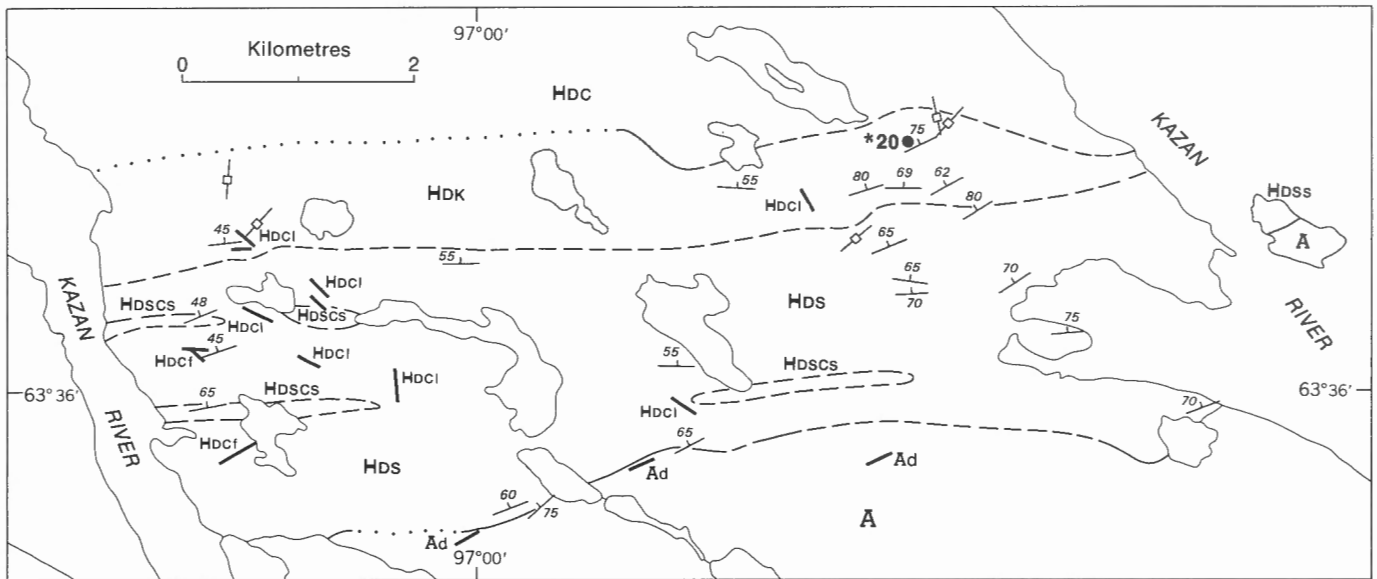
Six occurrences of Kazan type mineralization are known from northwest of Bissett Lake northeastward to Christopher Island (Fig. 1). The U-Cu-Ag mineralization shows a direct relationship to the emplacement of lamprophyre dykes and can be hosted within the South Channel conglomerate or lower portions of the Kazan arkose. Mineralization at occurrences 6, 7, 9, 10, and 11 is hosted within the giant crossbedded unit of the Kazan Formation whereas occurrence 8 is within the South Channel conglomerate. Lithologies at occurrence 11 differ to a degree from occurrences 7, 9 and 10 in that the arkose contains thick siltstone laminae, desiccation cracks and mudstone rip-up chips as well as features indicative of the giant crossbedded unit. This suggests that this occurrence is within a transitional zone between fluvial and eolian deposits.

Occurrence 8 is within the South Channel conglomerate approximately 12-15 m from the basal unconformity. The mineralization is localized within the matrix of the conglomerate adjacent to narrow north-trending biotite-feldspar porphyry dykes related to the Christopher Island Formation (Plate 19A, B). The dykes were not observed to cut the basement complex but this is probably only a function of exposure. The conglomerate at this location is massive, unsorted and pebble supported with framework clasts consisting of mica schist, garnet amphibolite, white quartz

and granitic gneiss to 15 cm in size, the last two lithologies predominating (Plate 20). The matrix comprises medium sand to silt size quartz, feldspar and muscovite cemented by hematite and calcite. Extensive chlorite is present in the areas of mineralization along with hematite and calcite. The subrounded to subangular shape of the framework clasts and high muscovite content of the matrix characterizes the South Channel conglomerate at this location. The unconformity surface between the conglomerate and basement gneiss is a vertical plane striking 060°. The retrograded white to pinkish white cataclastic biotite-potassic feldspar augen gneiss at the basal unconformity plane does not exhibit any features indicative of regolith development.

Angularity of the framework clasts and immaturity of the conglomerate matrix suggest that the basal South Channel Formation at this location is a lag deposit developed on the pre-Dubawnt basement complex. The steepness of the unconformity may be due to local block faulting. This basal conglomerate is strikingly similar to the basal conglomerate of the Martin Formation, Beaverlodge District, Saskatchewan (Tremblay, 1972; Plates 17, 18).

The Kazan arkose in the region of occurrence 6 on Christopher Island exhibits the features characterized by the type occurrences 7, 9 and 10. However as illustrated in Figure 3, this occurrence is situated near a late northwest fault which transects Christopher Island. In spite of the highly fractured nature of the Kazan arkose and abundant fractures containing copper and uranium minerals occurrence 6 and the remaining five occurrences are unified by the lithological and spatial relationships between arkose and dyke complexes, and alteration and metallic assemblages. Secondary minerals associated with the fracture controlled mineralization include francevillite-curienite series, uranophane, iriginite and powellite.



#### HELIKIAN (Hd)

**HdC** CHRISTOPHER ISLAND FM:  
trachyte lava; l, lamprophyre  
dyke; f, feldspar porphyry

**HdK** KAZAN FORMATION: arkose,  
minor conglomerate

**HdSC** SOUTH CHANNEL FORMATION:  
c, conglomerate, s, minor  
sandstone lenses

#### ARCHEAN AND/OR APHEBIAN (A)

**A** Granitic and granodioritic  
gneiss, diabase dykes (d)

Geological boundary (defined,  
approximate, assumed) .....

Bedding .....

Quartz veining .....

Uranium occurrence ..... **20**●

GSC

\*See Figure 1 and Appendix 1 for number reference

**Figure 8.** Geology of uranium occurrence 20, Thirty Mile Lake area (65 P/10).  
Mapped by A.R. Miller 1976, 1978 and A.N. LeCheminant 1975, 1978.

Occurrence 20 is located at the western end of Thirty Mile Lake approximately 2.5 km north of the unconformity (Fig. 8). Here, the South Channel conglomerate consists predominantly of cobble to granule size gneissic clasts set in a pink arkosic matrix. Mudstone and arkose lenses are interbedded with the conglomerate and locally mudstone rip-up chips are present within the conglomerate. The medium grained Kazan arkose is gradational from the conglomerate through a zone of interbedded coarse pebbly and sand size crossbedded arkose. The clastic sequence dips north at moderate attitudes (Fig. 8). Minor calcite-quartz veining is present within the arkose. Numerous fine grained northwest-to north-trending biotite lamprophyre dykes intrude the pebbly arkose. Narrow non-radioactive bleached contact aureoles are present in the adjacent arkose.

The radioactive zone occurs within medium to fine grained arkose at the contact with a conglomerate channel scour. The massive conglomeratic channel scour contains coarse rounded granitic gneiss, and white quartz predominantly 2-10 cm in size and is in erosional contact with a red to reddish pink mudchip-bearing arkose. The arkose is cemented by dolomite, hematite and minor calcite. Erratic radioactivity is confined to a narrow 10 to 15 cm wide band of maroon arkose along the contact of the channel scour. Trace element analyses of two specimens of radioactive arkose contained 66.9 and 153 ppm uranium, 23 and 45 ppm copper, 23 and 65 ppm lead and 0.3 and 0.2 ppm

silver, respectively. Anomalous uranium, lead and silver abundances are present compared to unmineralized Kazan arkose (Appendix 2G).

#### Petrography of the Kazan Arkose

Macey (1973) described the petrography of the South Channel and Kazan redbeds, their detrital mineralogy, secondary cements and sedimentological parameters. The Kazan arkose is plagioclase rich and has a plagioclase-potassic feldspar ratio varying from 1.4 to 6.3. This range is based on detrital grain abundances disregarding secondary silicate overgrowths. The plagioclase rich nature of the Kazan arkose compared to typically potassic feldspar rich arkoses coupled with the rapid deposition of the immature South Channel-Kazan sedimentary sequence into a tectonically controlled basin suggests that the distinctive detrital feldspar mineralogy of the Kazan arkose is directly related to a plagioclase rich provenance area rather than to processes of weathering, mineral stability and preservation.

Walker (1967), Waugh (1970a, b), and Kessler (1978) have described various diagenetic features that affect desert sandstone deposits and their ultimate conversion to redbeds. Based on modern analogues, the factors that contribute to formation of redbeds include a desert environment where iron-bearing detrital grains are altered and Eh-pH conditions favour the formation of ferric oxide and subsequent

conversion to the characteristic red pigments. These conditions are commonly met in hot, dry environments where a low water table and alkaline ground water prevail. In Kazan arkose hematite is a common cement coating framework and matrix grains but because of its ubiquitous distribution the timing of hematite cementation, during or after deposition of the sediments, is questionable. However textural relationships exhibited by the various cements in the Kazan arkose suggests sequential deposition of hematite, albite, and carbonate. Walker (1967) stated that formation of hematite is the result of destruction of iron-bearing detrital grains. The provenance area for the Kazan and South Channel redbeds contains biotite- and hornblende-bearing felsic gneisses and metavolcanics with associated paragneisses. In spite of a provenance area that would have contributed mafic detritus, mafic minerals or relict textures suggesting their presence are rare to absent especially within the Kazan arkose. This scarcity of iron-bearing minerals suggests that the red pigments have been ultimately derived from the alteration of mafic detritus. Hematite mantles the original rounded to subrounded grains of detrital quartz and feldspar and is in turn overgrown by authigenic albite. This relationship implies a timing of the hematite and albite cements and suggests an early postdepositional period of hematite cementation.

The plagioclase-rich Kazan arkose is highly indurated with authigenic albite overgrowths on potassic feldspar but predominantly on plagioclase. The dusted appearance of sericitic rounded to subrounded detrital feldspar in contrast to the unaltered albite overgrowths indicate that albite is of a postdepositional diagenetic origin. In addition, the authigenic overgrowths display optical continuity with the original twinned plagioclase grains. The authigenic albite overgrowths create subhedral prismatic outlines on rounded detrital clasts (Plate 21). The development of prismatic authigenic overgrowths on detrital silicates has been documented in several eolian sequences (Waugh, 1970a; Glennie et al., 1978) and in wadi and eolian dune environments (Kessler, 1978). The authigenic cements of quartz and potassic feldspar commonly occur in optical continuity on detrital silicates. These overgrowths are interpreted to have been precipitated slowly from ground waters concentrated with the appropriate elements. The enriched groundwater was created by the solution of micron size detrital fragments generated by abrasion in eolian environments (Waugh, 1970b). The high plagioclase content of the Kazan arkose may have created optimum conditions

for a high chemical activity of sodium and aluminum in the groundwater systems to permit precipitation of authigenic albite.

Carbonate is present throughout the redbed formations and, in the Kazan arkose, occurs as anhedral grains interstitial to the framework grains. Authigenic albite overgrowths display euhedral grain margins against anhedral interstitial carbonate. This relationship suggests that the carbonate cement is post albite.

At the western end of Thirty Mile Lake (NTS area 65 P/10) a basal carbonate-cemented arkose of the South Channel Formation rests on felsic gneisses. These units are crosscut by a lamprophyre dyke belonging to the Christopher Island Formation. Carbonate has been remobilized into the dyke margins where the dyke intrudes carbonate-cemented arkose (LeCheminant, personal communication, 1978). The relationship, at this locality, indicates that the carbonate cement is pre-Christopher Island dyke emplacement. Textures and mineral assemblages, to be described later, within altered Kazan arkoses peripheral to alkaline dykes are interpreted to be the result of thermal anomalies generated during emplacement.

#### Lithological Relationships Associated With Kazan Type Mineralization

Lamprophyre dykes related to the Christopher Island Formation intrude the basement complex, South Channel, Kazan and Christopher Island formations. In supracrustal rocks the intrusions are present as single units or as dyke swarms, the latter consisting of a series of parallel to subparallel dykes and radiating dykelets of variable widths. They are characterized by major dykes up to 6 m in width with subsidiary dykes as narrow as 0.5 m in width. The major dykes exhibit narrow chilled margins with vertical to subvertical contacts with the host sedimentary rocks. The intrusive complexes from the various occurrences exhibit excellent continuity along strike. Near occurrences 10 and 11, the northerly trending dyke complex can be traced for approximately 3.5 km. In spite of the continuity, mineralization is locally concentrated within the adjacent altered sediments and rarely within the intrusive rocks as shown by one dyke containing 356 ppm uranium (Appendix 2B). These intrusions from four occurrences contain 6.1-23.9 ppm uranium (Appendix 2B) and are similar to the uranium abundances within the Christopher Island lavas, 3.0-13.1 ppm (Blake, 1980).

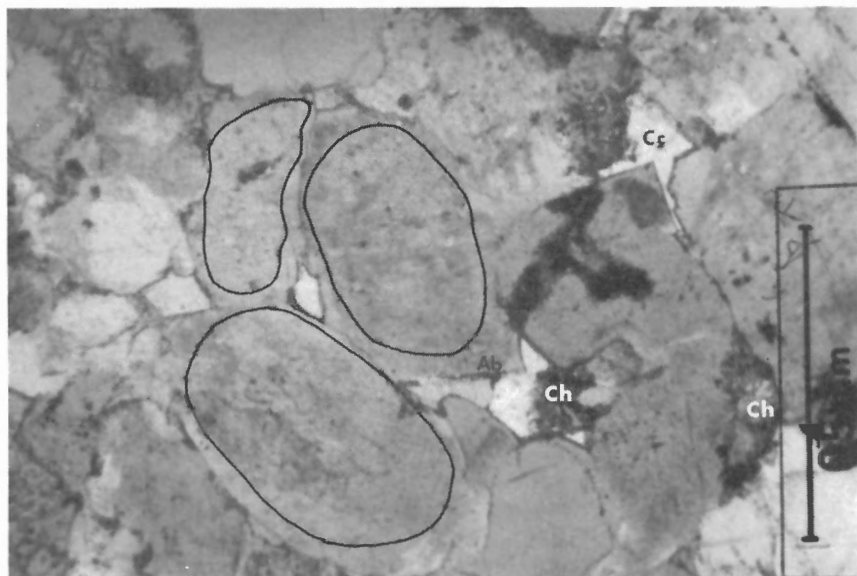


**Plate 21**

Photomicrograph of authigenic albite overgrowths (Ab) on rounded detrital plagioclase grains, outlined in black, and associated with interstitial chlorite (Ch) and calcite (Cc), pink altered zone, occurrence 9, transmitted light. (GSC 203591-U)

Chemical analyses of the lamprophyres from various occurrences plot within the alkaline field but are displaced compared to the equivalent lavas (Fig. 2, Appendix 2B). The shift to lower total alkali contents may be the result of intensive propylitization. Propylitization has resulted in extensive chlorite and calcite after mafic phenocrysts and very fine grained calcite disseminated through the trachytic to felted biotite-feldspar groundmass.

Partially to completely propylitized subhedral phenocrysts of biotite and plagioclase are common throughout all of the dykes. Rare relict textures suggest that olivine was a phenocryst along with biotite and plagioclase. Pseudomorphs of hematite after euhedral magnetite microphenocrysts are present throughout the trachytic groundmass. These textures and phenocryst types are similar to the stocks north of and on Christopher Island. The dyke

system at occurrence 7 contains subhedral to euhedral hornblende and clinopyroxene in addition to the above phenocrysts.

All dykes are xenolithic to various degrees ranging from microxenoliths of embayed resorbed quartz, 1-2 mm in size, to lithic macroxenoliths up to 30-40 cm in size and are characteristically subrounded to rounded in shape. Xenoliths are commonly white vein quartz or granodioritic to granitic gneiss. However, at occurrence 7 exotic fragments of fluorite-bearing biotite clinopyroxenite are present as well as the above common xenoliths. The biotite clinopyroxenite xenoliths exhibit a cumulate texture with intercumulus feldspar. Fluorite is present as lensoid grains along biotite cleavage planes in the biotite-clinopyroxenite xenolith and in biotite phenocrysts enclosed within the feldspathic groundmass of the dyke. This xenolith resembles ultramafic layers in alkaline intrusions within the basement complex (Morrison, 1977; LeCheminant et al., 1977). Locally, segments of massive aphanitic porphyritic dykelets at occurrence 7 are choked with a heterogenous assortment of rounded to subrounded Kazan siltstone, mudstone and arkose, granodioritic gneiss and white quartz ranging from 1 mm to 5 cm in diameter. The rounded form of all the xenoliths may be the result of attrition during emplacement of the fluidized trachytic magma.

Thermal aureoles occur within the Kazan arkose peripheral to the lamprophyre dykes. The alteration assemblages related to the thermal aureoles are of variable widths ranging from 1 m up to 100 m. The narrow aureoles occur within segments of the Kazan Formation characterized by thinly bedded fluvial arkose and siltstone-mudstone units. In contrast, wide thermal aureoles occur within thickly bedded sand units such as the giant crossbedded Kazan arkose.

Thermal aureoles are characterized by a pronounced colour variation. This accompanied by secondary alteration minerals and related textures as well as whole rock and trace-element analyses permit a three fold subdivision of the altered Kazan arkose. Colour alteration is gradational between zones and varies from white through mottled pink and pink to a cherry red. The white altered zone occurs nearest the intrusive complex grading horizontally outward into the pink and red altered rocks.

### Petrography of the Altered Kazan Arkose Associated With Mineralization

#### White Altered Kazan Arkose

This altered zone is present adjacent to the dyke complex and is characterized by pinkish white to white hues compared to the typical pink hues of the Kazan arkose. Hematite is sporadically disseminated as fine relict knots interstitial to clastic grains and as relict films along grain edges. The interstitial carbonates have been recrystallized with the development of euhedral dolomite (Plate 22). Calcite is present as very fine sugary grains (0.1-0.3 mm) interstitial to clastic grains and intergrown with fine grained subhedral to euhedral

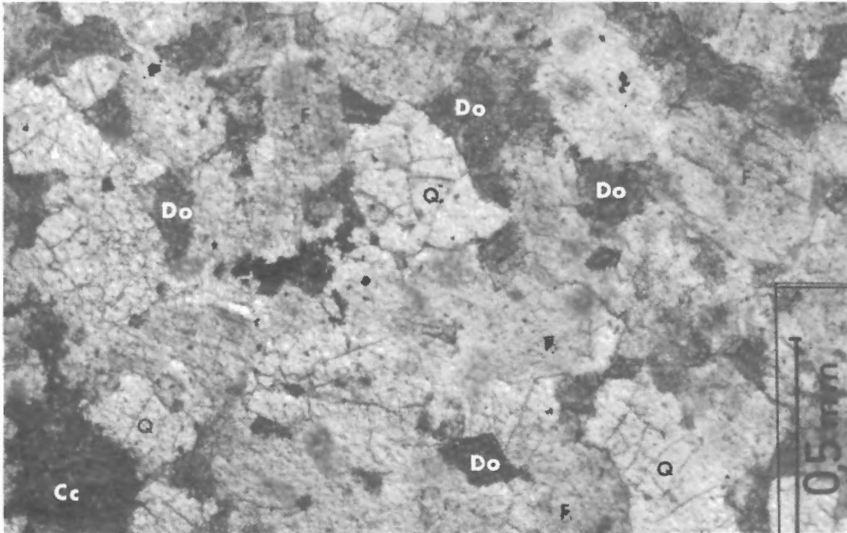


Plate 22

Photomicrograph of recrystallized carbonates, anhedral calcite (Cc) and subhedral to euhedral dolomite (Do) interstitial to quartz (Q) and feldspar (F), white altered zone, occurrence 9, transmitted light. (GSC 203591-V)

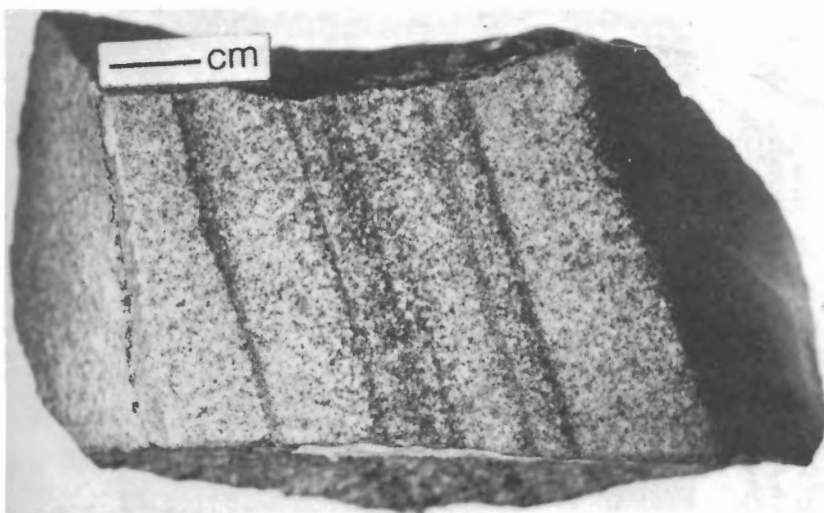
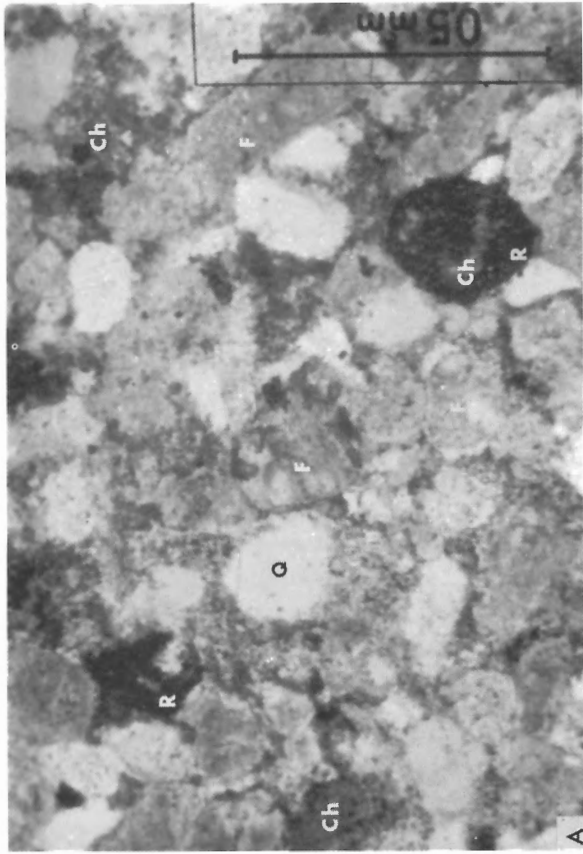
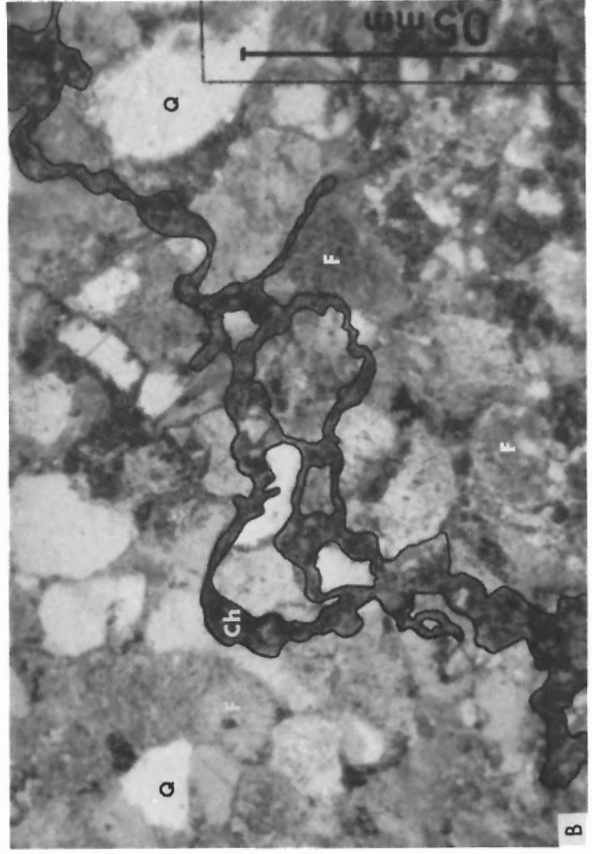


Plate 23

Photograph of chloritized arkose, white altered zone, with chlorite growth concentrated along silty laminae, occurrence 7, analysis 5, Appendix 2C. (GSC 203345-G)



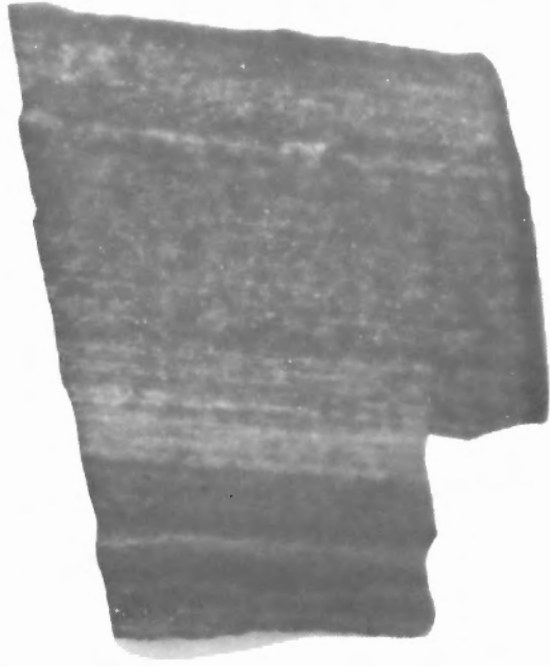
**A.** Photomicrograph of chlorite (Ch) and secondary anatase (R) interstitial to framework clasts, feldspar (F) and quartz (Q), occurrence 9, transmitted light. (GSC 203591-W)



**B.** Photomicrograph of chlorite stylolitic structure within altered arkose. Note the tortuous character and incorporation of detrital quartz (Q) and feldspar (F) into the structure, occurrence 10, transmitted light. (GSC 203591-X)



**C.** Photograph of red altered arkose with chlorite stylolite subparallel to bedding, occurrence 7, analysis 7, Appendix 7, Appendix 2E. (GSC 203345-B)



**D.** Autoradiograph of Figure 24C showing very finely disseminated uranium mineralization. Note the stylolite is very weakly radioactive. (GSC 203591-Y)

dolomite grains (0.2-0.4 mm). The recrystallized carbonates commonly display a mosaic texture. Chlorite, variety clinocllore, is intergrown with the recrystallized carbonates but is not as abundant as in the pink and red altered zones. Chlorite can be locally concentrated in siltstone-mudstone laminae imparting a light green hue to the laminae compared to the white sandy beds (Plate 23). Very fine grained clusters of subhedral to euhedral anatase are associated with interstitial carbonates and chlorite. Anhedral barite is locally associated with the interstitial carbonates.

*Pink Altered Kazan Arkose*

The pink altered arkose is characterized by a variety of macro- and micro-structures, recrystallization textures, and an increase in the secondary chlorite and anatase contents. Chlorite is common in the pink zone as very fine interstitial grains (< 0.05-0.15 mm), as fine radiating interstitial rosettes intergrown with carbonates (0.1-0.2 mm), and as fine stylolitic-like structures (Plate 24A, B, C, D). The interstitial chlorite is clinocllore with a MgO content of 27.74-29.34 weight per cent and an FeO content of 8.24-12.10 weight per cent (Table 4). The narrow stylolitic-like structures (0.20-1.00 mm) consist principally of chlorite with minor carbonate and anatase and can either parallel or crosscut bedding planes. The veinlets are highly tortuous following detrital grain contacts. Stylolitic structures consisting of illitic clays with associated uranium and sulphide mineralization will be described later.

The pink hues of this zone are the result of the retention of hematite as a film coating detrital quartz, feldspar and interstitial carbonates. Hematite is also present as very fine interstitial anhedral grains or anhedral bladed aggregates. A distinct megascopic texture of the pink zone is the localized concentration of roughly circular knots (2-3 mm in size) of an extremely fine grained mixture of recrystallized red hematite and chlorite. The area between the knots is relatively hematite poor (Plate 25A, B, C). The recrystallized red hematite and individual knotted texture suggests that iron has been remobilized and recrystallized during alteration of the Kazan arkose.

Anhedral to euhedral dolomite is associated with interstitial anhedral calcite but is less abundant than in the white altered zone. Anatase is more abundant than in the white

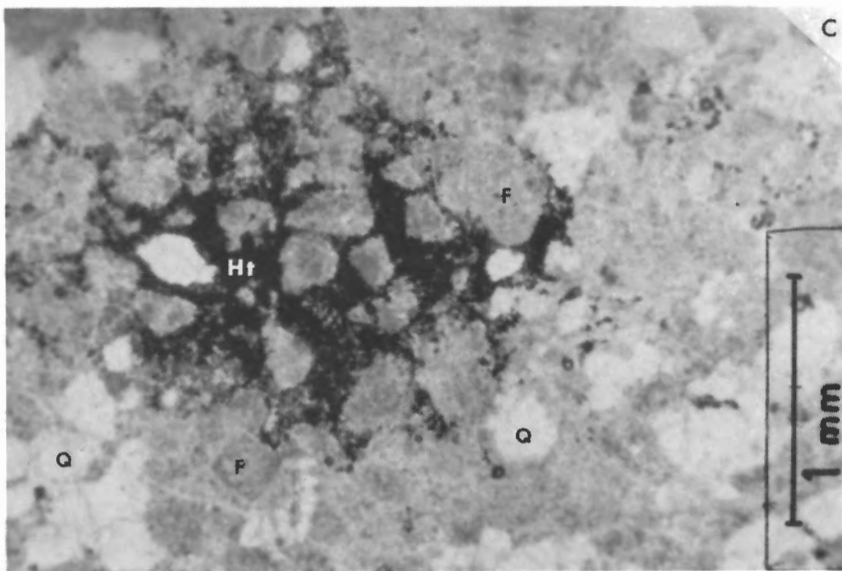
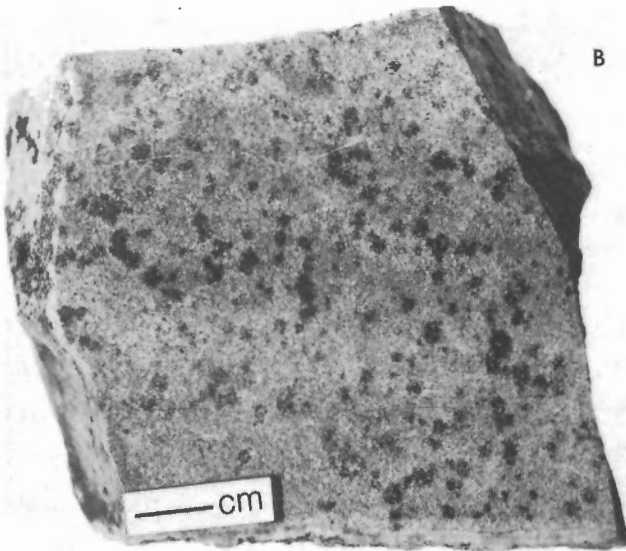
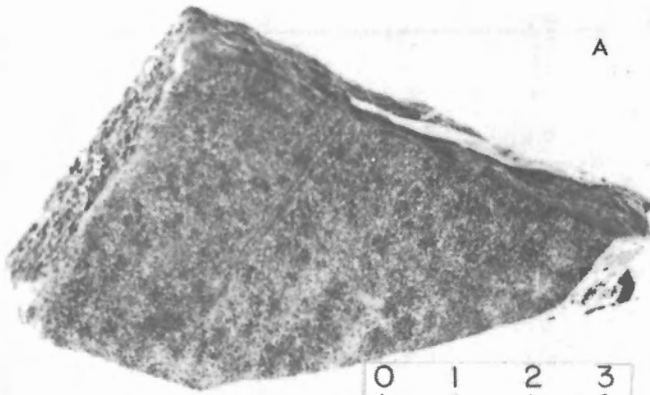


**Plate 25.**

**A.** Blotchy arkose, pink altered zone, occurrence 10, analysis 14, Appendix 2D. (GSC 203591-Z)

**B.** Blotchy arkose adjacent to Martell intrusion, analysis 5, Appendix 2F. (GSC 203345-J)

**C.** Photomicrograph of Figure 25A showing recrystallized hematite (Ht) with chlorite interstitial to framework clasts of feldspar (F) and quartz (Q). Note the hematite depleted character adjacent to the hematite-chlorite knot. (GSC 203592)

Table 4

## Electron microprobe analyses of chlorite associated with the Kazan type mineralization

Analysis	1	2	3	4	5	6	7	8	9	10
Occurrence	9	9	9	9	9	9	9	9	9	10
Alteration Zone	Pink	Pink	Pink	Pink	Pink	Red	Red	Red	Red	Red
SiO <sub>2</sub>	29.90	30.17	31.23	30.83	30.44	32.70	32.45	24.47	25.03	27.37
TiO <sub>2</sub>	0.04	0.00	0.00	0.08	0.06	0.04	0.04	0.07	0.06	0.08
Al <sub>2</sub> O <sub>3</sub>	17.16	18.01	18.45	17.20	16.47	15.05	15.41	19.47	20.42	19.04
Cr <sub>2</sub> O <sub>3</sub>	0.05	0.07	0.04	0.04	0.06	0.03	0.02	0.05	0.08	0.19
FeO	8.24	12.10	11.09	9.38	9.27	0.57	0.56	41.89	39.59	24.58
MnO	0.06	0.10	0.04	0.06	0.02	0.18	0.12	0.10	0.00	0.11
MgO	28.23	27.74	28.67	29.34	28.59	28.73	30.78	3.50	5.45	15.73
CaO	0.16	0.02	0.02	0.04	0.18	0.28	0.20	0.00	0.00	0.00
Na <sub>2</sub> O	0.00	0.12	0.00	0.00	0.00	0.32	0.00	0.00	0.00	0.00
K <sub>2</sub> O	0.01	0.00	0.06	0.01	0.00	0.52	0.06	0.00	0.00	0.08
Total	83.85	88.33	89.60	86.98	85.09	78.42*	79.64*	89.55	90.63	87.18
Fe/Mg	.376	.562	.498	.412	.324	.026	.023	15.4	9.36	2.01
Structural formula based on 28 oxygen										
Si <sup>+4</sup>	6.005	5.872	5.941	6.000	6.059	6.710	6.541	5.534	5.497	5.776
Al <sup>+6</sup>	1.995	2.128	2.059	2.000	1.941	1.290	1.459	2.466	2.503	2.224
Al	2.069	2.004	2.079	1.947	1.924	2.351	2.203	2.725	2.784	2.514
Ti	0.006	0.000	0.000	0.012	0.009	0.006	0.006	0.012	0.010	0.013
Fe <sup>+2†</sup>	1.384	1.722	1.764	1.478	1.543	0.098	0.094	7.923	7.272	4.338
Fe <sup>+3†</sup>	--	0.237	--	0.047	--	--	--	--	--	--
Mn	0.010	0.017	0.006	0.009	0.003	0.031	0.021	0.019	0.000	0.020
Mg	8.451	8.046	8.129	8.510	8.481	8.785	9.247	1.180	1.784	4.947
Ca	0.034	0.004	0.004	0.008	0.038	0.062	0.043	0.000	0.000	0.000
Na	0.000	0.045	0.000	0.000	0.000	0.127	0.000	0.000	0.000	0.000
K	0.003	0.000	0.015	0.003	0.000	0.136	0.015	0.000	0.000	0.022
ΣZ	8.000	8.000	8.000	8.000	8.000	8.000	8.000	8.000	8.000	8.000
ΣY	11.957	12.085	11.997	12.016	11.998	11.596	11.629	11.859	11.850	11.854

\*Average 3.38 wt% CuO

†Iron redistributed according to Finger, 1972.

Analyst: A.G. Plant

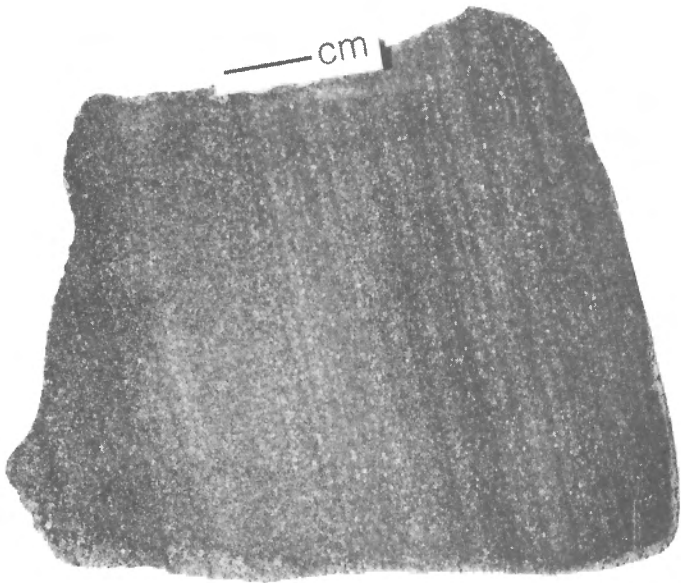


Plate 26A

Photograph of red altered arkose with native copper 10 000 ppm Cu, and 2820 ppm U analysis 6, Appendix 2E. Note the uniform hue distribution due to intense hematitization compared to Plates 23 and 25A. (GSC 203345-D)

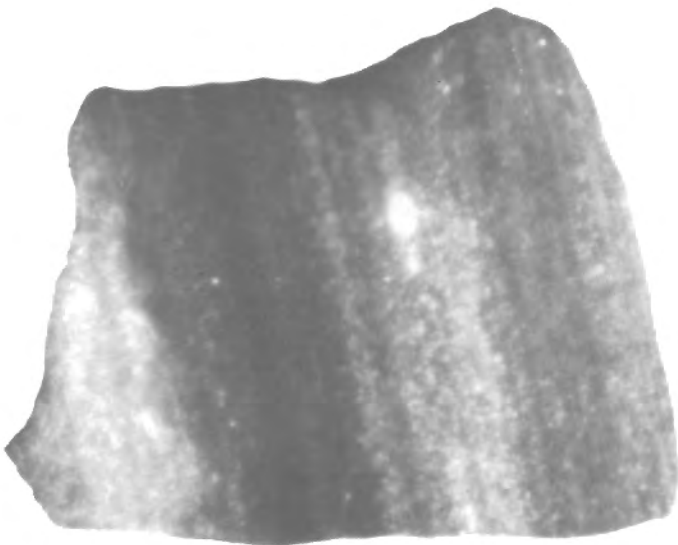
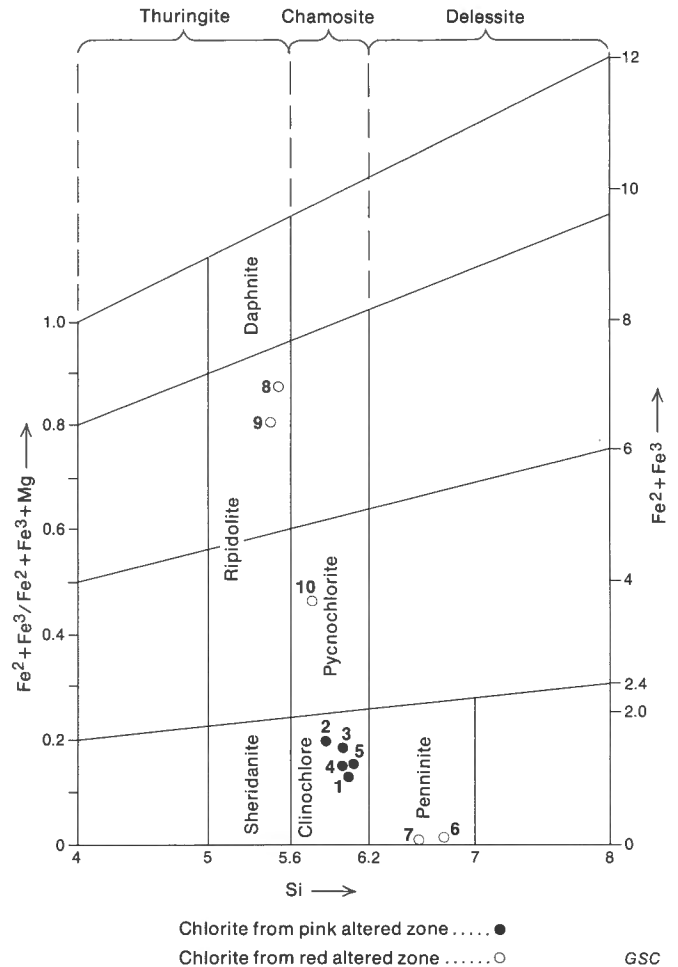


Plate 26B

Autoradiograph of Plate 26A showing the intense impregnation of uranium minerals along the bedding planes. (GSC 203592-A)



Numbered symbols refer to chlorite analyses from Table 3

**Figure 9.** Compositional variation of interstitial chlorites associated with the Kazan type mineralization (after Hey, 1954). Numbered data points refer to chlorite analyses, Table 4.

altered zone and occurs as aggregates of subhedral crystals and microscopic geoid-like structures. These ovoid to round structures (0.1-0.2 mm in diameter) occupy interclastic areas and consist of a rim of inwardly terminated anatase crystals. The central areas of these structures can be filled with euhedral anatase crystals, chlorite, and/or calcite. Disseminated interstitial sulphides and uranium phases occur with the carbonate and chlorite assemblages. Anhedral barite is common through the interstitial carbonate cement.

#### Red Altered Kazan Arkose

The cherry red alteration zone resembles barren deep maroon hematite-cemented Kazan arkose except for the very high radioactivity and malachite-coated fractures (Plate 26A, B). The intense red hue of this zone is the result of a hematite pigment coating all grains and impregnated through detrital feldspar and interstitial cements. In plain light, detrital feldspar grains and authigenic albite overgrowths have a bluish grey hue due to micron size iron oxide inclusions.

Interstitial sparry carbonates are abundant in this alteration zone. Minor dolomite is intergrown with calcite and barite and is anhedral in form compared to the euhedral character within the white and pink altered zones. Calcite is



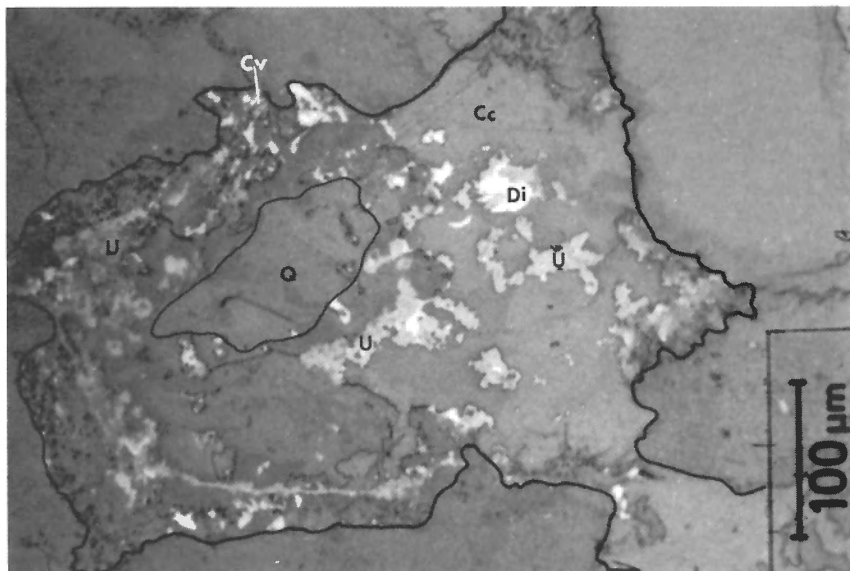


**Plate 27**

Photomicrograph of fine grained covellite (Cv) and digenite (Di) mantled by and associated with very fine grained uraniferous titanates (U). Mineralization is concentrated within an interclastic area, outlined in black and is associated with interstitial calcite (Cc) and detrital quartz (Q), occurrence 9, reflected light. (GSC 203592-B)

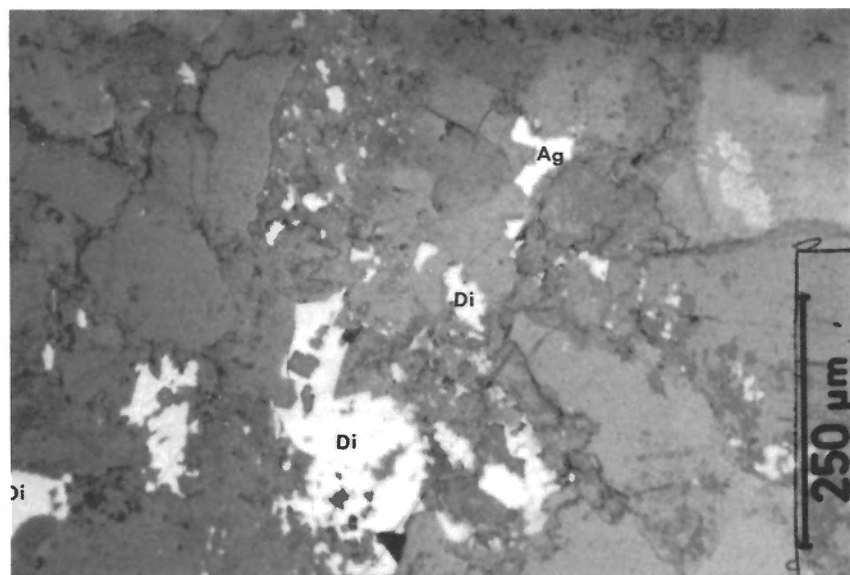


**Plate 28**

Photomicrograph of interstitial digenite (Di) and native silver (Ag) from pink altered zone, occurrence 9, reflected light. (GSC 203592-C)

the predominant carbonate species and electron microprobe energy dispersive spectra indicate the presence of low Mg and high Mg calcites. Anatase aggregates and geoid-like anatase structures are intergrown with calcite and chlorite and can be mantled by pitchblende and uraniferous titanates.

Interstitial chlorite is present throughout the cherry red altered zone and contains variable FeO and MgO contents, which result in a compositional range from low iron penninite through pycnochlorite to ripidolite (Table 4; Fig. 9). Analyses of chlorite (Table 4, analyses 6, 7) associated with native copper bearing altered arkose averaged of 3.38 per cent CuO. The copper is interpreted as submicron size inclusions. Trace amounts of chlorine were identified in the spectra of some chlorite grains. The variation in chlorite composition is interpreted as a reflection of the two stage process of mineralization to be discussed later. Interstitial sulphides, native metals and uranium oxides are concentrated in the cherry red alteration zone.

#### Ore Mineralogy of Kazan Type Mineralization

The alteration envelope peripheral to the Christopher Island dyke complex contains lead, iron, iron-copper and copper sulphides, native metals and uranium oxides. The distribution of the mineralization is erratic across the thermal aureole, however, there is a progressive increase in the tenor of the silver-copper-uranium mineralization from the white altered zone adjacent to the dyke complex through to the cherry red altered zone.

The metallic ore minerals identified include digenite, covellite, chalcopyrite, bornite, pyrite, galena, native copper and silver, pitchblende and titanium-uranium phases. These last phases are extremely fine grained (0.05 mm and less) and have not been identified by X-ray diffraction. Energy dispersive spectra indicate variable titanium, uranium and silicon contents. These phases will be referred to as uraniferous titanates. The mineralization has two modes of occurrence: 1) an impregnated assemblage of the above sulphides, uranium oxide, uraniferous titanates and native

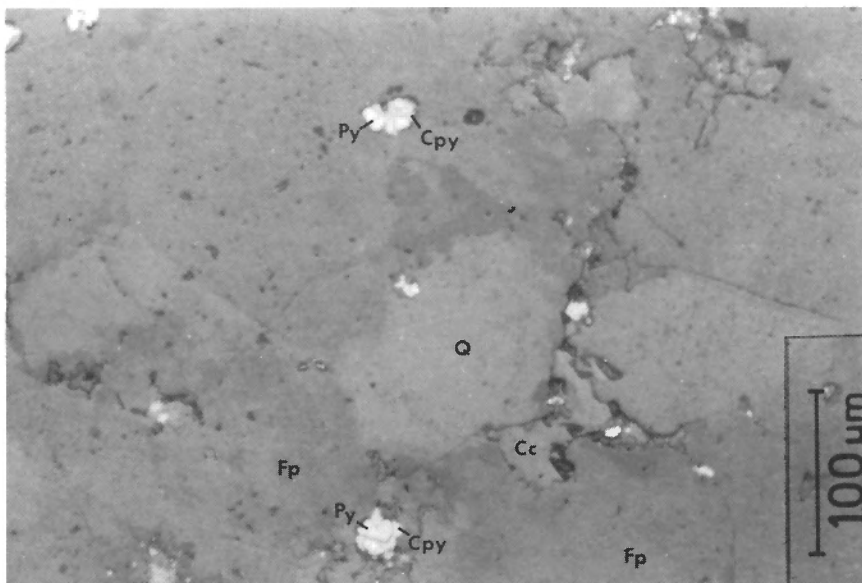


Plate 29

Photomicrograph of chalcopyrite (Cpy) mantling anhedral pyrite (Py) interstitial to detrital feldspar (Fp), quartz (Q) and calcite (Cc), from chalcopyrite-pyrite-bornite sulphide assemblage, pink altered arkose, occurrence 9, reflected light. (GSC 203592-D)

metals associated with interstitial carbonates, chlorite, barite and anatase, and 2) narrow stylolitic structures and fractures that consist of pitchblende-complex uraniferous phases-clay-carbonate and minor sulphide. The former mode is the most prevalent.

Arkose of the white altered zone contains very sparsely and erratically disseminated interstitial digenite and covellite. No uranium minerals were identified in this zone.

Sulphides and uranium oxides are disseminated throughout the pink altered zone and occur principally as impregnated concentrations interstitial to the framework detritus and to a minor extent in stylolitic structures. Because of the extremely fine grain size of the metallic minerals and their very finely disseminated nature within the interclastic areas, the term assemblage will be used to describe the association of various sulphide minerals and native metals even though mutual contact may not occur in all cases.

Very fine grained impregnated sulphides occur within interstitial volumes and along grain contacts of authigenic albite overgrowths. Two impregnated interstitial sulphide assemblages are present within the pink altered zone: 1) digenite-covellite, and 2) pyrite-chalcopyrite.

The most common assemblage, digenite-covellite, occurs as very fine equant anhedral and irregular wispy grains (0.3 mm and less) within interclastic areas and as irregularly shaped grains conforming to the outline of interclastic volumes (Plate 27). The very fine grained covellite and digenite are disseminated amongst interstitial carbonates, chlorite, anatase and barite and can occur as discrete grains or intergrowths. Other sulphides that can be associated with digenite-covellite include pyrite, bornite and/or chalcopyrite. Minor native copper and native silver also are present (Plate 28). The metallic minerals are generally disseminated through the sand beds and siltstone laminae but locally the siltstone laminae can be highly impregnated with sulphides and native metals.

Small areas within the pink altered arkose contain a chalcopyrite-pyrite assemblage in contrast to the common digenite-covellite assemblage. Pyrite occurs as euhedral to anhedral grains (0.1-0.2 mm) and is commonly mantled or embayed by chalcopyrite (Plate 29). Minor bornite as discrete grains can be associated with chalcopyrite-pyrite.

Pitchblende and uraniferous titanates are intimately associated with concentrations of interstitial sulphides, carbonates, and chlorite. Pitchblende, the most abundant uranium mineral, is present as extremely fine grained mats that partially or completely mantle sulphides (Plate 30). Locally, pitchblende displays very fine delicate colloform textures on sulphides or occurs as discrete colloform buckshot aggregates within and along the grain margins of interstitial carbonate (Plate 31). The complex uraniferous phases (0.05 mm and less) can be intergrown with pitchblende mats, mantle very fine grained sulphides, or be intergrown with chlorite, calcite and anatase. Anhedral to subhedral galena (<0.01 mm in size) is always associated with interstitial concentrations of uranium phases (Plate 32). Galena formation is interpreted in part to result from the radioactive decay of uranium minerals.

Fine stylolitic structures, 0.2-1.0 mm in width, crosscut and parallel bedding planes throughout the pink and red altered arkose. These structures are tortuous in form following the margins of detrital grains and authigenic overgrowths (Plate 33). The assemblage most commonly present in these structures is chlorite and anatase with minor digenite or pyrite but can include clay minerals, carbonate, pitchblende and uraniferous titanates. X-ray powder diffraction patterns of the clay minerals resemble those of glauconite and celadonite. The stylolitic structures are commonly simple but composite forms are present with carbonate or pyrite-pitchblende-carbonate veinlets superimposed upon chloritic and/or illitic clay-bearing stylolitic structures (Plate 34). The presence of fine illitic bands within chloritic stylolitic structures suggests that the clay has developed from chlorite in response to a low temperature alteration under alkaline conditions with a high concentration of potassium (Garrels and Christ, 1965).

Anhedral to subhedral opaque knots ranging up to 0.5 mm in diameter are distributed within and along the margins of the stylolitic structures. In detail, the knots consist of an extremely fine grained mixture of equant anhedral to irregular anhedral grains of pitchblende with minor uraniferous titanates set in illitic clay and uraniferous clay (Table 6; Plates 35A, B; 36A, B). Two analyses of the illitic clay hosting extremely fine grained pitchblende contain 5.1 and 10.1 weight per cent UO<sub>2</sub>. The high uranium contents may result from submicron sized pitchblende inclusions

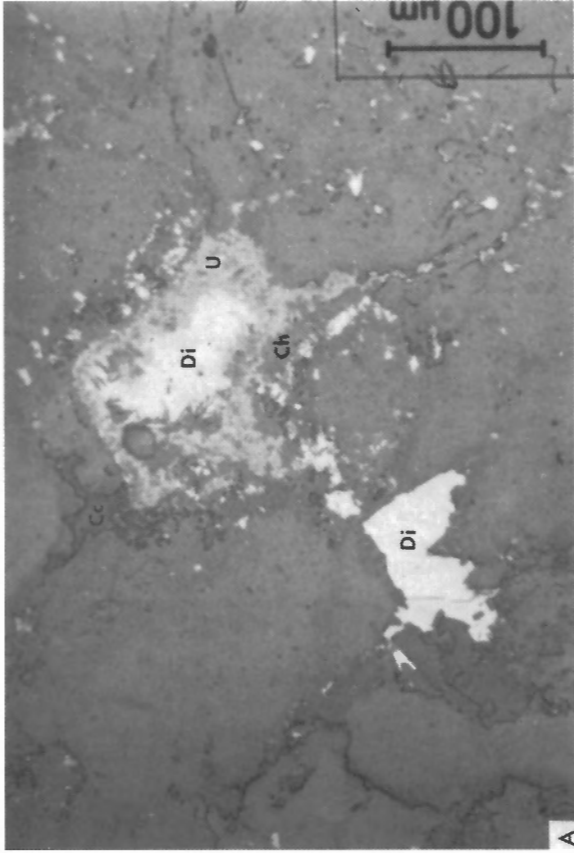


**Plate 30**

**A,B.** Photomicrographs of extremely fine grained (grey) pitchblende and uraniferous titanates, collectively marked as U, mantled and intergrown with interstitial (white) digenite (Di), associated with interstitial calcite (Cc) and chlorite (Ch), occurrence 9, reflected light. (A – GSC 203592-E, B – GSC 203592-F)

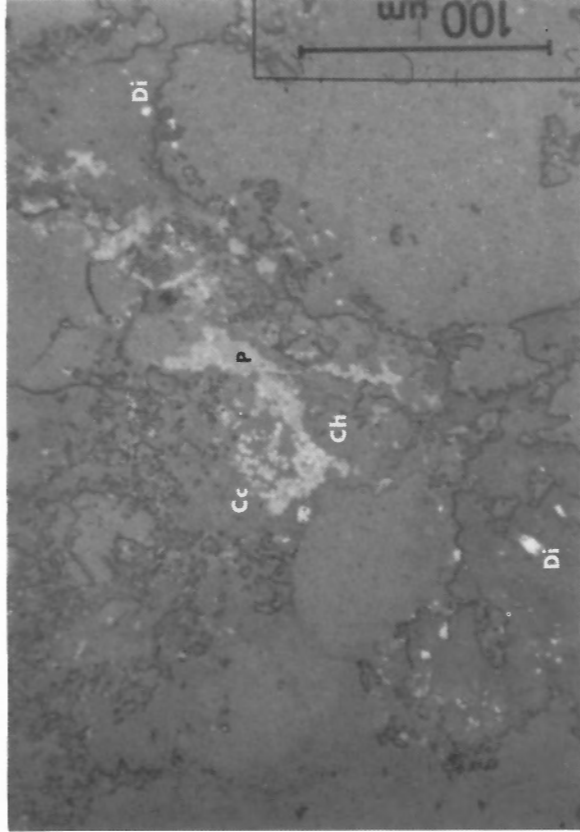
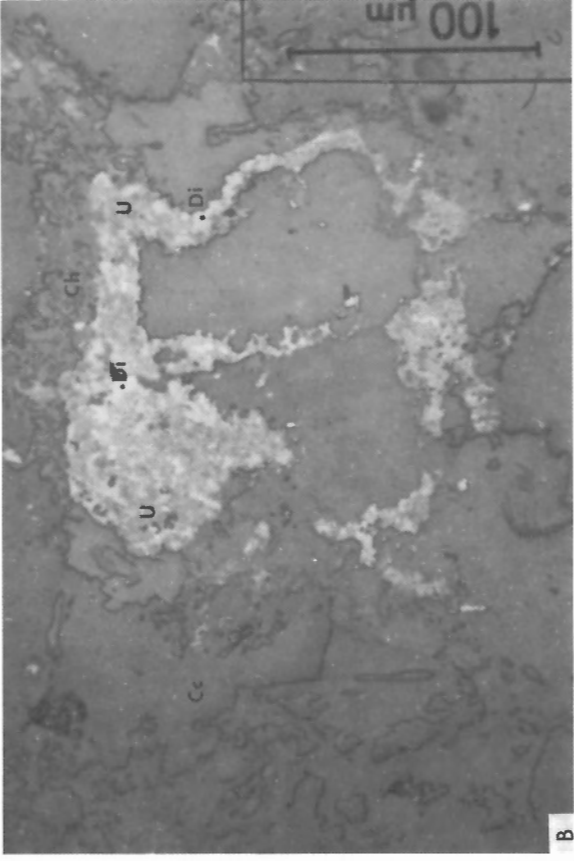


**Plate 31**

Photomicrograph of extremely fine grained interstitial mats and colloform pitchblende (P) associated with interclastic assemblages of chlorite (Ch) and calcite (Cc). Digenite (Di) is present as discrete grains and as extremely fine wispy grains (white areas) in grey pitchblende mats, red altered zone, occurrence 9, reflected light. (GSC 203592-G)

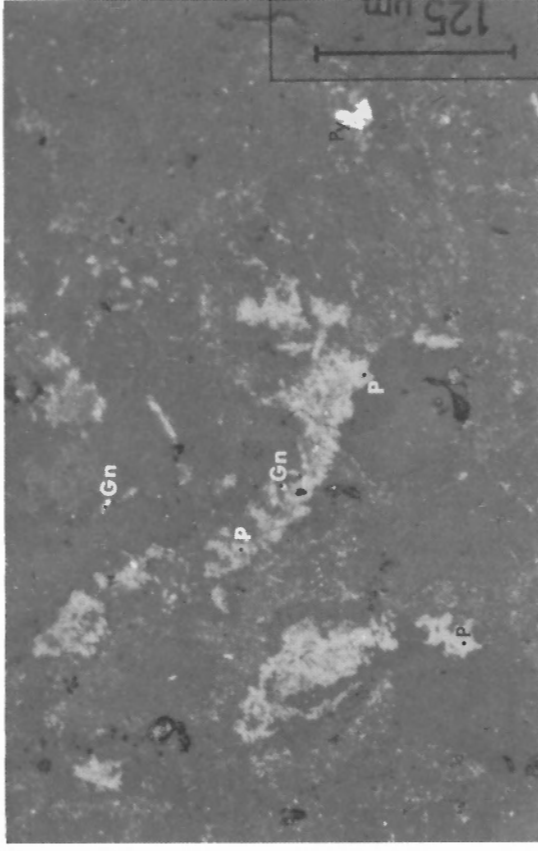


**Plate 32**

Photomicrograph of interstitial wispy pitchblende (P) associated with very fine grained anhedral galena (Gn) and subhedral pyrite (Py), pink altered zone, occurrence 10, reflected light. (GSC 203592-H)

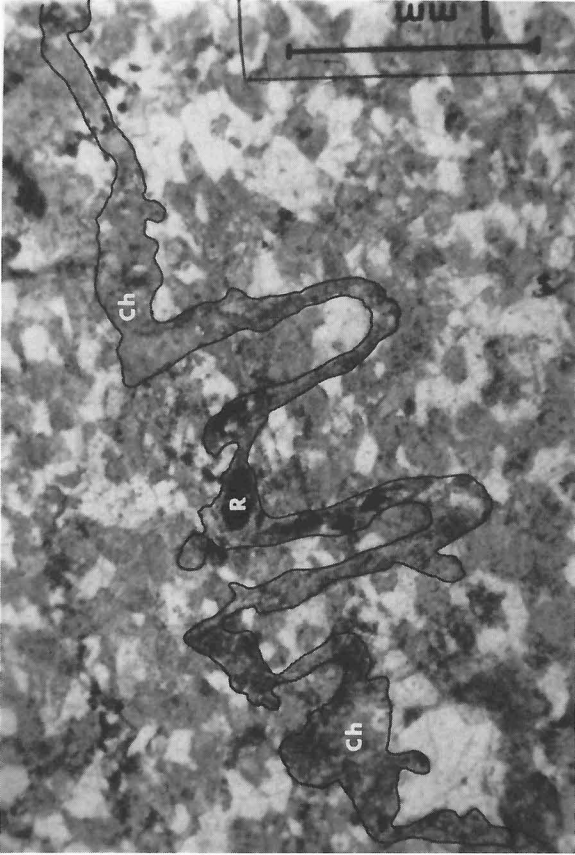


**Plate 33**

Photomicrograph of tortuous chloritic stylolitic structure, chlorite variety clinoclone (Ch), with anatase aggregate (R), pink altered chlorite bearing arkose, occurrence 10, transmitted light. (GSC 203592-I)

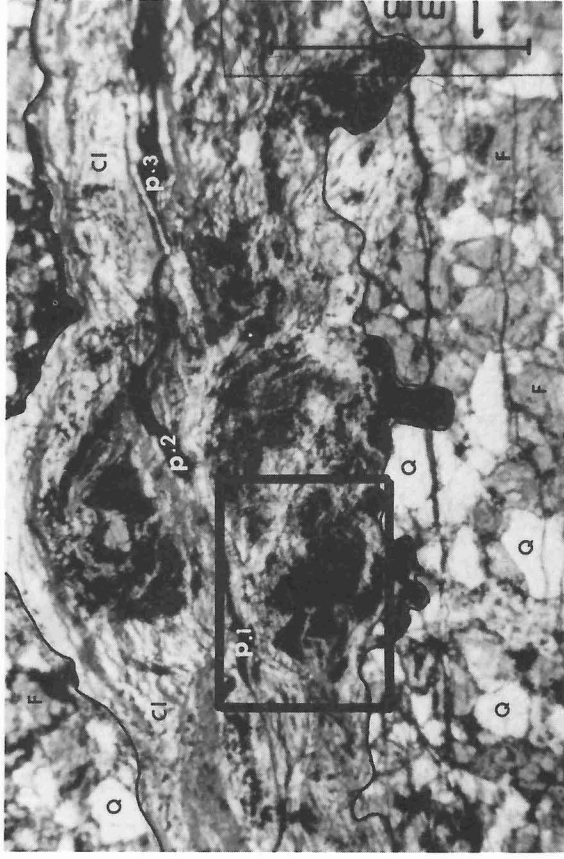


**Plate 34**

Photomicrograph of complex clay-bearing stylolitic structure from the pink altered zone, occurrence 10, transmitted light. The black outline marks the limit of the illitic clay (Cl) stylolite within a chalcopyrite-pyrite-bornite bearing altered arkose. Host arkose consists of quartz (Q) and feldspar (F) and chlorite. Opaque areas represent knots of pitchblende. The dots labelled P1,2,3 are the locations of analyzed veinlet pitchblende listed in Table 7, grains 1,2,3, respectively. Detail of the rectangular area is shown in Plates 35 and 36. (GSC 203592-J)

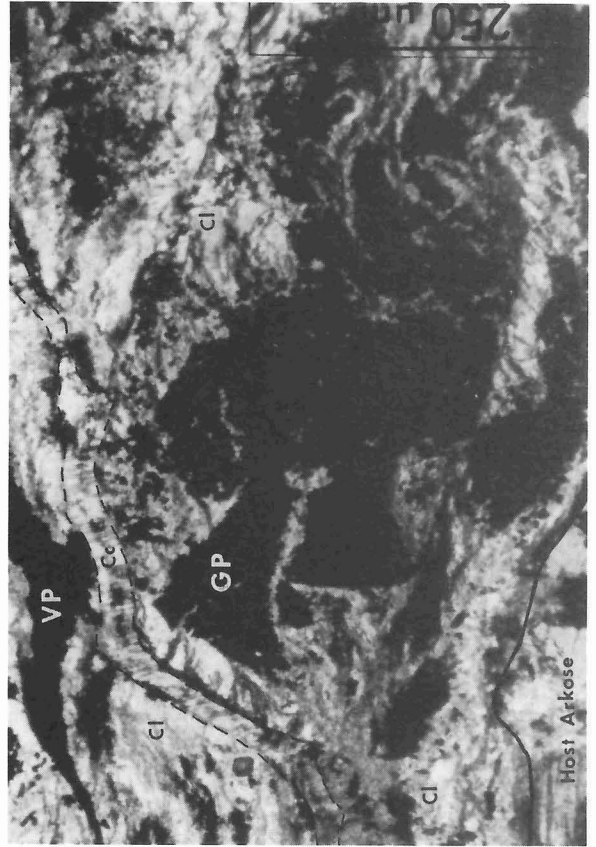
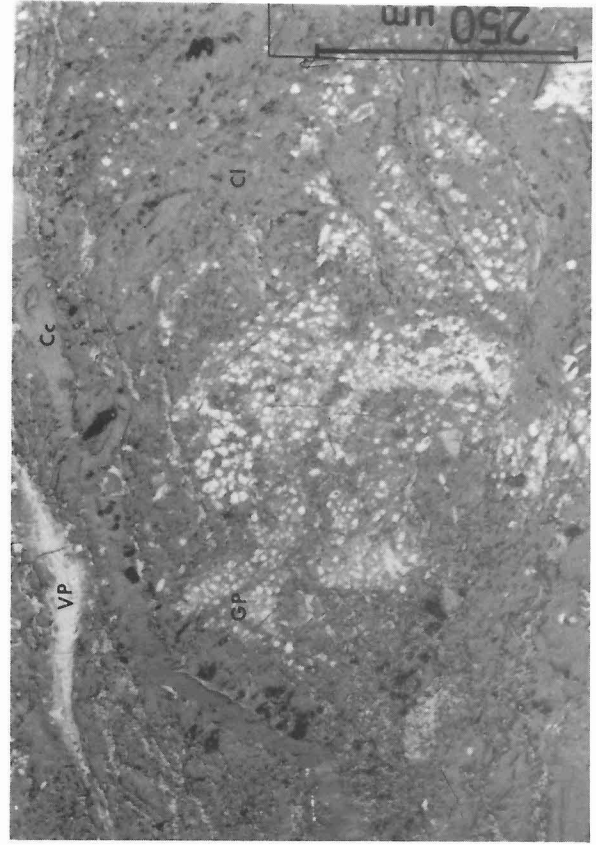


**Plate 35**

A. Photomicrograph of granular (GP) and veinlet (VP) pitchblende varieties hosted within an illitic (Cl) stylolitic structure. Note the subhedral form of the granular pitchblende knots. Calcite (Cc) veinlet crosscuts stylolite, occurrence 10, transmitted light. (GSC 203592-K)



B. Photomicrograph of Plate 35A showing the very fine grained granular pitchblende (GP) and veinlet pitchblende (VP), reflected light. (GSC 203592-L)

Table 5

Electron microprobe analyses of illitic clay associated with Kazan type mineralization, occurrence 10

Analyses	1	2	3	4	5	6
SiO <sub>2</sub>	46.35	46.30	46.48	47.10	41.14	42.83
TiO <sub>2</sub>	0.15	0.20	0.10	0.08	0.31	0.27
Al <sub>2</sub> O <sub>3</sub>	28.55	26.86	27.99	29.02	22.65	25.78
Cr <sub>2</sub> O <sub>3</sub>	0.08	0.01	0.03	0.04	0.07	0.05
FeO	5.25	5.75	4.85	4.47	7.03	4.67
MnO	0.08	0.09	0.03	0.00	0.22	0.08
MgO	2.40	2.57	2.22	2.25	2.61	1.99
CaO	0.13	0.50	0.21	0.23	2.71	0.76
Na <sub>2</sub> O	0.59	0.73	0.79	0.83	1.06	0.48
K <sub>2</sub> O	4.59	8.02	7.67	8.08	7.95	8.02
UO <sub>2</sub>	N.A.	N.A.	N.A.	N.A.	10.1	5.3
Total	88.17	91.03	90.37	92.10	95.85*	90.23*
Structural formula based on 20 oxygen and 4(OH)						
Si	5.9773	5.9560	5.9635	5.9269		
Al <sup>+4</sup>	2.0227	2.0440	2.0365	2.0731		
Al <sup>+6</sup>	2.3181	2.0297	2.1975	2.2323		
Ti	0.0145	0.0193	0.0096	0.0076		
Fe	0.5662	0.6186	0.5204	0.4704		
Mn	0.0087	0.0098	0.0033	0.0000		
Mg	0.4613	0.4927	0.4245	0.4220		
Ca	0.0180	0.0689	0.0289	0.0310		
Na	0.1475	0.1821	0.1965	0.2025		
K	0.7552	1.3162	1.2555	1.2972		
OH(Calc)	4.0000	4.0000	4.0000	4.0000		
<p>*Due to the very fine grain size of the granular pitchblende (Table 6, analyses 4,5,6,7; Plates 34,35,36) the high UO<sub>2</sub> contents may be due to submicron size pitchblende inclusions within the hosting illitic clay.</p> <p>N.A. = Not analyzed</p> <p>Analyst: A.G. Plant</p>						

Table 6

Electron microprobe analyses of pitchblende and U-Ti phases associated with Kazan type mineralization

Analysis	1	2	3	4	5	6	7	8	9	10
Texture	Impregnated pitchblende and U-Ti phase			Granules within stylolite				Veinlets within stylolite		
Occurrence	9	9	10	10	10	10	10	10	10	10
Wt %				Grain 1	Grain 2	Grain 3	Grain 4	Grain 1	Grain 2	Grain 3
U	41.6	61.2	74.3	64.6	64.2	65.1	63.2	73.7	73.4	73.1
Pb	0.8	2.1	2.1	17.1	17.2	17.1	14.3	6.3	6.4	6.3
Th	0.00	0.00	0.00	N.D.	N.D.	N.D.	N.D.	N.D.	N.D.	N.D.
Ca	1.0	2.3	2.9	1.4	1.3	1.4	1.5	2.9	2.7	3.1
Ti	15.2	2.6	0.5	0.2	0.2	0.2	2.9	0.0	0.1	0.1
Fe	0.00	0.1	1.3	0.3	0.2	0.2	0.5	0.5	0.4	0.4
Si	5.2	3.8	0.6	N.A.	N.A.	N.A.	N.A.	N.A.	N.A.	N.A.
Al	1.0	0.4	0.1	N.A.	N.A.	N.A.	N.A.	N.A.	N.A.	N.A.
Zr	0.3	0.00	0.2	N.A.	N.A.	N.A.	N.A.	N.A.	N.A.	N.A.
Cu	2.8	3.8	N.D.	N.A.	N.A.	N.A.	N.A.	N.A.	N.A.	N.A.
S	0.3	0.7	0.00	N.A.	N.A.	N.A.	N.A.	N.A.	N.A.	N.A.
Total	68.20	77.20	82.40	83.6	83.1	84.0	82.4	83.4	83.0	83.0

N.D. = Not detected

N.A. = Not analyzed

Analyst: A.G. Plant

within the fine grained clay or from incorporation of uranium into the clay structure. The restriction of pitchblende and uraniferous titanates to the subhedral outlines of opaque knots suggests that this assemblage may have resulted from the alteration of subhedral pitchblende deposited in chloritic stylolites. The chloritic stylolites were subsequently subjected to argillic alteration and the development of uraniferous titanates and perhaps uraniferous illitic clay. These complex mineral clusters can be crosscut by pyrite-pitchblende-calcite veinlets (Plates 35A, B; 36A, B).

The cherry red altered zones are enclosed within the pink altered zone but occur near the outer margin of the alteration envelopes. These zones are roughly lensoid in plan and contacts though gradational from the pink altered arkose transect bedding. The metallic assemblage of the cherry red altered zone is digenite-covellite-native silver and copper, the abundance of native copper characterizes this zone. Native copper is present as irregular grains occupying interstitial areas with carbonates, chlorite, anatase and barite (Plate 37). Locally native copper is concentrated within silty laminae as the sole copper mineral but is associated with digenite-covellite in the sandy beds. Bornite is present but rare with the latter assemblage. Pitchblende and complex uraniferous phases display textures similar to those in the pink altered zone. Pitchblende mantles on subhedral anatase grains and geoid-like structures are common. Similarly very fine grained galena is associated with the interstitial pitchblende mats that mantle sulphide minerals and anatase. Secondary minerals identified from the mineralized and altered zones of occurrences 7, 8, 9, 10 and 11 include malachite, uranophane, boltwoodite, francevillite-curienite series, and minor brochantite.

Electron microprobe analyses of uranium bearing oxides from various textural associations within the altered arkoses contain varying abundances of the major elements U, Pb and Ca (Table 6). Analyses of pitchblende from the impregnated textural variety of occurrences 9 and 10, contain 61.2 and 74.3 weight per cent U with low Pb levels of 2.1 weight per cent accompanied by minor and trace amounts of Ca, Ti, Fe, Si, Al and Zr (analyses 2, 3, Table 6). Copper contents of a uraniferous titanate and pitchblende, analyses 1 and 2, respectively, are 2.8 and 3.8 weight per cent. The extremely fine intergrowths of these phases with covellite-digenite suggest that the copper may be present as submicron sized inclusions. The minor and trace element abundances of the above pitchblendes are similar to pitchblende from the Beaverlodge district (Morton and Sassano, 1972).

Analyses of the textural varieties of pitchblende from a stylolitic structure from occurrence 10 exhibit different abundances of the major elements U, Pb and Ca. The very fine grained anhedral granular pitchblende set in the illitic clay and uraniferous illitic clay contain greater Pb abundances (14.3-17.2 wt. %) compared to pitchblende from the pyrite-calcite veinlets (6.3-6.4 wt. % Pb) which crosscut the former. Similarly the calcium content of the very fine granular pitchblende is lower (1.3-1.5 wt. % Ca) than the veinlet pitchblende (2.7-3.1 wt. % Ca). Calcium exhibits a direct relationship with uranium and is probably substituting for uranium in the pitchblende structure.

Oxide proportions of the elements analyzed yield low totals suggesting the pitchblende may be hydrous. The systematic variation in the U, Pb and Ca contents of the

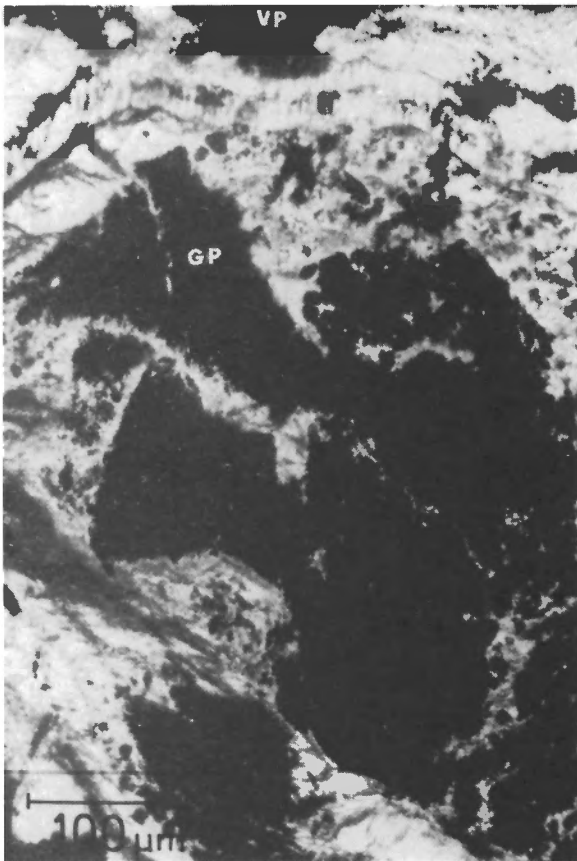


Plate 36A

Photomicrograph of opaque granular pitchblende (GP) knots and veinlet pitchblende (VP), occurrence 10, transmitted light. (GSC 203592-M)

pitchblendes within the stylonitic structure and the cross-cutting relationship exhibited by the pitchblende associated with pyrite-calcite-veinlets indicate that remobilization has occurred. Furthermore comparison of Pb abundances in stylonitic pitchblendes to those in impregnated pitchblendes may indicate that several generations of uranium deposition are present in the altered arkose. Very fine grained galena associated with the impregnated pitchblende may explain the low Pb content of this textural variety (analyses 2 and 3, Table 6).

#### Geochemistry of the Kazan Type Mineralization

Whole rock chemistry and trace element abundances were obtained on Kazan arkose from the following environments: 1) unaltered arkose distant from known mineralization (Appendix 2G), 2) altered arkose from the various alteration zones associated with mineralization peripheral to dyke complexes (Appendix 2C, D, E), and 3) altered arkose adjacent to the Martell intrusions with which no mineralization is associated (Appendix 2F). The analytical data were used to establish background values with which to compare altered and mineralized arkose and to document any variation across the alteration envelope.

#### Sodium and Potassium

$\text{Na}_2\text{O}/\text{K}_2\text{O}$  ratios for the fluvial crossbedded arkose range from 0.6-1.96 whereas ratios from two giant cross

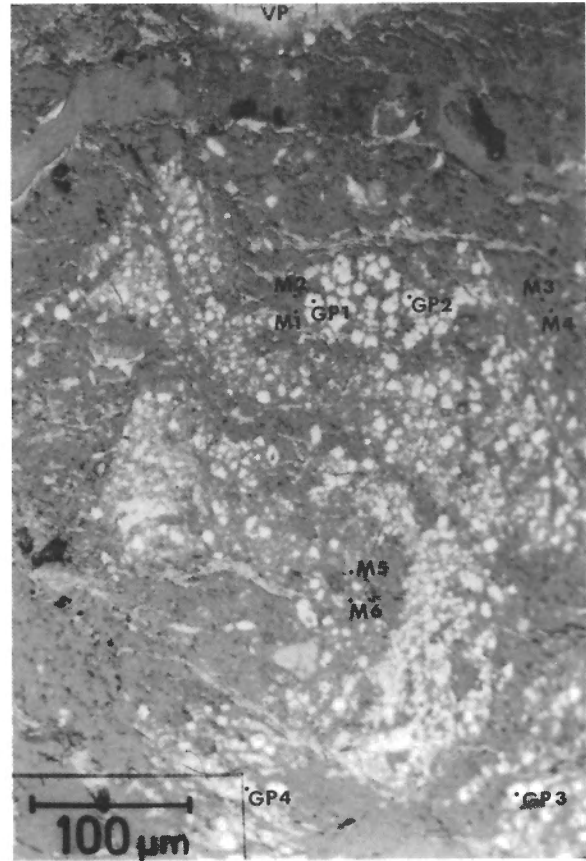


Plate 36B

Photomicrograph of Plate 36A showing veinlet pitchblende (VP) and granular pitchblende (GP) set in illitic clay. The grains marked GP1,2,3,4 are the locations of analyzed granular pitchblendes listed in Table 6, Grains 1,2,3,4 respectively. The grains marked M1,2,3,4,5,6 are the locations of analyzed illitic clay (Table 5), hosting granular pitchblende, reflected light. (GSC 203592-N)

bedded units are 2.6 and 17.3. Mineralized occurrences 7, 9, 10 and 11 occur in giant crossbedded arkose and have  $\text{Na}_2\text{O}/\text{K}_2\text{O}$  ratios ranging from 1.95 to 35 with an average of 3.7. The higher values of the giant crossbedded units interpreted as eolian deposits compared to thinly bedded arkosic units interpreted as fluvial deposits suggest that the giant crossbedded units may have acted as a paleoaquifer within the Kazan Formation permitting more extensive albitization due to a higher primary permeability.

Albite is the major silicate cementing the arkose whereas carbonate is the major non-silicate cementing mineral. Whole rock  $\text{Na}_2\text{O}$  contents are a reflection of the detrital plagioclase abundance and the degree of authigenic albitization. The variation of  $\text{Na}_2\text{O}$  vs.  $\text{CO}_2$  is inverse as shown by Figure 10. This relationship along with the petrographic textures supports the interpretation that carbonate occupies the interstitial volumes not filled by authigenic albite. This inverse relationship is a factor controlling the quantity of epigenetic silver-copper-uranium mineralization within the thermally altered aureoles.

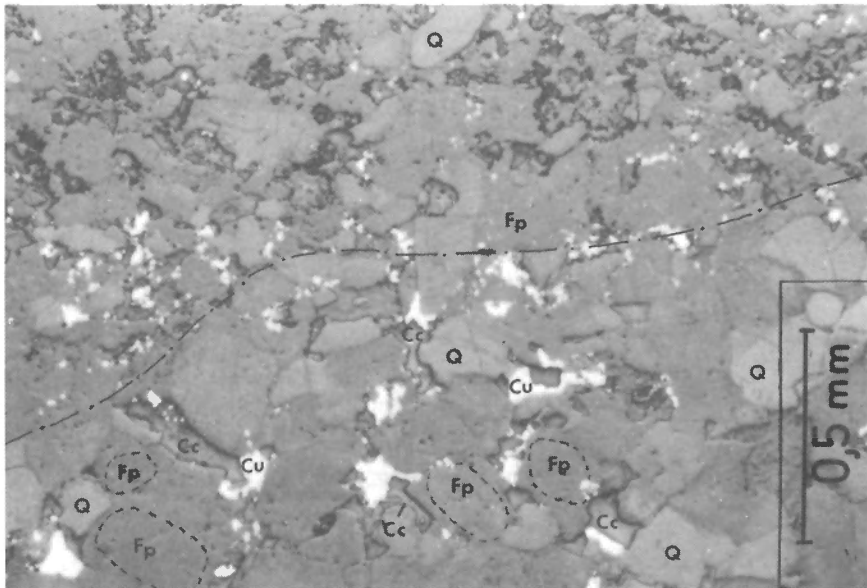


Plate 37A

Photomicrograph of native copper (Cu) interstitial to quartz (Q) and hematite impregnated feldspar (Fp). Native copper associated with very fine grained interstitial calcite (Cc) and chlorite, occurrence 9, reflected light. Dashed-dot line represents the interface between silt laminae and sand bed. (GSC 203592-O)

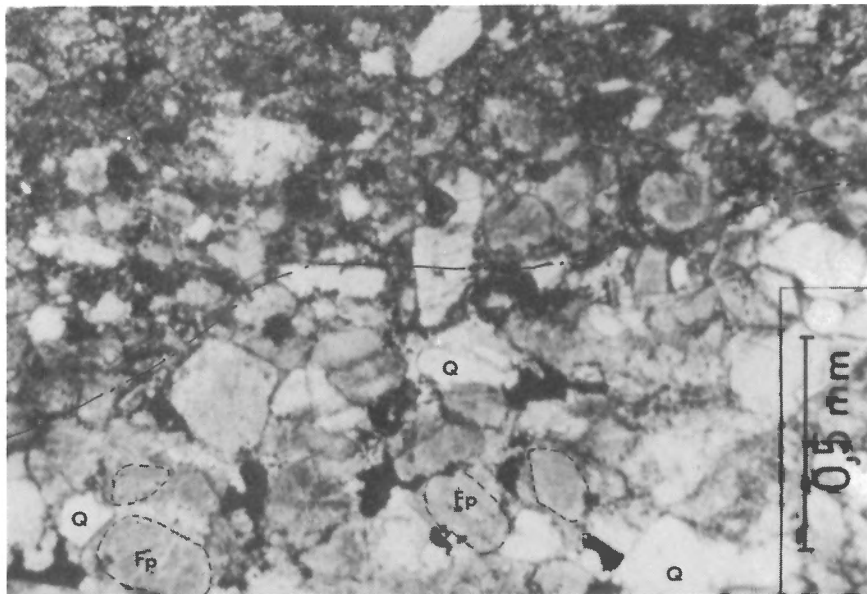


Plate 37B

Photomicrograph of Plate 37A showing the interstitial distribution of native copper amongst detrital quartz (Q) and feldspar (Fp). Note the euhedral hematitized albite overgrowths on rounded hematitized feldspar cores. (GSC 203592-P)

## Iron

The distribution of ferric and ferrous iron was determined on most samples of Kazan arkose. However only total iron,  $Fe_2O_3_T$ , is reported for some samples due to difficulty in determining FeO by titration. Inability to determine an accurate titration point may be due to the presence of a strong reducing agent possibly uranium oxide or native metal (copper). The principal alteration superimposed upon the Kazan arkose by the thermal regimes of the dyke complexes is leaching, remobilization and recrystallization of the iron oxide cement. This has resulted in distinctive colour zones and textures.

The oxidized state of the unaltered pink to maroon Kazan arkose is displayed by the greater ferric than ferrous oxide contents (Appendix 2G). The white altered zone of thermal aureoles is reduced containing greater FeO abundances with respect to  $Fe_2O_3$  which contrasts with the oxidized state of the pink and red altered zones (Appendix 2C, D, E). Calculated as  $FeO_T$ , the total iron content increases across the alteration envelope from 0.73 weight per cent in the white altered zone, 0.99 weight per cent in the pink altered zone to 1.27 weight per cent in the red altered zone compared with 0.90 weight per cent for the unaltered Kazan arkose. However no relationship exists across the alteration envelopes between  $FeO_T$  and uranium, copper, molybdenum, vanadium or silver. The lack of a relationship between iron and the other metals may be due to continued iron redistribution by groundwater after deposition of the uranium-copper-silver mineralization.

## Magnesium

Within the white altered zone, the Mg-bearing minerals are dolomite and clinocllore; the latter is minor in abundance compared to dolomite. The increased dolomite content is reflected as higher MgO values in the white alteration zone compared to the pink and cherry red zones (Appendix 2C, D, E).

## Carbonate

The silver-copper-uranium mineralization occurs principally as impregnated concentrations interstitial to framework grains and associated with recrystallized cements, chlorite and anatase. The concentration of copper has a weak positive correlation with  $CO_2$  (Fig. 11). This relationship along with the  $Na_2O$  vs.  $CO_2$  correlation suggests that the arkosic beds not sealed off by authigenic albite overgrowths contained sufficient interstitial permeability to permit fluid migration and ore deposition.



## Copper

The copper contents of the unaltered Kazan arkose range from 6 to 46 ppm with an average value of 17 ppm which was taken as a background value for the Kazan arkose. The distribution of copper through the white, pink and red altered zones is variable and overlapping however the copper content increases horizontally away from the dyke complex as shown by 7-620 ppm in the white zone, 7-13 000 ppm in the pink to 20-18 000 ppm within the cherry red zone (Appendix 2C, D, E).

## Silver

Silver analyses of unmineralized arkose indicate that the background abundance is below the 0.1 ppm detection limit. Silver has been concentrated within the thermal envelope with contents varying from <0.1 ppm to 20 ppm.

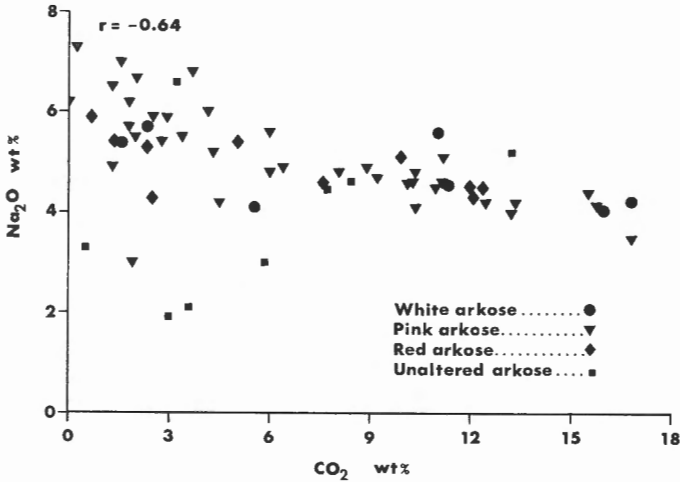


Figure 10.  $\text{Na}_2\text{O}$  vs.  $\text{CO}_2$  for altered and unaltered arkose, Kazan type mineralization.

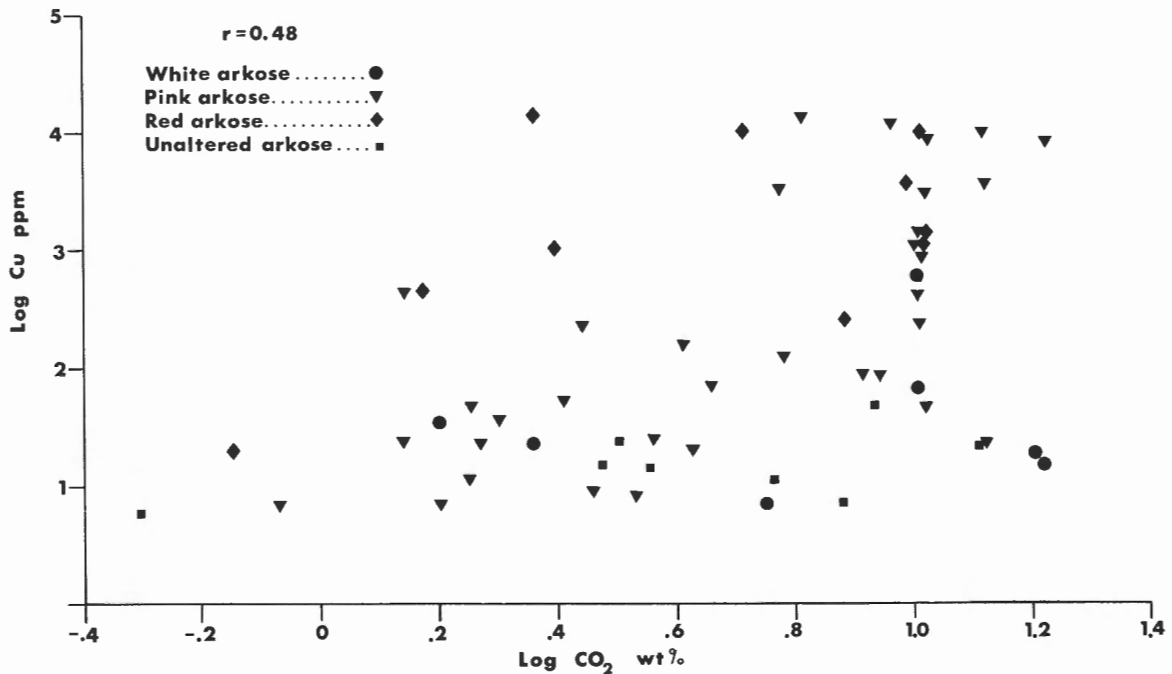


Figure 11.  $\text{Log Cu}$  vs.  $\text{log CO}_2$  for altered and unaltered arkose, Kazan type mineralization.

The distribution of silver increases across the alteration envelope in the same manner as copper (Appendix 2C, D, E). The distribution pattern of silver vs. copper (Fig. 12B,  $r = 0.83$ ) suggests that these elements acted similarly under the physiochemical parameters controlling metal deposition.

## Uranium

The uranium contents of eight unaltered Kazan arkose samples range from 0.9 to 4.1 ppm, with an average value of 2.0 ppm taken as back-ground. The uranium contents of the various colour altered zones are variable and overlapping between zones but increases away from the dyke complex: 0.6-12.0 ppm in the white zone, 1.2-1470 ppm in the pink zone to 820-2820 ppm within the cherry red zone (Appendix 2C, D, E). Uranium is associated with several elements across the mineralized aureole. The high correlation of U vs. Pb (Fig. 13D;  $r = 0.86$ ) reflects the association of finely disseminated galena with the interstitial uranium phases and minor lead contents of the uranium bearing phases. Similarly the variations of U vs. Cu (Fig. 13A) and Ag vs. U (Fig. 12A) reflect the textural relation of uranium phases mantling the interstitial copper sulphides and associated native silver.

## Vanadium

No vanadium bearing minerals were identified; however the arkosic beds within the thermal aureoles have anomalous vanadium abundances well above the background level set for the Kazan arkose (<10 ppm, Appendix 2G). Vanadium increases across the alteration envelope from 10-51 ppm in the white zone, through <10-160 ppm in the pink zone to 25-310 ppm within the cherry red zone. The distribution of vanadium exhibits a direct relationship with uranium (Fig. 13C,  $r = 0.63$ ) and no relationship with copper ( $r = 0.38$ , not shown).

## Molybdenum

Background molybdenum abundances for the unaltered Kazan arkose are 1-2 ppm. Within the alteration envelope,

molybdenum contents range from background values to 154 ppm with the higher abundances occurring with higher uranium contents in the pink and cherry red zones (Fig. 13B). Molybdenum shows a direct correlation with uranium ( $r = 0.57$ ) but shows no relation with copper distribution ( $r = 0.26$ , not shown).

#### Zinc

Unmineralized Kazan arkose contains a wide range in zinc abundances (3-55 ppm). The distribution of zinc within the thermal envelopes displays an even larger distribution, 4-124 ppm. Zinc shows no correlation with the other metals even though the average value for the altered arkosic zone (35 ppm) is one and a half times that of the unmineralized Kazan (21 ppm).

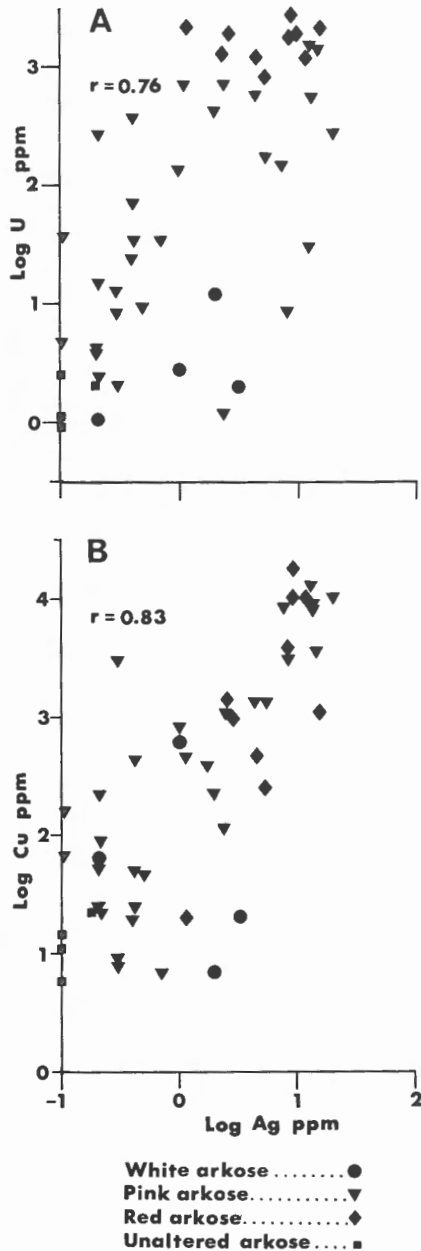


Figure 12. Log U, log Cu vs. log Ag for altered and unaltered arkose, Kazan type mineralization.

#### Barium

Barium contents of the thermal aureole show a wide distribution from 85-4900 ppm reflecting the erratic distribution of interstitial barite cement. Barium contents of the unaltered Kazan exhibit a wide range (430-1900 ppm) but lower in absolute values compared to the thermal aureoles.

#### Fluorine

No fluorite has been identified associated with the silver-copper-uranium mineralization. Three high grade uranium specimens from occurrences 7, 9, and 11 contain very low levels of fluorine, 84, 93, and 101 ppm respectively (Appendix 2E). This is in contrast to the high fluorine contents 455-2710 ppm from the dyke complexes associated with these thermal aureoles (Appendix 2B).

#### Geochemistry of the Altered Kazan Arkose Adjacent to the Martell Intrusions

The contact aureoles within the Kazan arkose adjacent to the Martell intrusions exhibit the following features which are similar to the altered rocks peripheral to the dyke complexes: 1) a zonal distribution of colour-altered rocks except that cherry red altered zones were not observed, 2) recrystallization and remobilization textures developed in the primary cements, and 3) the development of silicates and oxides in response to the thermal anomalies of the intrusions. The contact aureoles exhibit carbonate contents ranging from 0.0-7.5 weight per cent  $\text{CO}_2$  and very high  $\text{Na}_2\text{O}/\text{K}_2\text{O}$  ratios ranging from 3.6 to 42 (Appendix 2F). Petrographic textures and chemical data suggest that extensive albitization may have significantly reduced the original permeability and porosity of the Kazan arkose to later fluid migration.

Uranium contents range from 1.7 to 10.7 ppm and are complemented by above background abundances of copper and vanadium similar to the relationships in the mineralized arkose associated with dyke complexes. Barium levels range from 89-420 ppm, significantly lower than either the unaltered Kazan arkose or the mineralized zones associated with the dyke complexes. Zinc levels in the Martell contact aureoles (6-46 ppm) are comparable to those of the unaltered Kazan (5-55 ppm) but less than the zinc contents (4-124 ppm) in the dyke aureoles. The distribution of ferrous and ferric iron with the Martell contact aureoles are comparable to the pink altered zones peripheral to the dyke complexes.

#### Genetic Model for the Kazan Type Mineralization

A genetic model for the Kazan type mineralization is governed by three fundamental factors: 1) a source rock, 2) a mechanism capable of remobilizing and transporting the elements, and 3) a structural or chemical environment for deposition of the transported elements. These factors should account for the observed physical and chemical characteristics of the uranium-copper-silver occurrences in the Kazan Formation: 1) the stratigraphic distribution of the occurrences, 2) their spatial relationship to intrusive complexes, and 3) the variation and distribution of elements within the occurrences.

Multivariate statistical analysis of the chemical data from 54 samples of mineralized and altered Kazan arkose was undertaken to define relationships among the geochemical variables. Factor analysis expresses associations among original variables in terms of a smaller number of new variables. Results of R-mode factor analysis indicate two interrelated metal associations: U-Pb-Ag-V-Mo-Cu-Fe and Cu-Ag. These two elemental associations and the textural relationships of the sulphides and uranium oxides in the altered arkose suggest a two stage process for the silver-copper-uranium mineralization.

Certain inferences concerning the groundwater system prevailing in the redbed sequence can be made from the authigenic minerals cementing the Kazan Formation. The extensive development of authigenic albite on detrital feldspar and the lack of diagenetic alteration of the detrital feldspar indicate that the groundwater flowing through the Kazan Formation was most probably neutral to alkaline (Garrels and Christ, 1965). Carbonate is a ubiquitous cement throughout the Kazan Formation. Garrels and Christ (1965) stated that water in contact with  $\text{CaCO}_3$  is alkaline at pH 8 depending on the partial pressure of  $\text{CO}_2$ . In addition, the presence of hematite cement through the lower redbed sequence suggests the groundwater was oxidized. Therefore the various authigenic cements suggest that the groundwater system flowing through the Kazan Formation was neutral to alkaline and oxidizing.

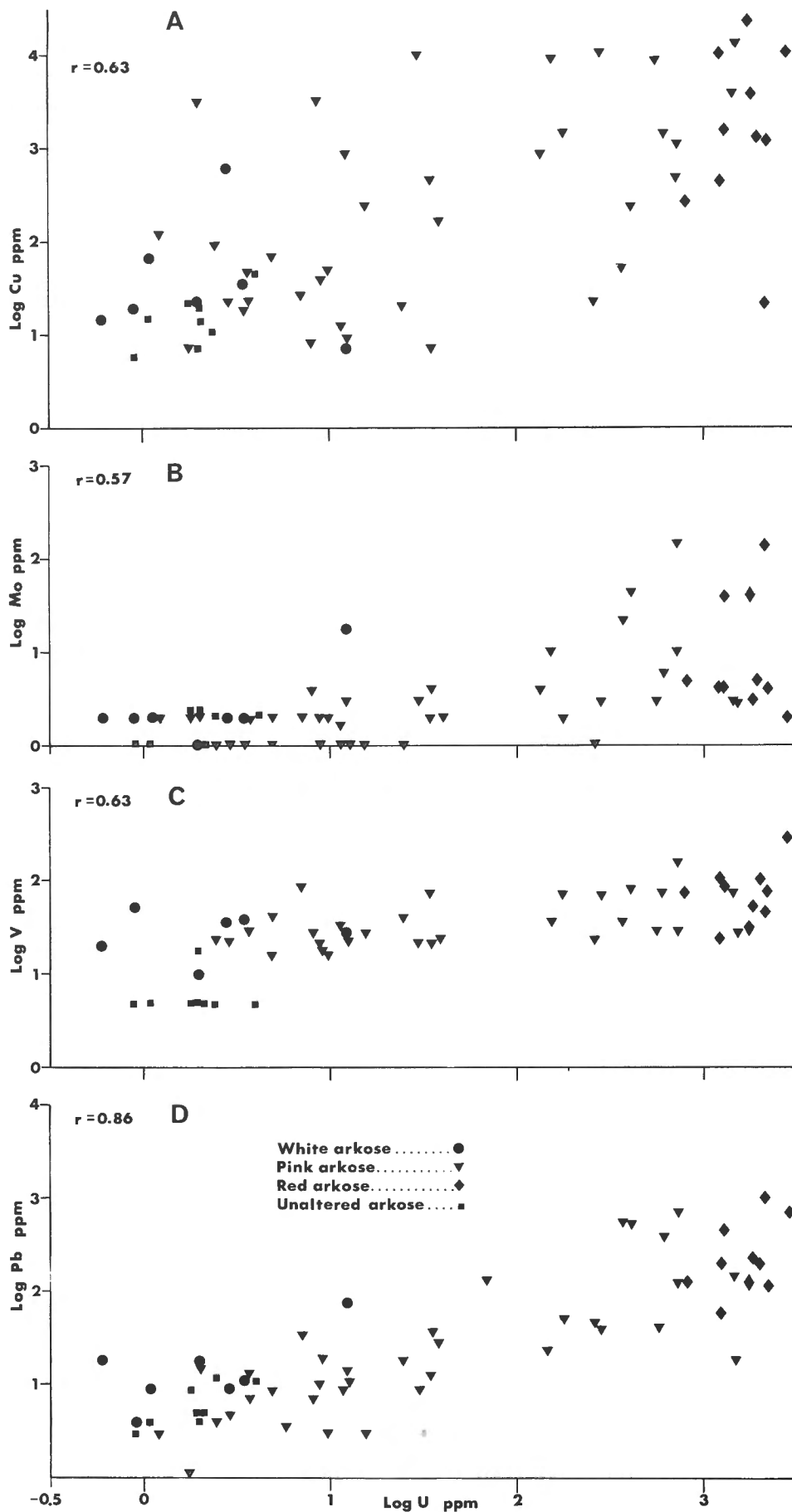
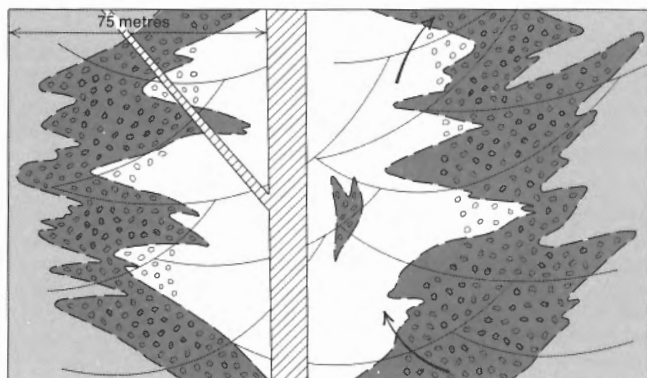
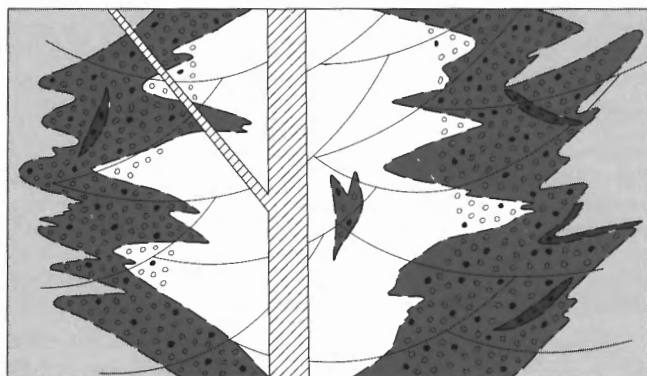


Figure 13. Log Cu, log Mo, log V, log Pb vs. log U for altered and unaltered arkose, Kazan type mineralization.



Phase 1. Hydrothermal alteration and Cu-Ag deposition associated with a convective circulation cell.



Phase 2. Uranium deposition along redox front during renewed basinward groundwater flow.

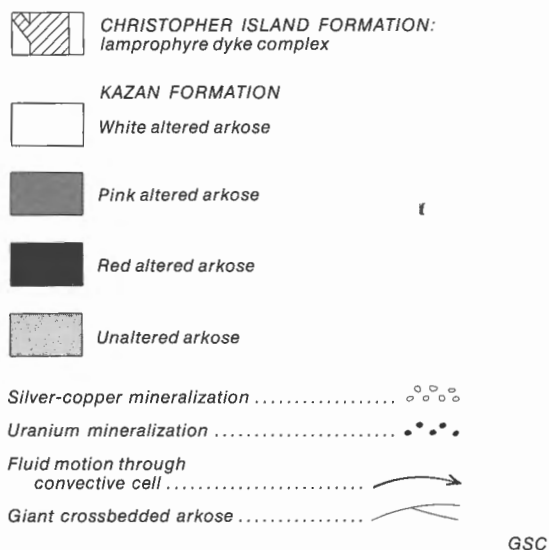


Figure 14. Schematic cross-sectional model for the Kazan type U-Cu-Ag mineralization.

The uranium-copper-silver mineralization is situated within thermal aureoles that were created during emplacement of the Christopher Island intrusive complexes. The emplacement of magma into water-bearing supracrustal rocks results in fluid convection due to the thermal anomaly. Convecting hydrothermal systems created by cooling plutons are controlled by the host rock permeability, distribution of permeable horizons, pluton size and level of emplacement (Norton and Knight, 1977; Cathles, 1977; Norton, 1978).

Active geothermal systems such as Tuscany, Italy and the Wairakei geothermal area, New Zealand demonstrate the capacity of volcanic-plutonic regions to circulate a vast volume of fluid with dissolved metal components through permeable rocks for distances up to tens of kilometres (Elder, 1965, 1977; Ewers, 1977).

The alkaline dykes and Martell laccoliths and sills are interpreted as hypabyssal intrusions emplaced within a supracrustal sequence estimated at 1000-1500 m thick. Authigenic cements in the Kazan arkose and pervasive hydration and carbonatization of the Christopher Island volcanic rocks indicate the presence of groundwater interactions on the supracrustal sequence. Thus the Christopher Island dyke complexes were interpreted to have been intruded into water-bearing sediments. Emplacement of alkaline magmas into water-bearing sedimentary rocks would create differential heating of connate water and result in the development of convective circulation cells peripheral to the dyke complexes (Fig. 14, phase 1).

The silver-copper-uranium mineralization occurs near the base of the Kazan Formation and is commonly hosted within the giant crossbedded arkose. These arkoses interpreted as eolian deposits may have represented a very permeable horizon compared to the thinner bedded fluvial arkose which has a greater siltstone-mudstone component. Interbedding of units with differential permeability may be analogous to sandstone uranium deposits of the southwest United States where the sandstone aquifer is bounded by impermeable claystone horizons (Harshman, 1972).

Where the permeability was greatest, in the giant crossbedded units, the effects of the heated groundwater would be the widest. The geochemical effect on the Kazan arkose was the creation of the reducing to oxidizing zones away from the dyke, recrystallization of the carbonate cements and crystallization of chlorite throughout the thermal aureole. Associated with these variations, copper-iron and copper-sulphides and silver were deposited within the outer segments of the thermal aureoles in response to varying temperature, Eh and possibly pH conditions (Fig. 14, phase 1). Thus the presence of copper and iron-copper sulphides would create a suitable reducing environment for later uranium concentrations (Fig. 14, phase 2).

The source rock for uranium concentrated within the Kazan arkose could have been 1) Apehbian and Archean gneisses which were the provenance for the plagioclase-rich arkose, 2) the lamprophyre dyke complexes, or 3) the overlying Christopher Island volcanic rocks.

The basement complex along the southern margin of the Baker Lake basin consists of belts of Archean(?) meta-volcanic and metasedimentary rocks with a felsic ortho- and paragneiss complex which were weakly metamorphosed during the Late Apehbian. Allanite and uranothorite bearing pegmatites, gneiss and the presence of disseminated uranium-sulphide mineralization within leucocratic gneiss indicate that uranium and thorium were present and were remobilized during Late Apehbian deformation and metamorphism. Thus it is possible that the basement complex may have contributed uranium as detrital minerals or in solution during South Channel-Kazan sedimentation. However, considering the age (Archean and Apehbian) of the source rocks and their lithologies, granulites, metavolcanic rocks and felsic gneiss complexes, the redbeds are not interpreted as a significant source of uranium.

Uranium and thorium are characteristically enriched in alkaline rock series compared to subalkaline series. The partitioning of the radioactive elements during magma differentiation has been attributed to the volatile component of a magma, in particular the halogens

(Sorensen, 1977; Alder, 1977). Tilsley (1978) suggested that degassing of a uranium-rich magma during emplacement into a shallow intrusive environment can partition uranium into the gaseous magmatic fluids.

The lamprophyre dyke complexes intruding the Kazan sediments are xenolithic but are not characterized by brecciated country rocks, typical of fluidized breccia pipe and dyke complexes. If uranium was added to the Kazan arkose through gaseous transfer during intrusion and subsequent cooling, the metal association in the mineralized Kazan arkose is not similar to the Ti-Mo-Zr-Th-U elemental association typical of fluidized breccia structures such as at Poços de Caldas, Brazil (de Andrade Ramos and Fraenkel, 1974). In addition, the absence of a fluorine association with the Kazan mineralization based on petrography and limited chemical analyses is in contrast with the common relationship present in the Brazilian breccia structures. Thus based on field and geochemical relationships, a gaseous transfer of uranium into the adjacent arkose is not interpreted to be a significant process in the formation of Kazan type mineralization.

The Christopher Island volcanic rocks within the Baker Lake basin contain anomalous uranium abundances and represent a potential source rock for uranium concentrations in the underlying Kazan arkose. The subaerial alkaline potassic-rich volcanic lavas of the Christopher Island Formation lie mainly within the trachybasalt-trachyandesite-trachyte compositional fields (Blake, 1980) and are enriched in various incompatible elements including uranium. The intrusions display similar textures, mineralogy and alteration to those of the overlying alkaline lavas described by Blake (1980). Phenocrysts or their altered equivalents from the Christopher Island volcanic and intrusive rocks include biotite/phlogopite, plagioclase, potassic feldspar and less commonly olivine, clinopyroxene and hornblende. These are set in a very fine grained feldspathic groundmass and/or devitrified glass.

A high uranium abundance is a fundamental petrogenic characteristic of alkaline potassic-rich volcanic series. Civetta and Gasparini (1977) reviewed the uranium abundances of various volcanic series and demonstrated that continental potassic alkaline volcanic suites typified by the alkaline lavas from the Roman and Neopolitan volcanic provinces in Italy can contain 5-47 ppm U. Mittempergher (1970) and Locardi and Mittempergher (1971) have documented uranium, thorium, and sulphide occurrences associated with the Quaternary potassic alkaline volcanic rocks of Central Italy. Their estimates of uranium abundances for these alkaline volcanic rocks range from 25-50 ppm. Locardi and Mittempergher (1971) described the relationship of altered and mineralized volcano-sedimentary rocks associated with Pleistocene alkaline potassic volcanism. The mineralized horizons are hydrostatically not stratigraphically controlled and are related to the distribution of the present aquifers. Uranium contents of 3.0 to 13.1 ppm for alkaline mafic and felsic lavas from the eastern Baker Lake basin (Blake, 1980) and 6.1 to 23.9 ppm for dyke and subvolcanic stocks intruding the Kazan Formation (Appendix 2A, B) compare with the uranium abundances of recent alkaline volcanic rocks from Italy. The areal extent and volume of Christopher Island Formation rocks in the eastern Baker Lake basin suggest that the volcanic rocks could have acted as the source rock for epigenetic uranium mineralization within the underlying Kazan arkose.

The distribution of uranium, between various phenocrysts and between phenocryst and groundmass have been investigated by Dostal et al. (1976), Dostal and Capedri (1975), and Nagasawa and Wakita (1968). These studies indicated that uranium is partitioned into the groundmass of volcanic rocks compared to the hosted phenocrysts and is enriched in phenocrysts of biotite and clinopyroxene relative to plagioclase and olivine.

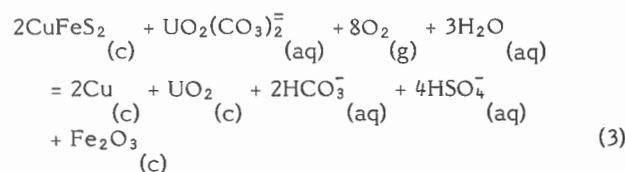
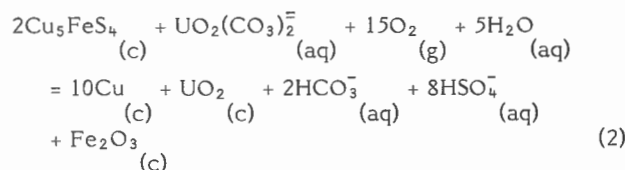
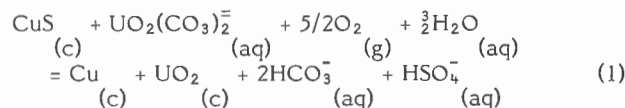
The supracrustal rocks of the Eastern Baker Lake basin have not been affected by regional metamorphism. However the aphanitic porphyritic mafic to felsic volcanic rocks have been propylitized to varying degrees (Blake, 1980) similar to the altered dyke complexes and subvolcanic stocks (Appendix 2A, B). Blake (1980) suggested that the chloritization and carbonatization is an early deuteric process.

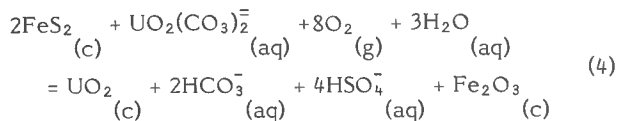
Rosholt and Noble (1969) have demonstrated that uranium can be depleted from the hydrated glassy groundmass of silicic volcanic rocks by groundwater leaching. Capaldi et al. (1971) have documented the effects of early postdepositional zeolitization, hydration and the remobilization of U, Th and Ra from a recent alkalic trachytic tuff in Italy. Uranium is differentially mobilized with respect to thorium in aqueous solutions under oxidizing conditions.

The extensive carbonate and chlorite development in the phenocrysts and glassy to aphanitic groundmass of the Christopher Island volcanic rocks suggests that the altering fluids were probably neutral to alkaline and oxidizing (Garrels and Christ, 1965). Hostetler and Garrels (1962) stated that under oxidizing neutral to alkaline conditions with a high partial pressure of CO<sub>2</sub>, uranium is transported as uranyl dicarbonate and tricarbonatocomplexes. Vanadium exhibits a geochemical behaviour similar to uranium under these conditions. With suitable geochemical parameters prevailing for solution of uranium, vanadium, and possibly molybdenum, these elements would be incorporated into the groundwater system and circulated throughout the South Channel conglomerate, Kazan arkose, and the Christopher Island volcanic rocks.

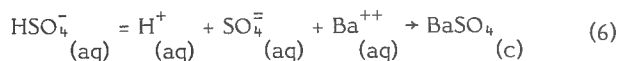
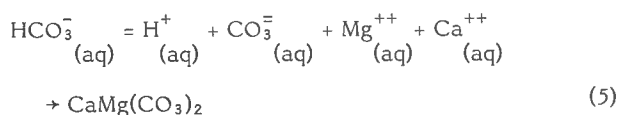
Pitchblende and complex uranium titanates phases mantle epigenetic hydrothermal sulphide and silver mineralization throughout the pink altered zone of the thermal aureoles. The cherry red altered zone within the peripheral portions of the thermal aureoles is characterized by native copper, a high uranium content, and an intense hematite impregnation through the framework silicates and authigenic cements. Native copper coexisting with covellite and/or digenite in the pink and cherry red altered zones is a metastable assemblage (Craig, 1974a). The mineralogical and chemical features of the cherry red altered arkose are interpreted as the product of a redox reaction superimposed upon the pink altered arkose during uranium deposition.

The following empirical equations represent possible reactions between epigenetic sulphide mineralization and uranium-bearing connate groundwaters flowing through the Kazan Formation. These four reactions are suggested to account for the observed metallic mineral assemblages within the pink and cherry red altered arkose:





The following two reactions are suggested to account for the observed cements with the mineralized and altered arkose:



Oxidized aquifer systems with a neutral to slightly alkaline pH range would represent the optimum chemical conditions for the transmission of uranium-bearing connate groundwaters through the Kazan Formation.

The oxidized state of the redbeds suggests a continuous supply of oxidized groundwaters through the Kazan aquifer. Carbonated lavas and calcite cemented redbeds represent an optimum pH environment for the transportation of uranium possibly as uranyl dicarbonate. Thus uranium-bearing alkaline and oxidized connate groundwaters would be stable on migration through carbonate and hematite cemented arkose.

Uranium bearing groundwater, however, entering the reducing environment created by the disseminated epigenetic sulphide concentrations would become unstable. Uranium would be precipitated according to the first four redox reactions. These reactions appear to account for the mineralogical assemblages observed across the alteration envelopes. Within the white altered zone, the low copper content is complemented by low uranium contents both ranging at or near background levels. The increased sulphide content of the pink altered rocks represented a zone of greater reducing potential to the uraniferous groundwater and resulted in higher uranium tenor compared to the white zone. Minor native copper associated with the copper and copper-iron sulphides is interpreted as an oxidation product of the first three redox reactions.

The mineralogical and geochemical features that characterize the cherry red altered arkose are interpreted to result from an intensive oxidation during uranium-bearing groundwater interaction with the pink altered arkose. Several products result from the three redox reactions involving copper and copper-iron sulphides. The high native copper content and uranium content (820-2820 ppm) suggest extensive oxidation of the epigenetic sulphide assemblage. The intensive hematization of framework clasts and authigenic cements is interpreted to result from the liberation of iron derived during oxidation of copper-iron and iron sulphides. Sulphide oxidation is accompanied by the generation of hydrogen carbonate and sulphate complexes. Reaction of these complexes with magnesium, calcium and barium ions (equations 5 and 6) in solution within the groundwater may explain the distribution of high Mg calcite and barite within the mineralized zones. The two varieties of chlorite present within the cherry red altered zone are interpreted to reflect two superimposed processes. The low iron chlorite similar to those of the white and pink zones is thought to have formed during hydrothermal alteration generated during dyke emplacement. The high iron chlorite is interpreted to have formed during ground water interaction with the epigenetic sulphides and is associated with native copper, pitchblende and intensive hematite alteration, all of

which characterize this alteration zone. The geochemical anomalies of molybdenum and vanadium associated with the mineralized zones may result from the scavenging of these elements by hematite, the latter a product resulting from the redox reactions between uranium-bearing groundwater and epigenetic sulphides.

#### COMPARISON OF THE GEOLOGY AND MINERALIZATION OF THE EASTERN BAKER LAKE BASIN AND THE BEAVERLODGE DISTRICT, SASKATCHEWAN

Isolated remnants of several Proterozoic redbed successions occur throughout the Churchill Province. Donaldson (1968) suggested a correlation between the Martin Formation, Beaverlodge District, Saskatchewan and the South Channel and Kazan formations. The redbed sequences and the underlying basement complexes in both areas have much in common (Table 7). For more detailed descriptions of the geology of each area the reader is referred to Tremblay (1972), Beck (1969), LeCheminant et al. (1976, 1977), Blake (1980), Macey (1973), and Donaldson (1965, 1966, 1967, 1968).

The basement complex in the Beaverlodge area, termed the Tazin Group, consists of an interlayered sequence of quartz-feldspathic gneisses, metasedimentary and mafic metavolcanic rocks and various metasomatic rocks ranging in composition from granite to granodiorite (Tremblay, 1972). The Tazin Group were regionally metamorphosed to lower amphibolite facies at about 2550-2450 Ma. Extensive granitization and recrystallization occurred between 2300-2000 Ma and culminated in pegmatite formation at about 2000 Ma. The 2300-2000 Ma granitization may represent a mid-Aphebian orogenic event. These events were followed by retrograde metamorphism to greenschist facies during the Hudsonian orogeny. The Hudsonian imprint is reflected by chloritized biotites that indicate ages of about 1800 Ma (K-Ar) (Tremblay, 1972).

The Tazin Group has been subjected to polyphase folding, faulting and fracturing. The main structural fabric of the Beaverlodge area is represented by isoclinal or open northeast- and north-trending folds related to the mid-Aphebian orogenic event. The first period of extensive faulting may be associated with the early northeast folds and is expressed as wide zones of mylonitic and brecciated rocks that affected only the Tazin Group. The second period of faulting affected the Tazin and Martin rocks and is characterized by narrow clean-cut fractures that trend northwest, northeast, and north. The Martin Formation is folded about a northeasterly axis, the limbs of which are truncated by late northeast faults.

The basement to the Dubawnt Group rocks in the eastern Baker Lake basin consists of mafic and felsic gneisses and mafic to ultramafic intrusive complexes. In the area of Christopher Island, the eastern termination of the Baker Lake basin, a gabbroic-noritic anorthosite complex intrudes granulitic and granitoid gneisses. In the Thirty Mile Lake area, the basement consists of northwest- to west-trending belts of Archean metavolcanic and metasedimentary rocks infolded with gneissic quartz monzonite and granodiorite, cataclastic augen and mylonitic gneiss and granitic gneiss. This complex has been affected by several phases of deformation. The earliest events involved development of west- to northwest-trending isoclinal folds which were accompanied by amphibolite grade metamorphism. In the Thirty Mile Lake area the latest phase of deformation is represented by narrow east- to northeast-trending shear zones. Extensive greenschist grade retrogression is present in and adjacent to these shear zones. The development of late brittle deformation features marginal to the Dubawnt Group rocks in the Thirty Mile Lake area is similar to the first period of faulting in Beaverlodge area (Tremblay, 1972).

Table 7

Comparison of the geology and uranium occurrences in the eastern Baker Lake basin, N.W.T. and Beaverlodge District, Saskatchewan

	Eastern Baker Lake Basin	Beaverlodge District
Basement Complex		
Name	no formal name	Tazin Group
Age	Archean and Aphebian granulite,	Archean, Aphebian(?)
Lithologies	granulite, anorthosite, felsic ortho and paragneiss complex, infolds of metavolcanic rocks.	quartzo-feldspathic gneisses, amphibolites and areas of metasedimentary and metavolcanic rocks.
Metamorphism	amphibolite facies metamorphism at $\approx 2500(?)$ Kenoran event.	lower amphibolite facies metamorphism $\approx 2550-2450$ Ma (K-Ar) Kenoran event.
	deformation and metamorphism of mafic dykes intruding gneiss complex, mid-Aphebian event(?).	granitization between 2300-2000 Ma, mid-Aphebian event (K-Ar on pegmatites).
	greenschist retrogression at $\approx 1800$ Ma (K-Ar).	greenschist retrogression at $\approx 1800$ Ma (K-Ar).
Deformation	west to northwest folds; east and east-northeast fault – mylonite structures associated with basin development.	early northeast and north trending folds associated with granitization; early faults represented by wide mylonite zones in gneisses and granitic rocks.
Supercrustal rocks		
Name	Dubawnt Group	Martin Formation
Lithologies	South Channel Formation (0-1800 m) polymictic conglomerate Kazan Formation (0-1000 m) plagioclase-rich arkose and siltstone	basal conglomerate member (0-760 m) polymictic conglomerate lower and upper arkose member and siltstone member lower arkose (915-2440 m) upper arkose (245-2135 m) siltstone (305-1830 m) potassium feldspar rich clastic units.
	Pitz Formation (maximum 100 m) Christopher Island Formation (minimum 300 m) subaerial alkaline lavas, $K_2O/Na_2O > 1$ agglomerates and tuffs with synvolcanic sills, stocks, laccoliths and dykes (Martell intrusions).	no equivalent Porphyritic basalt-andesite member (to 1065 m) alkali basalt flows $K_2O/Na_2O < 1$ (plateau basalt type) with gabbroic sills.
Depositional environment	Thelon Formation (maximum 150 m) east-northeast trending tectonically controlled basin(s) with braided river-alluvial fan deposits.	Athabasca Formation northeast trending elongated basin(s) with braided river deposits.
Deformation	late northwest-trending faults transecting all of the Dubawnt Group; very minor folding associated with late faults; east and east-northeast fault affected and controlled basal clastic deposition.	late northwest, northeast, and north-trending faults affecting Tazin Group and Martin Formation; northeast folding of Martin Formation.
Mineralization Distribution	Predominantly within Dubawnt Group rocks near the basal unconformity surface, minor within gneisses.	Predominantly within the Fay Complex and Donaldson Lake Gneiss of the basement Tazin Group; minor within the Martin Formation.

A. Syngenetic	rare occurrences in basement gneiss complex and pegmatites.	remnants of metasediments in granitic and granitoid rocks; pegmatites, and areas of granitic rocks.
Mineralogy	uraninite, uranothorite, molybdenite, allanite, monazite.	uraninite, monazite, uranothorite.
Age	unknown	≈ 2000 Ma, related to latest phases of extensive granitization and recrystallization.
B. Epigenetic		
1. Fracture controlled mineralization in basement gneisses and cover rocks.	associated with fracturing, brecciation and minor mylonitization related to late northwest faulting.	within zones of extensive mylonitization, and brecciation and closely spaced fracturing related to the late brittle deformation.
Mineralogy	two metallic associations 1 simple mineralogy: pitchblende with pyrite, chalcopyrite, bornite, galena and minor molybdenite, sphalerite, or uraniferous titanates. 2 complex mineralogy: pitchblende with Cu and Cu-Ag selenides and minor electrum	two metallic associations 1 simple mineralogy: pitchblende with pyrite, chalcopyrite, galena, sphalerite and clausthalite, some brannerite. 2 complex mineralogy: pitchblende with native Au, Ag and Cu, arsenides, sulphides, selenides and antimonides.
Alteration assemblages:	hematite, chlorite, quartz, white and pink calcite, barite, cerussite	hematite, chlorite, quartz, white to buff carbonate
Age	very limited age data occurrence 13, simple mineralogy, discordant 1813 Ma occurrence 4, complex mineralogy discordant 1516 Ma	abundant age data 1780 ± 20 Ma for occurrences of simple mineralogy 1140 ± 50 Ma for occurrences of complex mineralogy remobilization ages of 270 ± 20 Ma and 100 to 0 Ma
2. Kazan type mineralization	impregnation and microfracture mineralization in altered Kazan arkose peripheral to lamprophyre dyke complexes	no equivalent
Mineralogy	pitchblende, uraniferous titanates, digenite, covellite, chalcopyrite, bornite, native copper and silver, pyrite, galena	
Alteration assemblage	Chlorite, carbonate recrystallization, iron leaching and recrystallization	
Age	unknown	
3. Diatreme breccia-structure	infilling of brecciated country rock peripheral to alkaline stock	no equivalent
Mineralogy	pitchblende, chalcopyrite, sphalerite, pyrite	
Alteration assemblage:	hematite, quartz, calcite, dolomite, barite, chlorite.	
Age	unknown	



An east- to northeast-trending diabase dyke swarm intrudes the basement rocks in the Thirty Mile Lake area. The dyke swarm has been metamorphosed and is deformed by the late narrow shear zones. Diabase dykes and various gneissic lithologies have been cut by unmetamorphosed and undeformed east to southeast lamprophyre dykes which are related to the Christopher Island Formation.

Redbed successions in both areas are unmetamorphosed and rest with angular unconformity upon the basement gneisses. The Martin Formation has been subdivided into three distinct lithological units that grade from a discontinuous basal conglomerate through crossbedded arkose and terminates with siltstone sedimentation. Alkali basalt flows ( $K_2O/Na_2O < 1$ ), plateau basalt type, and related gabbroic sills are present within the arkosic sandstones (Tremblay, 1973). The incorporation of volcanic detritus within some arkosic units indicates contemporaneous sedimentation and volcanism, possibly with minor disconformities. Structurally the Martin Formation is folded about a northeast trending axis, the limbs of which are truncated by late regional faults. This deformation may be related to the latest phases of the Hudsonian Orogeny. The redbed sequence is considered to span an interval 1830 Ma to 1650 Ma indicating an age of late Apehbian or early Paleohelikian (Tremblay, 1972). The depositional environment is interpreted as an intercratonic basin, controlled by marginal normal faults, into which the clastic detritus was transported by braided fluvial streams.

In comparison, the Dubawnt Group was subdivided into a similar sequence of fining upward rock units beginning with the basal South Channel conglomerate and grading into the Kazan arkose and siltstone. The plagioclase-rich Kazan arkose infers a plagioclase-rich provenance region compared to the potassic feldspar-rich Martin arkose inferring a granitic source area. In the Christopher Island area, the Christopher Island Formation is conformable and gradational from Kazan sedimentation. To the west, volcanic rocks of the Christopher Island Formation are unconformable on the basal clastic redbeds. Subaerial Christopher Island volcanic rocks belong to the alkaline potassic-rich basalt series ( $K_2O/Na_2O > 1$ ) and are associated with abundant pyroclastic units whereas the Martin Formation volcanic rocks belong to the alkalic plateau basalt series. The related intrusive equivalents to the Christopher Island volcanic rocks, the Martell intrusions, occur as dyke complexes, sills and laccoliths within the Kazan arkose and Christopher Island volcanic rocks similar to the gabbroic sills within the Martin arkose. The alkaline volcanism of the Christopher Island Formation implies a rift style of tectonics. Christopher Island volcanic rocks are anomalous in their uranium abundances (range 3.0 to 13.1 ppm) compared to the Martin basalts (average 1.1 ppm, Tremblay, 1970). The South Channel, Kazan, and Christopher Island formations are not folded but extensively faulted about northwest and northeast directions. The Rb-Sr age of 1786 Ma from Christopher Island volcanic rocks represents a minimum age for the lower redbeds and suggests that the redbeds are very late Apehbian to Paleohelikian. Normal faults parallel to the margins of the Baker Lake basin and various sedimentological characteristics of the basal redbed sequence suggest that the Dubawnt Group was deposited in fault controlled basins into which detritus was carried by alluvial fan-braided river systems strikingly similar to the tectonic and sedimentological environment of the Martin Formation.

Robinson (1955) and Tremblay (1972) recognized three types of uranium mineralization in the Beaverlodge district: 1) epigenetic fracture controlled mineralization (the most common), 2) disseminated syngenetic concentrations in pegmatitic bodies, granitoid rocks, and remnant meta-sedimentary rocks and 3) superimposed supergene concentrations.

The epigenetic fracture-controlled mineralization at Beaverlodge is localized predominantly within the basement complex with only minor mineralization within the supercrustal rocks. The basement mineralization is controlled by late fracture systems that parallel earlier zones of mylonitization and brecciation. The uranium mineralization is associated with intensive hematitization, silicification, chloritization, and carbonatization. In contrast, the epigenetic fracture controlled mineralization in the Baker Lake basin is predominantly within the supercrustal rocks. The mineralization is controlled by narrow northwest-trending zones of brecciation and fracturing accompanied by an assemblage of alteration minerals similar to Beaverlodge. The metallic assemblages in both districts are principally pitchblende accompanied by varied amounts of pyrite, chalcopyrite, bornite, galena, sphalerite, molybdenite and minor uraniferous titanates or various selenides, native gold and silver.

The epigenetic uranium-copper-silver mineralization within the altered Kazan arkose peripheral to alkaline dykes represents the most common occurrence of base metals and uranium in the lower redbeds of the Dubawnt Group. This type of mineralization is not present within the Martin Formation even though the lower arkosic unit is intruded by gabbroic dykes and sills.

In the Beaverlodge district, erratically disseminated, uranium-thorium and thorium-rich minerals are present as syngenetic concentrations within pegmatites and radioactive paragneisses. The presence of uranothorite-bearing pegmatites and disseminated molybdenum-uranium-bearing minerals in augen gneiss along the southern margin of the eastern Baker Lake basin may be equivalent to the syngenetic occurrences of the Beaverlodge district.

Two U-Pb ages on pitchblende from the eastern Baker Lake basin permit only limited comparison to the abundant age data available from the Beaverlodge District (Tremblay, 1972; Koepfel, 1968). Some inferences can be made from the lithological and structural similarities of both basins. In the Beaverlodge district the first major episode of uranium redistribution and mineralization was associated with intense fracturing at about 1780 Ma; the counterpart in the Baker Lake basin may be the fracture controlled mineralization in the basement gneisses near Kazan Falls which is dated at 1813 Ma. In addition, the discordant 1516 Ma date from fracture controlled U-Se-Cu-Ag-Au mineralization on Christopher Island may be related to this first period of mineralization.

Several periods of remobilization, 1140 and 300 Ma, have been demonstrated in the fracture controlled mineralization in the Beaverlodge District. In the eastern Baker Lake basin, U-Pb dates on the sandstone mineralization are in progress, however the variation of U/Pb ratios of pitchblendes from these occurrences indicate remobilization has occurred within the uranium-copper-silver bearing zones.

Tremblay (1972) stated that the epigenetic fracture filling mineralization at Beaverlodge was the result of the remobilization of uranium by metamorphic-hydrothermal fluids derived from uraniferous metasedimentary rocks during the Hudsonian Orogeny. In contrast the principal source rock for the epigenetic mineralization in the Baker Lake area is the uraniferous alkaline potassic-rich volcanic rocks of the Christopher Island Formation. Uranium liberated during propylitic alteration of the volcanic rocks and moved into the groundwater systems was concentrated in epigenetic sulphide zones of high reducing potential or deposited by hydrothermal fluids that were channelled along late fracture zones.

## REFERENCES

- Alder, H.H.  
1977: Geochemical factors contributing to uranium concentration in alkalic igneous rocks; in *Recognition and Evaluation of Uraniferous Areas*, Proceedings of a Symposium in Vienna, 1975, p. 35-43.
- de Andrade Ramos, J.R. and Fraenkel, M.O.  
1974: Uranium occurrences in Brazil; in *Formation of Uranium Ore Deposits*, International Atomic Energy Agency, Vienna, p. 637-658.
- Barton, P.B., Jr. and Toulmin III, P.  
1964: The electrom-tarnish method for the determination of the fugacity of sulfur in laboratory sulfide systems; *Geochimica et Cosmochimica Acta*, v. 28, p. 619-640.
- Beck, L.S.  
1969: Uranium deposits of the Athabasca region; Department of Mineral Resources, Province of Saskatchewan, Report 125, 139 p.
- Bernardini, G.P. and Catini, A.  
1968: The Cu-Se system; *Mineralium Deposita*, v. 3, p. 375-380.
- Bigarella, J.J.  
1972: Eolian environments: Their characteristics, recognition and importance; in *Recognition of Ancient Sedimentary Environments*, J.K. Rigby and W.K. Hamblin (ed.); Society of Economic Paleontologists and Mineralogists, Special Publication 16, p. 12-62.
- Blake, D.H.  
1980: Volcanic rocks of the Paleohelikian Dubawnt Group in the Baker Lake-Angikumi Lake area, District of Keewatin, N.W.T.; Geological Survey of Canada, Bulletin 309, 39 p.
- Blake, D.H., Miller, A.R., and Schau, Mikkel  
1977: Potassic volcanic rocks of the Paleohelikian Dubawnt Group and associated Cu, U, and Se mineralization, Christopher Island region, District of Keewatin, N.W.T.; Geological Association of Canada, Programs with Abstracts, v. 2, p. 8.
- Capaldi, G., Civetta, L., and Gasparini, P.  
1971: Fractionation of the  $^{238}\text{U}$  decay series in the zeolitization of volcanic ashes; *Geochimica et Cosmochimica Acta*, v. 35, p. 1067-1072.
- Carmichael, I.S.E., Turner, F.J., and Verhoogen, J.  
1974: *Igneous Petrology*; McGraw-Hill Book Co., 739 p.
- Cathles, L.M.  
1977: An analysis of the cooling of intrusives by ground water convection which includes boiling; *Economic Geology*, v. 72, p. 804-826.
- Civetta, L. and Gasparini, P.  
1977: A review of U and Th distributions in recent volcanics from southern Italy; *Magmatological and geophysical implications*; U.S. Energy Research and Development Administration, Conference No. Conf-720805-P2, The Material Radiation Environment II; Volume 2, p. 483-515. (believed to be published in the 1970s)
- Coleman, J.M.  
1969: Brahmaputra River: Channel processes and sedimentation; *Sedimentary Geology*, v. 3, p. 129-239.
- Craig, J.R.  
1974a: The Cu-S system in Sulfide Mineralogy; Mineralogical Association of Canada, Short Course Notes edited by P.M. Ribbe, p. 58-63.
- Craig, J.R. (cont.)  
1974b: The Cu-Fe-S system in Sulfide Mineralogy; Mineralogical Association of Canada, Short Course Notes edited by P.H. Ribbe, p. 64-76.
- Donaldson, J.A.  
1965: The Dubawnt Group, Districts of Keewatin and Mackenzie; Geological Survey of Canada, Paper 64-20.  
1966: Geology Schultz Lake, District of Keewatin; Geological Survey of Canada, Map 7-1966.  
1967: Two Proterozoic clastic sequences: A sedimentological comparison; Geological Association of Canada Proceedings, v. 18, p. 33-54.  
1968: Proterozoic sedimentary rocks of Northern Saskatchewan (74N); in Report of Activities, Part A, Geological Survey of Canada, Paper 68-1A, p. 131.
- Dostal, J. and Capedri, S.  
1975: Partition coefficients of uranium for some rock-forming minerals; *Chemical Geology*, v. 15, p. 285-294.
- Dostal, J., Capedri, S., and Dupuy, C.  
1976: Uranium and potassium in calc-alkaline volcanic rocks from Sardinia; *Lithos*, v. 9, p. 179-183.
- Elder, J.W.  
1965: Physical processes in geothermal areas; American Geophysical Union, Geophysical Monograph, v. 8, p. 211-239.  
1977: Model of hydrothermal ore genesis; Geological Society of London, I.M.M. Special Publication 7, p. 4-13.
- Ewers, G.R.  
1977: Experimental hot water-rock interactions and their significance to national hydrothermal systems in New Zealand; *Geochimica et Cosmochimica Acta*, v. 41, p. 143-150.
- Ewers, G.R. and Keays, R.R.  
1977: Volatile and precious metal zoning in the Broadlands geothermal field, New Zealand; *Economic Geology*, v. 72, p. 1337-1354.
- Finger, L.W.  
1972: The uncertainty in the calculated ferric iron content of a microprobe analysis; Carnegie Institution Year Book 1971, Annual Report of the Director, Geophysical Laboratory 1971-72, p. 600-603.
- Freeman, W.E. and Visher, G.S.  
1975: Stratigraphic analysis of the Navajo sandstone; *Journal of Sedimentary Petrology*, v. 45, no. 3, p. 651-668.
- Garrels, R.M. and Christ, C.L.  
1965: *Solutions, Minerals and Equilibria*; Harper and Row, 450 p.
- Gibbins, W.A., Seaton, J.B., Laporte, P.J., Murphy, J.D., Hurdle, E.J., and Padgham, W.A.  
1977: Mineral Industry Report 1974. Northwest Territories; Canada, Indian Affairs and Northern Development, E.G.S., 1977-5.
- Glennie, K.W., Mudd, G.C., and Nagtegaal, P.J.C.  
1978: Depositional environment and diagenesis of Permian Rotliegendes sandstones in Leman Bank and Sole, Pit areas of the UK southern North Sea; *Journal of Geological Society of London*, v. 135, p. 25-34.

- Harris, D.C., Cabri, L.J., and Kaiman, S.  
1970a: Athabascaite: A new copper selenide mineral from Martin Lake, Saskatchewan; *Canadian Mineralogist*, v. 10, pt. 2, p. 207-215.
- Harris, D.C., Cabri, L.J., and Murray, E.J.  
1970b: An occurrence of a sulphur-bearing berzelianite; *Canadian Mineralogist*, v. 10, pt. 4, p. 737-740.
- Harshman, E.N.  
1972: Geology and uranium deposits, Shirley Bodin area, Wyoming; U.S. Geological Survey, Professional Paper 745, 82 p.
- Henley, R.W.  
1973: Solubility of gold in hydrothermal in chloride solutions; *Chemical Geology*, v. 11, p. 73-88.
- Hey, M.H.  
1954: A new review of chlorites; *Mineralogical Magazine*, v. 30, p. 277-292.
- Hostetler, P.B. and Garrels, R.M.  
1962: Transportation and precipitation of uranium and vanadium at low temperatures, with special reference to sandstone-type uranium deposits; *Economic Geology*, v. 57, no. 2, p. 137-167.
- Kessler, L.G. II  
1978: Diagenetic sequence in ancient sandstones deposited under desert climatic conditions; *Journal of Geological Society of London*, v. 135, p. 41-49.
- Koepfel, V.  
1968: Age and history of the uranium mineralization of the Beaverlodge area, Saskatchewan; *Geological Survey of Canada, Paper 67-31*, 111 p.
- Kvacek, M.  
1973: Selenides from the uranium deposits of western Moravia, Czechoslovakia. Part I, Berzelianite, umangite, eskebornite; *Acta Universitatis Carolinae Geologica*, Rost Vol. No. 1-2, p. 23-36.
- Laporte, P.J.  
1974a: North of 60°, Mineral Industry Report, 1969 and 1970. Vol. 2, Northwest Territories East of 104° West Longitude; Canada, Indian Affairs and Northern Development, E.G.S. 1974-2.  
1974b: North of 60°, Mineral Industry Report, 1971 and 1972. Vol. 2 of 3, Northwest Territories East of 104° West Longitude; Canada, Indian Affairs and Northern Development, E.G.S. 1974-2.
- Laporte, P.J., Gibbins, W.A., Hurdle, E.J., Lord, C., Padgham, W.A., and Seaton, J.B.  
1978: Northwest Territories, Mineral Industry Report, 1975; Canada, Indian Affairs and Northern Development, E.G.S. 1978-5.
- LeCheminant, A.N. and Miller, A.R.  
1978: Five types of uranium occurrences studied in Baker Lake basin; *Northern Miner Annual Review* Number, Nov. 30, vol. 64, no. 38, Section D, p. D1, D22.
- LeCheminant, A.N., Blake, D.H., Leatherbarrow, R.W., and deBie, L.  
1977: Geological studies: Thirty Mile Lake and MacQuoid Lake map-areas, District of Keewatin; in *Report of Activities, Part A, Geological Survey of Canada, Paper 77-1A*, p. 205-208.
- LeCheminant, A.N., Hews, P.C., Lane, L.S., and Wolf, J.M.  
1976: MacQuoid Lake (55M West Half) and Thirty Mile Lake (65P East Half) map areas, District of Keewatin; in *Report of Activities, Part A, Geological Survey of Canada, Paper 76-1A*, p. 383-386.
- LeCheminant, A.N., Leatherbarrow, R.W., and Miller, A.R.  
1979: Thirty Mile Lake Map Area, District of Keewatin; in *Current Research, Part B, Geological Survey of Canada, Paper 79-1B*, p. 319-327.
- Locardi, E. and Mittempergher, M.  
1971: Exhalative supergenic uranium thorium and marcasite occurrences in Quaternary volcanics of central Italy; *Bulletin Volcanologique*, v. 35, p. 173-184.
- Macey, G.  
1973: A sedimentological comparison of two Proterozoic red bed successions (the South Channel and Kazan Formations of Baker Lake, N.W.T. and the Martin Formation of Uranium City, Saskatchewan); Unpublished M.Sc. thesis, Carleton University, 176 p.
- Mittempergher, M.  
1970: Exhalative-supergenic uranium mineralization in the Quaternary alkaline volcanic rocks of central Italy; *Uranium Exploration Geology (IAEA-PL-391/7)*, p. 177-184.
- Morrison, I.R.  
1977: Petrology and petrochemistry of the Cookie Monster alkalic intrusion, District of Keewatin, N.W.T.; unpublished B.Sc. thesis, University of Western Ontario, 54 p.
- Morton, R.D. and Sassano, G.P.  
1972: Reflectance and micro-indentation hardness vs. chemical composition in some Canadian uraninites; *Neues Jahrbuch fuer Mineralogie Monatshefte*, v. 8, p. 350-360.
- Nagasawa, H. and Wakita, H.  
1968: Partition of uranium and thorium between augite and host lavas; *Geochimica et Cosmochimica Acta*, v. 32, p. 917-921.
- Norton, D.  
1978: Sourcelines, source regions and pathlines for fluids in hydrothermal systems related to cooling plutons; *Economic Geology*, v. 73, p. 21-28.
- Norton, D. and Knight, J.  
1977: Transport phenomena in hydrothermal systems. Cooling plutons; *American Journal of Science*, v. 277, p. 937-981.
- Padgham, W.A., Seaton, J.B., Laporte, P.J., and Murphy, J.D.  
1976: Mineral Industry Report, 1973. Northwest Territories; Canada, Indian Affairs and Northern Development, E.G.S. 1976-9.
- Park, J.K., Irving, E., and Donaldson, J.A.  
1973: Paleomagnetism of the Precambrian Dubawnt Group; *Geological Society of America Bulletin*, v. 84, p. 859-870.
- Pringle, G.J. and Miller, A.R.  
1977: A study of Cu-S-Se minerals: Electron microprobe analysis and X-ray power data; in *Report of Activities, Part B, Geological Survey of Canada, Paper 77-1B*, p. 113-116.
- Reineck, H.E. and Singh, I.B.  
1975: *Depositional Sedimentary Environments*; Springer-Verlag, Berlin, 439 p.
- Reinhardt, E.W. and Chandler, F.W.  
1973: Gibson-MacQuoid Lakes map areas, District of Keewatin; in *Report of Activities, Part A, Geological Survey of Canada, Paper 73-1A*, p. 162-165.

- Robinson, S.C.  
1955: Mineralogy of uranium deposits, Goldfields, Saskatchewan; Geological Survey of Canada, Bulletin 31, 128 p.
- Rosholt, J.N. and Noble, D.C.  
1969: Loss in uranium from crystallized silicic volcanic rocks; *Earth and Planetary Science Letters*, v. 6, p. 268-270.
- Ruzicka, V.  
1971: Geological comparison between East European and Canadian uranium deposits; Geological Survey of Canada, Paper 70-48, 196 p.
- Schau, Mikkel and Hulbert, L.  
1977: Granulites, anorthosites and cover rocks, northeast of Baker Lake, District of Keewatin; in *Report of Activities, Part A*, Geological Survey of Canada, Paper 77-1A, p. 399-407.
- Schumm, S.A.  
1977: *The Fluvial System*; J. Wiley and Sons, New York, 338 p.
- Seward, T.M.  
1973: The complexes of gold and the transport of gold in hydrothermal ore solutions; *Geochimica et Cosmochimica Acta*, v. 37, p. 379-399.  
1976: The stability of chloride complexes of silver in hydrothermal solutions up to 350°C; *Geochimica et Cosmochimica Acta*, v. 40, p. 1329-1342.
- Shanks, W.C. and Bischoff, J.L.  
1977: Ore transport and deposition in the Red Sea geothermal system: a geochemical model; *Geochimica et Cosmochimica Acta*, v. 41, p. 1507-1519.
- Skinner, B.J., White, D.E., Rose, H.J., and Mays, R.E.  
1967: Sulfides associated with the Salton Sea geothermal brine; *Economic Geology*, v. 62, p. 316-330.
- Sorensen, H.  
1977: Features of the distribution of uranium in igneous rocks – Uranium deposits associated with igneous rocks; in *Recognition and Evaluation of Uraniferous Areas*, Proceedings of a Symposium in Vienna, 1975, p. 47-52.
- Tilsley, J.E.  
1978: Uranium mineralization in shallow intrusive environments; in *Uranium Deposits: Their Mineralogy and Origin*, Mineralogical Association of Canada, Short course edited by M.M. Kimberley, p. 281-289.
- Tremblay, L.P.  
1970: The significance of uranium in quartzite in the Beaverlodge area, Saskatchewan; *Canadian Journal of Earth Sciences*, v. 7, no. 2, p. 280-305.  
1972: Geology of the Beaverlodge Mining Area, Saskatchewan; Geological Survey of Canada, Memoir 367, 265 p.  
1973: Volcanic rocks of Beaverlodge Area; in *Volcanism and Volcanic Rocks*, Geological Survey of Canada, Open File 164, p. 15-27.
- Walker, T.R.  
1967: Formation of redbeds in modern and ancient deserts; *Geological Society of America Bulletin*, v. 78, p. 353-368.
- Wanless, R.K. and Loveridge, W.D.  
1972: Rubidium-strontium isochron age studies, Report 1; Geological Survey of Canada, Paper 72-23.
- Waugh, B.  
1970a: Formation of quartz overgrowths in the Penrith sandstone (Lower Permian) of Northwest England as revealed by scanning electron microscopy; *Sedimentology*, v. 14, p. 309-320.  
1970b: Petrology, provenance and silica diagenesis of the Penrith sandstone (Lower Permian) of Northwest England; *Journal of Sedimentary Petrology*, v. 40, no. 4, p. 1226-1240.
- Wine, G.D.  
1976: Geology of the Martell syenites, N.W.T., with emphasis on petrography and chemistry; unpublished B.Sc. thesis, University of British Columbia, 38 p.
- Wright, G.M.  
1967: Geology of the southeastern Barren Grounds, parts of the Districts of Mackenzie and Keewatin; Geological Survey of Canada, Memoir 350.



APPENDIX I  
LOCATION OF URANIUM OCCURRENCES

Occurrence Number	Company designation	NTS Map Sheet	Latitude	Longitude	Easting	Northing
1	68-2 <sup>1,2,3</sup>	56D/2	64°10'10"	94°33'34"	424190	7116640
2	71-2 <sup>2,3</sup>	56D/2	64°08'53"	94°32'48"	424750	7114240
3	69-9A <sup>2,3</sup>	56D/2	64°06'46"	94°37'14"	421050	7110380
4	69-9 <sup>1,3</sup>	56D/2	64°06'26"	94°37'22"	420940	7109780
5	71-4 <sup>2,3</sup>	56D/2	64°04'50"	94°31'36"	425550	7106690
6	68-1 <sup>1,3</sup>	56D/2	64°04'43"	94°33'06"	424320	7106500
7	75-3 <sup>3</sup>	55M/14	63°47'45"	95°07'38"	395210	7075820
8	75-5 <sup>3</sup>	55M/11	63°44'57"	95°14'08"	389690	7070790
9	74-1E <sup>3,4</sup>	55M/13	63°48'19"	95°33'17"	374190	7077640
10	74-1W <sup>3,4</sup>	55M/13	63°49'02"	95°35'07"	372750	7079040
11	75-6 <sup>3</sup>	55M/13	63°50'10"	95°35'22"	372620	7081150
12	71-5 <sup>3</sup>	55M/12	63°42'56"	95°40'27"	367900	7067880
13	68-4(69-4) <sup>1,2,3,4,5</sup>	55M/12	63°41'25"	95°46'27"	362830	7065280
14	68-4A(69-4A) <sup>2,4,5</sup>	55M/12	63°40'58"	95°43'55"	364890	7064350
15	—————	55M/12	63°43'26"	95°52'24"	358100	7069250
16	76-9E <sup>3</sup>	65P/9	63°40'04"	96°17'12"	634270	7062640
17	76-9W <sup>3</sup>	65P/9	63°40'04"	96°17'52"	633720	7062630
18	75-1 <sup>3</sup>	65P/9	63°39'25"	96°25'31"	627450	7061170
19	75-2 <sup>3</sup>	65P/10	63°44'57"	96°45'20"	610750	7070800
20	—————	65P/10	63°37'23"	96°56'43"	601850	7056450
1 Laporte, 1974a		4 Gibbins et al., 1977				
2 Laporte, 1974b		5 Padgham et al., 1976				
3 Laporte, et al., 1978						

APPENDIX 2  
WHOLE ROCK AND TRACE ELEMENT ANALYSES  
OF DUBAWNT GROUP ROCKS

A. Christopher Island subvolcanic stocks and volcanic rocks									
Analysis	1	2	3	4	Analysis	1	2	3	4
Occurrence	3	3	2	19	Occurrences	3	3	2	19
SiO <sub>2</sub>	41.1	52.2	44.8	52.3	Trace elements (ppm)				
TiO <sub>2</sub>	1.03	1.18	0.95	0.61	Ba	13000	2300	3700	1600
Al <sub>2</sub> O <sub>3</sub>	10.2	13.1	10.1	14.7	Sr	3400	750	1800	330
Fe <sub>2</sub> O <sub>3</sub>	3.2	2.2	2.8	3.0	V	160	110	90	92
FeO	4.7	3.9	3.9	2.3	U	4.9	8.3	3.5	87.3
MnO	0.09	0.08	0.10	0.16	Cu	30	67	110	12
MgO	13.1	8.1	10.0	4.8	Ag	0.2	0.2	N.D.	N.D.
CaO	8.0	5.2	7.9	6.1	Pb	9	4	6	1910
Na <sub>2</sub> O	0.3	1.2	0.3	3.4	Mo	2	2	2	2
K <sub>2</sub> O	3.9	5.7	6.4	5.0	Zn	83	73	73	100
P <sub>2</sub> O <sub>5</sub>	1.6	1.0	1.8	0.64	F	3300	3050	N.A.	N.A.
H <sub>2</sub> O <sub>T</sub>	4.9	3.1	2.4	3.1	Zr	390	430	430	370
CO <sub>2</sub>	6.0	3.3	8.0	4.2	Cl	600	400	N.A.	N.A.
S	0.32	0.20	0.0	0.21					
Total	98.44	100.46	99.45	100.52					
Analyses 1 and 2: stocks in the area of occurrence 3									
Analyses 3: central stock, occurrence 2									
Analyses 4: radioactive porphyritic trachyte, occurrence 19									
N.D. = Not detected                      N.A. = Not analyzed									

Appendix 2 (cont.)

B. Christopher Island lamprophyre dyke rocks associated with Kazan type mineralization											C. White altered arkose associated with the Kazan type mineralization										
Analysis	1	2	3	4	5	6	7	8	9		Analysis	1	2	3	4	5	6	7			
Occurrence	10	7	7	7	11	9	9	9	7		Occurrence	9	9	9	9	7	7	7			
SiO <sub>2</sub>	47.2	47.2	53.1	48.1	47.7	46.8	51.7	49.0	48.2		SiO <sub>2</sub>	58.0	56.0	47.2	49.0	73.5	66.1	70.6			
TiO <sub>2</sub>	0.73	0.66	0.78	0.71	0.87	0.73	0.53	0.70	0.55		TiO <sub>2</sub>	0.04	0.11	0.04	0.05	0.86	0.04	0.22			
Al <sub>2</sub> O <sub>3</sub>	11.6	14.5	17.5	14.1	12.6	11.4	14.6	13.0	14.0		Al <sub>2</sub> O <sub>3</sub>	10.0	10.5	9.0	9.0	12.3	13.0	14.9			
Fe <sub>2</sub> O <sub>3</sub>	3.9	6.0	0.8	3.0	5.1	8.1	3.5	4.3	3.9		Fe <sub>2</sub> O <sub>3</sub>	0.1	0.1	0.2	0.4	0.1	0.1	0.0			
FeO	3.1	1.8	4.8	4.0	0.7	0.8	1.4	2.4	2.8		FeO	0.2	0.7	0.5	0.5	0.3	0.7	1.3			
MnO	0.12	0.14	0.06	0.08	0.11	0.11	0.07	0.10	0.12		Fe <sub>2</sub> O <sub>3</sub> T										
MgO	8.0	6.1	4.6	8.8	7.5	10.3	4.4	8.2	4.4		MnO	0.05	0.06	0.07	0.13	0.03	0.08	0.03			
CaO	7.9	7.3	4.1	6.5	8.0	6.4	8.6	7.3	8.6		MgO	0.3	2.0	3.2	5.6	1.0	2.5	1.0			
Na <sub>2</sub> O	0.9	1.8	7.1	3.3	1.5	0.7	3.1	2.7	1.6		CaO	13.9	10.9	16.9	12.2	2.9	5.7	2.1			
K <sub>2</sub> O	5.7	4.8	0.1	2.1	5.9	5.3	3.2	4.0	3.0		Na <sub>2</sub> O	4.6	5.6	4.2	4.1	5.7	4.1	5.4			
P <sub>2</sub> O <sub>5</sub>	0.92	0.53	0.71	0.63	0.84	0.86	0.66	0.87	0.44		K <sub>2</sub> O	1.3	0.6	1.2	2.1	1.3	1.4	1.8			
H <sub>2</sub> O <sub>T</sub>	2.3	3.0	2.9	4.2	3.0	3.7	2.6	1.4	3.2		P <sub>2</sub> O <sub>5</sub>	0.05	0.08	0.06	0.06	0.08	0.05	0.14			
CO <sub>2</sub>	7.2	5.6	2.7	4.9	5.9	3.9	6.0	4.3	8.2		H <sub>2</sub> O <sub>T</sub>	0.3	0.3	0.4	0.4	0.6	1.1	0.9			
S	0.14	0.19	0.33	0.21	0.20	0.0	0.01	0.0	0.22		CO <sub>2</sub>	11.4	11.0	16.8	16.0	2.3	5.6	1.6			
Total	99.71	99.62	99.58	100.63	99.92	99.10	100.37	98.27	99.23		S	0.04	0.12	0.13	0.07	0.19	0.10	0.06			
Trace elements (ppm)											Total	100.28	98.07	99.90	99.61	101.16	100.57	100.05			
Ba	4900	3800	250	700	4700	4300	3300	5400	3800		Trace elements (ppm)										
Sr	1400	480	270	490	970	750	800	2700	390		Ba	1700	3300	1800	720	170	2600	930			
V	110	120	100	140	110	180	81	120	140		Sr	250	210	330	200	120	250	100			
U	10.7	12.8	23.9	8.0	7.1	8.3	6.1	11.5	356		V	<10	34	20	51	10	28	39			
Cu	37	34	8	7	24	25	27	50	4000		U	1.1	2.9	0.6	0.9	2.0	12.0	3.5			
Ag	0.1	0.3	0.3	0.1	N.D.	0.1	N.D.	0.3	11.0		Cu	66	620	15	19	22	7	34			
Pb	23	10	10	7	9	17	11	23	46		Ag	0.2	1.0	N.D.	N.D.	0.3	0.5	N.D.			
Mo	3	5	2	2	2	2	2	2	6		Pb	9	9	19	4	19	78	11			
Zn	56	92	230	148	43	51	39	58	90		Mo	2	2	2	2	1	18	2			
F	1650	2710	700	1030	1650	1650	455	1275	1115		Zn	4	16	62	68	32	73	27			
Zr	380	170	230	180	370	280	90	30	220		F	N.A.	N.A.	N.A.	N.A.	N.A.	N.A.	N.A.			
Cl	400	400	400	400	300	400	400	400	200		Cl										

N.D. = Not detected N.A. = Not analyzed



## Appendix 2 (cont.)

D. Pink altered arkose associated with the Kazan type mineralization														
Analysis	1	2	3	4	5	6	7	8	9	10	11	12	13	14
Occurrence	9	9	9	9	9	9	9	9	9	9	9	9	11	10
SiO <sub>2</sub>	64.0	57.9	58.2	50.2	56.0	58.0	57.0	56.5	74.1	49.0	67.3	61.7	73.2	63.5
TiO <sub>2</sub>	0.11	0.07	0.06	0.04	0.07	0.05	0.06	0.02	0.37	0.07	0.13	0.05	0.17	0.11
Al <sub>2</sub> O <sub>3</sub>	12.7	10.4	10.5	8.5	9.9	10.0	11.0	9.0	13.8	9.7	12.3	10.4	13.6	13.2
Fe <sub>2</sub> O <sub>3</sub>	0.0	0.4	0.5	0.5	0.5	0.8	0.3	0.5	1.7				0.9	3.0
FeO	0.2	0.3		0.0	0.2	0.2	0.6	0.0	0.1				0.1	0.0
Fe <sub>2</sub> O <sub>3</sub> T			0.5							0.5	1.3	1.1		
MnO	0.04	0.04	0.10	0.11	0.04	0.05	0.06	0.04	0.00	0.08	0.05	0.03	0.02	0.08
MgO	1.8	1.7	0.6	5.3	1.5	1.3	2.7	1.3	0.6	2.1	2.5	0.6	0.5	2.2
CaO	7.6	12.1	11.4	11.9	12.6	11.9	10.5	14.1	0.4	16.9	3.7	10.2	2.0	5.1
Na <sub>2</sub> O	5.6	4.6	4.7	4.1	4.6	4.5	5.1	4.2	6.2	4.4	5.4	4.8	6.2	6.0
K <sub>2</sub> O	1.1	1.2	1.6	1.5	1.5	1.8	1.4	1.6	2.1	1.4	1.6	1.4	0.3	1.3
P <sub>2</sub> O <sub>5</sub>	0.06	0.06	0.06	0.05	0.06	0.06	0.05	0.04	0.18	0.09	0.08	0.05	0.10	0.10
H <sub>2</sub> O <sub>T</sub>	0.8	1.0	1.0	0.5	0.6	0.7	0.5	0.3	0.4	0.3	1.1	0.6	0.4	1.4
CO <sub>2</sub>	6.0	10.1	9.2	15.8	11.2	10.9	11.2	12.5	0.0	15.5	2.8	8.1	1.8	4.1
S	0.02	0.10	0.18	0.14	0.14	0.10	0.04	0.08	0.08	0.25	0.00	0.00	0.06	0.18
Total	100.03	99.97	99.10	98.64	98.91	100.36	100.51	100.18	100.03	100.29	98.26	99.03	99.35	100.27
Trace elements (ppm)														
Ba	200	1200	1100	860	1400	1900	1200	1000	250	1200	2900	170	600	300
Sr	170	260	300	260	280	330	220	250	30	280	200	230	96	170
V	21	160	69	77	71	70	75	11	<10	37	28	24	16	25
U	8.8	722	269	1470	600	180	34.8	138	3.6	151	15.7	2.4	9.7	38.6
Cu	3200	1100	12000	3800	1400	1400	430	850	18	8900	240	90	50	160
Ag	8.4	2.4	20.0	14.0	4.3	5.3	0.4	1.0	N.D.	7.7	0.2	0.2	0.5	0.1
Pb	11	127	40	158	400	53	14	68	6	25	3	4	3	29
Mo	2	10	3	3	6	2	2	4	1	10	1	1	2	2
Zn	32	34	15	74	31	25	44	19	10	27	65	22	5	112
F	N.A.	N.A.	N.A.	N.A.	N.A.	N.A.	N.A.	N.A.	N.A.	N.A.	N.A.	N.A.	N.A.	N.A.

N.D. = Not detected

N.A. = Not analyzed

## Appendix 2 (cont.)

D. (cont.) Pink altered arkose associated with the Kazan type mineralization																											
Analysis	15	16	17	18	19	20	21	22	23	24	25	26	27														
Occurrence	10	7	7	7	7	10	11	11	9	9	9	9	7														
SiO <sub>2</sub>	56.7	71.5	68.7	69.2	74.8	70.8	46.3	64.8	53.0	59.0	59.2	53.0	70.2														
TiO <sub>2</sub>	0.09	0.16	0.16	0.16	0.18	0.25	0.08	0.27	0.06	0.08	0.03	0.05	0.14														
Al <sub>2</sub> O <sub>3</sub>	12.0	14.0	13.8	14.7	13.7	13.9	8.3	12.7	9.0	10.0	10.7	10.0	14.1														
Fe <sub>2</sub> O <sub>3</sub>	0.9	0.3	0.8	0.6	2.1	0.7	0.3	2.4		0.1	0.2	0.1	0.2														
FeO	0.0	0.8	0.2	0.8	0.0	0.2	0.1	0.0		0.4	0.2	0.7	0.8														
Fe <sub>2</sub> O <sub>3</sub> T									1.3																		
MnO	0.17	0.02	0.02	0.04	0.13	0.04	0.10	0.08	0.13	0.02	0.03	0.05	0.02														
MgO	3.8	0.5	0.5	1.3	0.1	0.8	0.8	2.0	5.4	1.5	0.9	3.6	0.5														
CaO	9.5	1.7	4.0	2.1	0.5	2.5	20.8	5.7	13.0	10.8	11.9	11.5	3.4														
Na <sub>2</sub> O	4.9	6.5	5.5	5.7	7.3	6.7	3.5	4.2	4.1	4.6	4.8	4.2	5.9														
K <sub>2</sub> O	1.2	2.0	2.0	1.7	0.8	1.8	1.1	1.6	0.8	1.6	1.5	2.4	1.7														
P <sub>2</sub> O <sub>5</sub>	0.08	0.13	0.11	0.10	0.11	0.15	0.09	0.15	0.06	0.06	0.04	0.06	0.11														
H <sub>2</sub> O <sub>T</sub>	1.8	0.6	0.6	1.0	0.6	0.6	0.7	1.1	2.3	0.8	0.4	0.5	0.7														
CO <sub>2</sub>	8.8	1.4	3.4	1.8	0.2	2.0	16.8	4.6	10.4	10.2	10.4	13.3	2.6														
S	0.15	0.60	0.09	0.03	0.20	0.21	0.33	0.03	0.10	0.11	0.06	0.10	0.20														
Total	100.19	100.21	99.88	99.23	100.72	100.65	99.30	99.63	99.65	99.27	100.36	99.56	100.57														
Trace elements (ppm)																											
Ba	400	2000	1700	430	810	880	1300	420	1000	1300	2600	2000	1600														
Sr	350	220	160	92	50	85	420	240	360	290	300	230	150														
V	<10	28	27	32	21	17	30	16	<10	80	<10	29	36														
U	12.2	737	8.1	11.7	36.3	9.3	572	4.9	2.0	409	3.7	3.8	364														
Cu	84	460	8	12	7	38	8200	68	3100	230	48	22	51														
Ag	N.D.	1.1	0.3	N.D.	0.7	N.D.	13.5	0.1	0.3	2.0	0.2	0.2	0.4														
Pb	15	715	7	9	38	19	42	9	15	535	13	7	550														
Mo	3	154	4	1	4	1	3	2	2	43	2	2	21														
Zn	54	124	19	58	5	27	18	37	50	28	13	47	73														
F	N.A.	N.A.	N.A.	N.A.	N.A.	N.A.	N.A.	N.A.	N.A.	N.A.	N.A.	N.A.	N.A.														
N.D. = Not detected      N.A. = Not analyzed																											

## Appendix 2 (cont.)

D. (cont.) Pink altered arkose associated with the Kazan type mineralization													
Analysis	28	29	30	31	32	33	34	35	36	37			
Occurrence	10	10	7	7	9	10	11	9	7	11			
SiO <sub>2</sub>	67.7	74.7	71.7	67.2	64.0	71.0	54.0	66.2	73.6	68.2			
TiO <sub>2</sub>	0.23	0.04	0.17	0.10	0.12	0.21	0.08	0.09	0.20	0.20			
Al <sub>2</sub> O <sub>3</sub>	14.1	12.8	13.1	13.0	11.0	13.4	10.0	11.0	13.4	12.6			
Fe <sub>2</sub> O <sub>3</sub>	2.2	0.2	1.1	1.1		0.8		0.2	0.9	1.8			
FeO	0.0	0.3	0.0	0.4		0.8		0.2	0.0	0.0			
Fe <sub>2</sub> O <sub>3T</sub>					0.4		0.4						
MnO	0.06	0.02	0.04	0.04	0.02	0.05	0.08	0.05	0.02	0.03			
MgO	1.3	0.7	1.1	0.9	0.2	0.7	0.6	2.1	0.5	0.8			
CaO	3.5	1.9	2.4	5.2	8.2	2.1	14.9	7.3	2.1	4.7			
Na <sub>2</sub> O	5.9	4.9	5.5	5.2	4.9	3.0	4.0	4.8	7.0	6.8			
K <sub>2</sub> O	1.4	1.6	2.5	1.9	1.4	5.4	1.0	1.3	0.2	0.3			
P <sub>2</sub> O <sub>5</sub>	0.14	0.07	0.14	0.12	0.08	0.14	0.10	0.08	0.17	0.11			
H <sub>2</sub> O <sub>T</sub>	0.8	0.5	0.8	0.8	0.4	0.6	0.6	1.0	0.5	0.5			
CO <sub>2</sub>	2.9	1.4	2.0	4.3	6.4	1.9	13.2	6.0	1.6	3.7			
S	0.07	0.04	0.18	0.10	0.4	0.08	0.4	0.25	0.09	0.18			
Total	100.30	99.17	100.73	100.36	97.52	100.18	99.36	100.57	100.28	99.92			
Trace elements (ppm)													
Ba	210	980	1500	1800	2900	820	1500	1800	85	700			
Sr	140	180	150	180	350	160	300	280	74	140			
V	24	23	41	40	27	22	21	<10	<10	84			
U	12.6	266	5.0	25.0	1480	2.9	30.2	1.2	1.8	7.0			
Cu	9	25	N.D.	20	13000	23	9900	120	7	26			
Ag	0.3	0.2	N.D.	0.4	13.0	N.D.	12.8	2.4	N.D.	0.4			
Pb	11	46	9	19	137	5	9	3	1	34			
Mo	1	1	1	1	3	1	3	2	2	2			
Zn	48	23	46	19	6	19	17	24	9	23			
F	N.A.	N.A.	N.A.	N.A.	N.A.	N.A.	N.A.	N.A.	N.A.	N.A.			
N.D. = Not detected      N.A. = Not analyzed													

Appendix 2 (cont.)

E. Red altered arkose associated with the Kazan type mineralization											F. Altered Kazan arkose adjacent to Martell Intrusions				
Analysis	1	2	3	4	5	6	7	8	9	10	1	2	3	4	5
Occurrence	9	9	9	9	9	9	7	11	11	10	Northing	7078110	7090240	7078190	7078540
											Eastings	369580	382460	369820	369610
SiO <sub>2</sub>	61.7	53.0	54.0	54.0	58.0	65.0	73.1	71.5	72.8	68.0	60.1	71.4	69.6	75.1	77.0
TiO <sub>2</sub>	0.14	0.09	0.08	0.08	0.08	0.17	0.15	0.17	0.24	0.19	0.10	0.13	0.11	0.06	0.07
Al <sub>2</sub> O <sub>3</sub>	11.4	11.0	10.0	9.5	10.0	12.0	13.6	12.3	12.3	12.0	11.2	13.2	10.3	14.8	13.8
Fe <sub>2</sub> O <sub>3</sub>	1.3	0.6	0.6	0.6	0.6	1.1	1.1	1.1	1.9	1.3	1.9	1.4	1.6	0.7	1.3
FeO	0.2	0.4	0.3	0.3	0.3	0.5	0.5	0.5	0.1	0.0	0.0	0.1	0.0	0.0	0.0
Fe <sub>2</sub> O <sub>3T</sub>			0.5		0.7	1.5	1.2			1.5					
MnO	0.02	0.03	0.05	0.06	0.06	0.03	0.01	0.07	0.04	0.05	0.09	0.04	0.09	0.00	0.01
MgO	1.2	1.0	2.0	2.4	1.8	0.7	0.6	0.8	0.7	0.5	1.5	0.7	2.5	0.7	0.3
CaO	8.8	14.0	13.9	13.5	12.0	6.4	1.0	3.3	1.9	3.0	9.7	2.5	5.8	0.1	0.8
Na <sub>2</sub> O	4.6	4.3	4.5	4.5	5.1	5.6	5.9	4.3	5.4	5.3	4.7	7.8	4.2	7.5	6.3
K <sub>2</sub> O	1.8	1.5	1.0	1.2	0.8	1.3	2.2	1.8	1.9	3.2	1.3	0.2	0.1	1.0	0.1
P <sub>2</sub> O <sub>5</sub>	0.08	0.07	0.09	0.06	0.07	0.12	0.12	0.08	0.13	0.15	0.07	0.09	0.14	0.08	0.06
H <sub>2</sub> O <sub>T</sub>	1.1	0.7	1.1	0.4	0.6	0.8	0.7	0.9	0.8	0.9	0.9	0.6	1.4	0.5	0.4
CO <sub>2</sub>	7.7	12.1	12.0	12.4	9.9	5.1	0.7	2.5	1.5	2.3	7.5	2.5	4.6	0.0	0.5
S	0.01	0.16	0.07	0.04	0.03	0.01	0.37	0.07	0.21	0.67	0.11	0.19	0.07	0.17	0.04
Total	100.05	98.95	99.29	99.04	99.14	98.73	99.65	99.39	99.92	97.76	99.17	100.85	100.51	100.71	100.68
Trace elements (ppm)															
Ba	1000	4900	690	820	390	1300	2400	1700	3900	1100	420	91	89	380	170
Sr	210	380	310	230	200	230	330	260	390	170	340	130	210	220	110
V	75	86	97	100	53	310	44	76	25	27	35	21	18	12	100
U	820.0	1300.0	1250.0	1960.0	1850.0	2820.0	2140.0	2190.0	1210.0	1750	5.8	3.0	1.7	3.7	10.7
Cu	260	1400	9800	1200	3500	10000	20	1100	480	18000	27	7	18	54	85
Ag	5.3	2.4	11.3	2.6	8.2	8.9	1.1	15.4	4.5	9.4	0.3	0.1	0.1	N.D.	0.3
Pb	129	485	205	205	230	730	1050	110	63	121	15	2	7	4	3
Mo	5	39	4	5	3	2	144	4	4	38	2	1	2	1	1
Zn	28	37	79	47	37	44	72	33	23	13	46	20	19	9	6
F	N.A.	N.A.	N.A.	N.A.	93	N.A.	84	101	N.A.	N.A.	N.A.	N.A.	N.A.	N.A.	N.A.

N.D. = Not detected      N.A. = Not analyzed

## Appendix 2 (cont.)

G. Unaltered Kazan arkose								
Analysis	1	2	3	4	5	6	7	8
Location	7086580 371620	7079040 378190	7079640 372730	7080120 374090	7086710 386090	7083490 378290	7074610 389040	7081220 372520
SiO <sub>2</sub>	77.2	59.5	56.7	73.7	64.0	75.3	63.7	69.0
TiO <sub>2</sub>	0.04	0.09	0.11	0.11	0.12	0.11	0.18	0.22
Al <sub>2</sub> O <sub>3</sub>	9.7	11.2	9.8	10.8	12.7	14.0	12.2	12.0
Fe <sub>2</sub> O <sub>3</sub>	0.1	0.8	0.7	0.6	1.0	0.7	1.4	
FeO	0.2	0.0	0.3	0.1	0.0	0.2	0.0	
Fe <sub>2</sub> O <sub>3</sub> T								1.8
MnO	0.01	0.12	0.10	0.02	0.07	0.00	0.04	0.03
MgO	0.7	3.0	2.3	1.0	2.7	0.1	0.7	1.1
CaO	3.2	8.5	10.6	4.1	6.6	1.1	7.3	4.0
Na <sub>2</sub> O	1.9	4.6	5.2	2.1	3.0	3.3	4.5	6.6
K <sub>2</sub> O	2.8	1.8	0.3	3.5	2.9	3.2	2.3	1.6
P <sub>2</sub> O <sub>5</sub>	0.07	0.10	0.11	0.13	0.14	0.11	0.15	0.13
H <sub>2</sub> O <sub>T</sub>	0.7	1.3	1.1	1.3	1.6	0.7	0.6	0.9
CO <sub>2</sub>	3.0	8.5	13.2	3.6	5.8	0.5	7.6	3.2
S	0.04	0.20	0.19	0.17	0.07	0.06	0.09	0.21
Total	99.66	99.71	100.71	101.23	100.70	99.38	100.76	100.79
Trace elements (ppm)								
Ba	430	590	880	710	660	1400	1900	350
Sr	130	850	980	140	390	160	180	200
V	<10	<10	<10	<10	<10	<10	18	<10
U	1.1	4.1	1.8	2.1	2.5	0.9	2.0	2.0
Cu	15	46	22	15	11	6	7	24
Ag	0.1	N.D.	N.D.	N.D.	0.1	0.1	N.D.	0.2
Pb	4	11	9	5	12	3	4	5
Mo	1	2	2	1	2	1	2	1
Zn	5	55	29	5	31	3	17	23
F	N.A.	N.A.	N.A.	N.A.	N.A.	N.A.	N.A.	N.A.
N.D. = Not detected      N.A. = Not analyzed								

APPENDIX 3

SUMMARY OF THE URANIUM OCCURRENCES IN THE EASTERN BAKER LAKE BASIN, NORTHWEST TERRITORIES

Occurrence	1	2	3	4	5	6	7	
Location	7116640N 424190E	7114240N 424750E	7110380N 421050E	7109780N 420940E	7109720N 421330E	7106690N 425550E	7106500N 424320E	7075820N 395210E
*Distance from basal Dubawnt unconformity	3.96 km N	1.52 km N	1.83 km S	2.42 km S	2.70 km S	4.84 km S	3.81 km N	2.80 km N
Occurrence type	Fracture controlled	Diatreme Breccia	Fracture controlled	Fracture controlled	Fracture controlled	Fracture controlled	Redbed and fractured controlled	Redbed
Host rock	Xenolithic alkaline dyke	Brecciated granulitic gneiss	Fractured Kazan arkose, Christopher Island intrusions and volcanic rocks(?) and volcanoclastic sediments	Fractured Christopher Island intrusion(?) -volcanic rock(?)	Fractured Kazan arkose	Xenolithic porphyritic biotite alkaline syenite stock	Fractured and altered Kazan arkose	Kazan arkose
Main mineralization control	N.W. fracture in dyke	Brecciated gneiss peripheral to alkaline stock	NW and N trending fractures	NW and N trending fractures	NW fracturing	NW fracturing	Altered arkose and NW fracturing	Lamprophyre dyke complex
Generalized geology	Alkaline dyke crosscutting granulitic gneisses	Alkaline stock and related dykes intruding granulitic gneiss	Intensely fractured and faulted sequence of conformable Dubawnt sediments, volcanics and/or related intrusions?	Intensely fractured and faulted sequence of conformable Dubawnt sediments, volcanics and/or related intrusions?	Fractured arkose with quartz stockwork	Alkaline stock intruding Christopher Island mudstone; stock intruded by N.W. trending sulphide bearing diabase	Altered giant cross-bedded Kazan arkose intruded by lamprophyre dyke; intensely fractured	Altered giant cross-bedded Kazan arkose peripheral to dyke complex
Uranium minerals	pitchblende	pitchblende	pitchblende	pitchblende	pitchblende	pitchblende	pitchblende	pitchblende, Ti-U phases
Sulphides, selenides or native metals	pyrite, molybdenite	chalcopyrite sphalerite pyrite	umangite, athabascaite, berzelianite, clausthalite, eucairite, electrum	umangite, athabascaite, berzelianite, clausthalite	marcasite, digenite, chalcocite	athabascaite berzelianite, eucairite	chalcopyrite	digenite, covellite, chalcopyrite, galena
Associated gangue minerals	chlorite, calcite	hematite, quartz, calcite, dolomite, white barite, chlorite	hematite, chlorite, calcite, cerussite, quartz	hematite, calcite, chlorite	white quartz, calcite	hematite calcite, chlorite	chlorite, calcite, barite	chlorite recrystallized carbonate and hematite, anatase
Secondary mineralization	uranophane, malachite	uranophane, kasolite, wölsendorffite	kasolite, wölsendorffite malacite	boltwoodite	uranophane	uranophane	francevillite-curienite series, iriginite, powellite, uranophane	malachite, boltwoodite
Stages of mineralization	undetermined	Two stages: 1)pitchblende 2)Cu-Fe and Zn sulphides	Three stages: 1)pitchblende 2)Cu-Ag and Cu selenides 3)noble metals	Two stages: 1)pitchblende 2)Cu-Ag and Cu selenides	undetermined	Two stages: 1)pitchblende 2)Cu-Ag and Cu selenides	undetermined	Two stages: 1)Cu-Fe, Cu, and Pb sulphides 2)pitchblende, U-Ti phases
Age (U/Pb)	-	-	-	Discordant 1516 Ma	-	-	-	-

\*Distance measured in plan view and at right angles from occurrence to basal Dubawnt unconformity.

Appendix 3 (cont.)

8	9	10	11	12	13	14	15	16
7070790N 389690E	7077640N 374190E	7079040N 372750E	7081150N 372620E	7067880N 367900E	7065280N 362830E	7064350N 364890E	7069250N 358100E	7062640N 634270E
0.1 km N	12.0 km N	13.7 km N	15.7 km N	1.6 km N	2.4 km S	2.5 km S	7 km S	1.0 km N
Redbed	Redbed	Redbed	Redbed	Fracture controlled	Fracture controlled	Fracture controlled	Disseminated-pegmatitic	Fracture controlled
South Channel conglomerate	Kazan arkose	Kazan arkose	Kazan arkose and siltstone	Christopher Island porphyritic biotite trachyte	Augen granodioritic gneiss	Augen granodioritic gneiss	K-feldspar augen-biotite gneiss	Christopher Island feldspar-biotite trachyte
Lamprophyre dyke complex	Lamprophyre dyke complex	Lamprophyre dyke complex	Lamprophyre dyke complex	NW fracturing	NW to N trending fracture zones with brecciation and mylonitization	NW to N trending fracture zones with brecciation	Disseminated in augen gneiss	
Altered conglomerate associated with dyke complex	Altered giant cross-bedded arkose peripheral to dyke complex	Altered giant cross-bedded arkose peripheral to dyke complex	Interbedded arkose-siltstone with minor giant cross-bedded arkose	Southerly dipping Christopher Island Formation flows and volcanoclastic sediments	E-W trend felsic augen gneisses with interlayer amphibolites	E-W trending felsic gneisses with interlayered amphibolites and metadiabase	Augen gneiss cut by diabase and amphibolite dykes	Series of Christopher Island flows
pitchblende	pitchblende, Ti-U phases	pitchblende, Ti-U phases, U-bearing illitic clay(?)	pitchblende	none identified	pitchblende	pitchblende	uraninite	Ti-U phase
chalcopryrite, digenite, covellite, bornite, galena	digenite, covellite, chalcopryrite, bornite, pyrite, native silver and copper, galena	digenite, covellite, chalcopryrite, pyrite, native silver and copper, galena	native copper, native silver, chalcocite, digenite	none identified	pyrite, chalcopryrite, native galena, molybdenite	chalcopryrite, bornite, pyrite, galena	molybdenite, monazite	chalcopryrite, galena
chlorite	chlorites, recrystallized carbonate (calcite, dolomite) and hematite, anatase	chlorite, recrystallized carbonate (calcite, dolomite) and hematite, anatase	chlorite, recrystallized carbonate, hematite, anatase	hematite, calcite	hematite, quartz, calcite, chlorite, specularite, pumpellyite prehnite	hematite, quartz, chlorite, calcite	-	chlorite, anatase, calcite
uranophane, boltwoodite, brochantite, malachite	malachite, boltwoodite	very limited exposure none observed	malachite, boltwoodite	none identified	kasolite, uranophane, wölsendorfite, betauranophane	uranophane, boltwoodite, wölsendorfite, malachite	none identified	malachite
undetermined	Two stages: 1)Cu-Fe, Cu, and Pb, Fe sulphide, native silver 2)pitchblende, U-Ti phases	Two stages: 1)Cu-Fe, Cu, Pb and Fe sulphides, native silver 2)pitchblende, U-Ti phases	Two stages: 1)Cu-Fe, Cu and Fe sulphides, native silver 2)pitchblende, U-Ti phases	undetermined	Two stages: 1)pitchblende 2)Cu-Fe, Fe, Pb and Mo sulphides	Two stages: 1)pitchblende 2)Cu-Fe, Fe and Pb sulphides	undetermined	undetermined
-	-	-	-	-	Discordant 1813 Ma	-	-	-

Appendix 3 (cont.)

Occurrence	17	18	19	20
Location	7062630N 633720E	7061170N 627450E	7070800N 610750E	7056450N 601850E
*Distance from basal Dubawnt unconformity	1.1 km N	0.44 km N	12.45 km N	2.2 km N
Occurrence type	Fracture controlled	Fracture controlled	Redbed	Redbed
Host rock	Christopher Island feldspar-biotite trachyte	Christopher Island biotite feldspar trachyte	Christopher Island biotite trachyte	Kazan arkose
Main mineralization control	NW fracturing	NW fracturing	Disseminated in amygdaloidal flowtop	Disseminated in arkose at contact with conglomerate channel scour
Generalized geology	Series of Christopher Island flows	Christopher Island flow overlying volcanoclastic sediments	Series of interbedded Christopher Island flows and volcanoclastic sediments	crossbedded Kazan arkose with coarse channel scours
Uranium minerals	pitchblende	pitchblende	none identified	none identified
Sulphides, selenides or native metals	pyrite, chalcopyrite, bornite, galena, sphalerite	chalcopyrite, bornite, galena	none identified	none identified
Associated gangue minerals	chlorite, quartz, hematite, barite	hematite, quartz, calcite, chlorite, orange barite	calcite, chlorite, hematite	dolomite
Secondary mineralization	kasolite, uranophane, malachite	chalcocite, digenite, malachite, uranophane, azurite	none identified	none identified
Stage of mineralization	undetermined	undetermined	undetermined	undetermined
Age (U/Pb)	-	-	-	-





